Synthetic Lipids for Drug Delivery Applications

by

Michael Weiwei Meanwell

BSc, University of British Columbia, 2014

A Thesis Submitted in Partial Fulfillment

of the Requirements for the Degree of

MASTER OF SCIENCE

in the Department of Chemistry

University of Victoria

Supervisory Committee

Synthetic Lipids for Drug Delivery Applications

by

Michael Weiwei Meanwell

BSc, University of British Columbia, 2014

Supervisory Committee

Dr. Thomas Fyles, Department of Chemistry
Supervisor

Dr. Peter Wan, Department of Chemistry
Departmental Member

Abstract

Supervisory Committee

Dr. Thomas Fyles, Department of Chemistry
Supervisor

Dr. Peter Wan, Department of Chemistry
Departmental Member

Solid lipid nanoparticles (SLNPs) and lipid-drug conjugates (LDCs) are two promising lipid nanoparticle (LNP) based drug delivery systems; this thesis explores new synthetic lipids that may circumvent the limitations of currently available components for LNPs with particular focus on the stability of LNP formulations.

Neutral polyethylene glycol lipids (PEG-lipids) have been designed, synthesized, and characterized with ESI-MS, for stabilizing SLNPs containing dsDNA oligomer. 1st and 2nd generation PEG-lipids investigated the effects of serinol and iminodiacetic acid backbone structures, respectively, and aliphatic chain sequences within the lipid anchors on the stability of SLNPs. Assays were developed to analyze LNP stability in both PBS buffer and PBS buffer with 10 % serum at different incubation temperatures. The results indicate that the hydrocarbon branching sequence offer additional SLNP stability over straight chain isomers.

LDC monomers were designed and synthesized to allow for the formulation of LDC nanocarriers for the thiopurine drugs. These hydrophobic LDC monomers were made by linking the polar thiopurine drug to a synthetic lipid. These synthetic lipids investigated branched and straight chain derivatives – the branched isomers once again demonstrated advantages in the stability of the LDCs.

Table of Contents

List of Tables

List of Figures

List of Schemes

List of Abbreviations

DCM: dichloromethane

DDQ: 2, 3 - dichloro-5,6-dicyano-1,4-benzoquinone

DIPEA: N, N - diisopropyl ethylamine

DMF: N, N - dimethylforamide

DMG-PEG: 1, 2 - dimyristoyl-*sn*-glycerol, methoxypolyethylene glycol

DMPC: 1, 2 - dimyristoyl-*sn*-glycero-3-phosphocholine

DMSO: dimethyl sulfoxide

DOTMA: 1, 2 - di-*O*-octadecenyl-3-trimethylammonium propane

dsDNA: double stranded deoxyribonucleic acid

DSG-PEG: 1, 2 - distearoyl-*sn*-glycerol, methoxypolyethylene glycol

DSPC: 1, 2 - distearoyl-*sn*-glycero-3-phosphocholine

DSPE-PEG: 1, 2 - distearoyl –*sn*- glycerol-3-phosphoethanolamine polyethylene glycol

EPC (14:0): 1,2 – dimyristoyl-*sn*-glycero-3-ethylphosphocholine

ESI-MS: electrospray ionisation mass spectrometry

EtOAc: ethyl acetate

Equiv.: equivalents

HBTU: N, N, N', N'- Tetramethyl-*O*-(1H-benzotriazol-1-yl) uronium hexafluorophosphate

HOBt: hydroxybenzotriazole

MeOH: methanol

NHS: N- hydroxysuccinimide

^{1}H-NMR: proton nuclear magnetic resonance

^{13}C-NMR: carbon-13 magnetic resonance

PEG: polyethylene glycol

R.T.: room temperature

RES: Reticuloendothelial System

siRNA: small interfering ribonucleic acid

TEM: transmission electron microscopy

TFA: trifluoroacetic acid

TLC: thin layer chromatography

List of Compounds

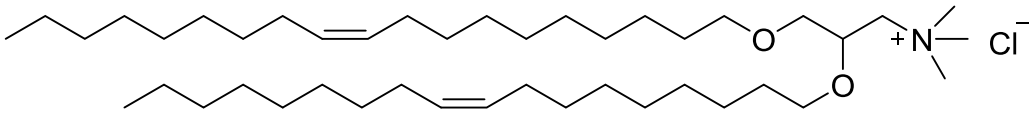

1-1

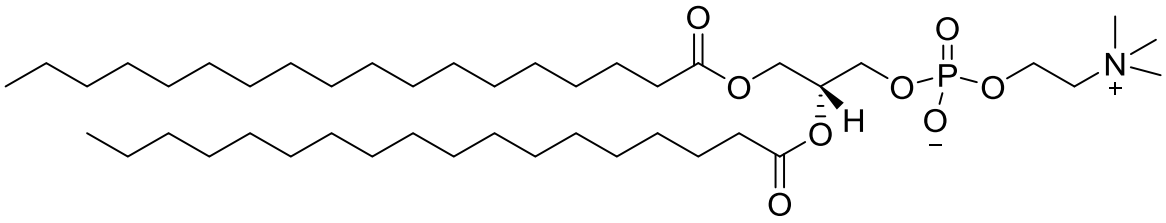

1-2

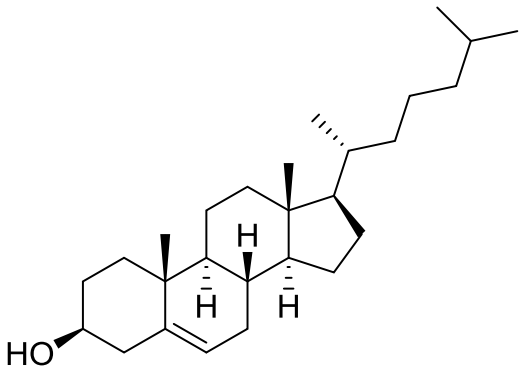

1-3

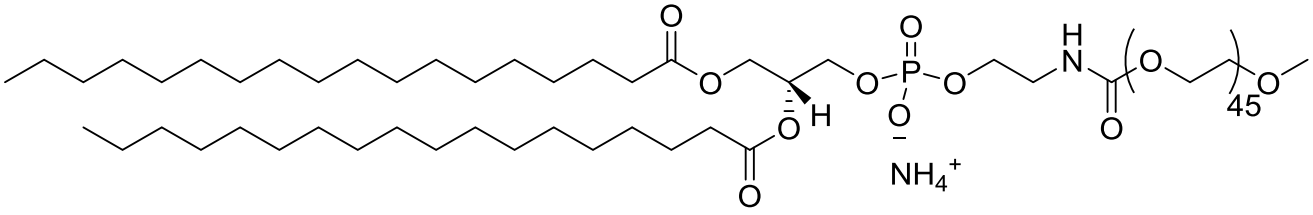

1-4

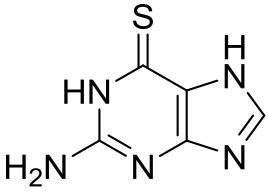

1-5

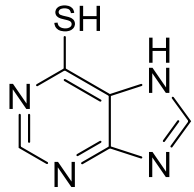

1-6

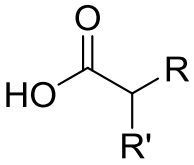

2-1(a-d)

a: R= $C_{12}H_{25}$; R'=H
b: R= $C_{14}H_{29}$; R'=H
c: R= C_8H_{17}; R'= C_6H_{13}
d: R= $C_{16}H_{33}$; R'=H

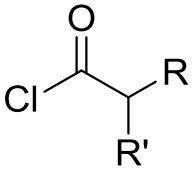

2-2(a-d)

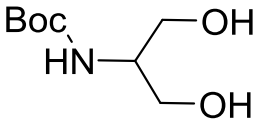

2-3

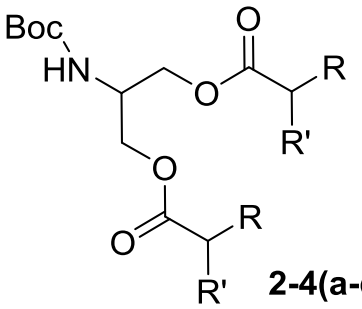

2-4(a-d)

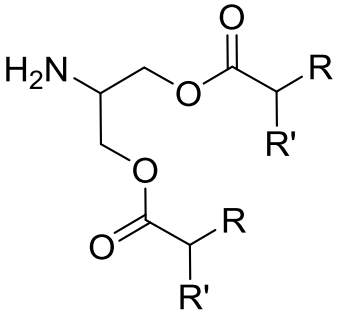

2-6(a-d)

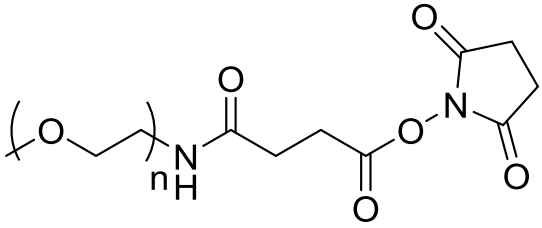

2-5

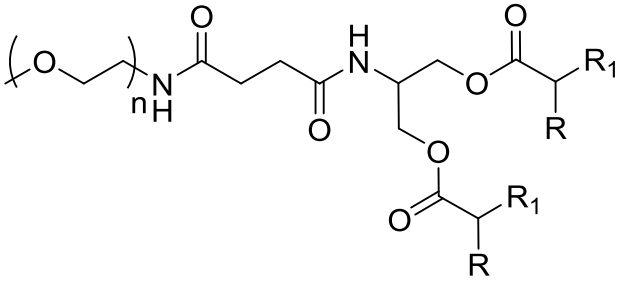

PEG-G$_1$-C14: R= $C_{12}H_{25}$; R'=H
PEG-G$_1$-C16: R= $C_{14}H_{29}$; R'=H
PEG-G$_1$-dC16: R= C_8H_{17}; R'= C_6H_{13}
PEG-G$_1$-C18: R= $C_{16}H_{33}$; R'=H

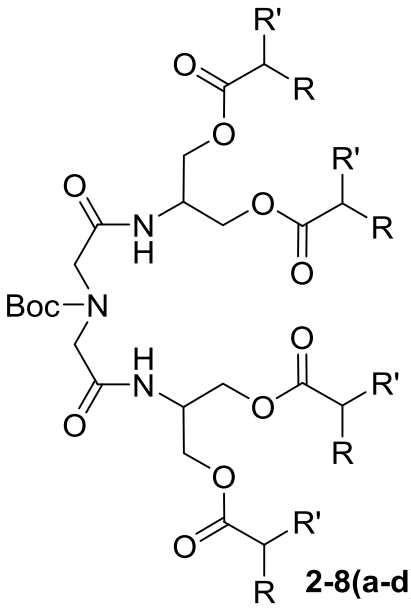

2-8(a-d)

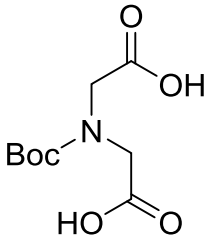

2-7

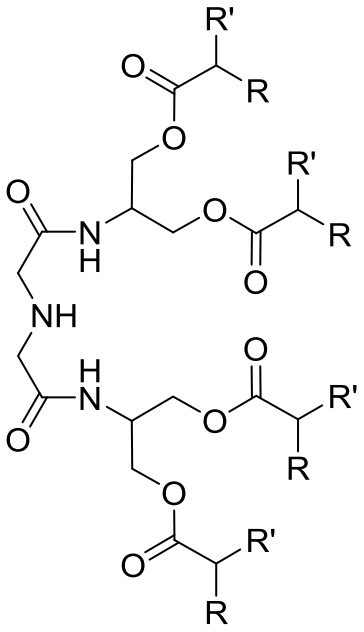

2-9(a-d)

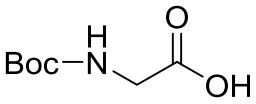

2-10

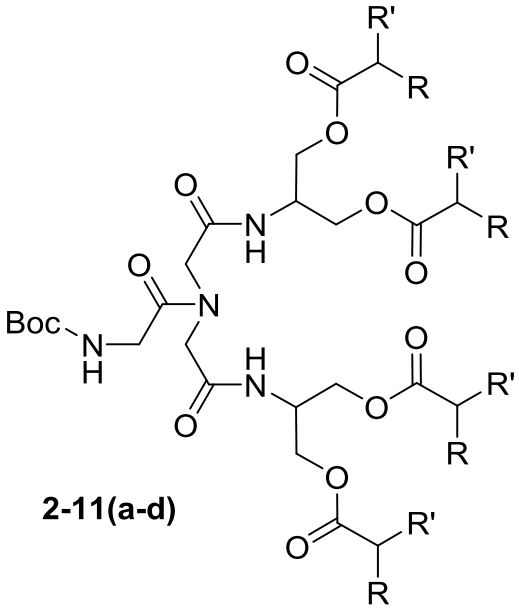

2-11(a-d)

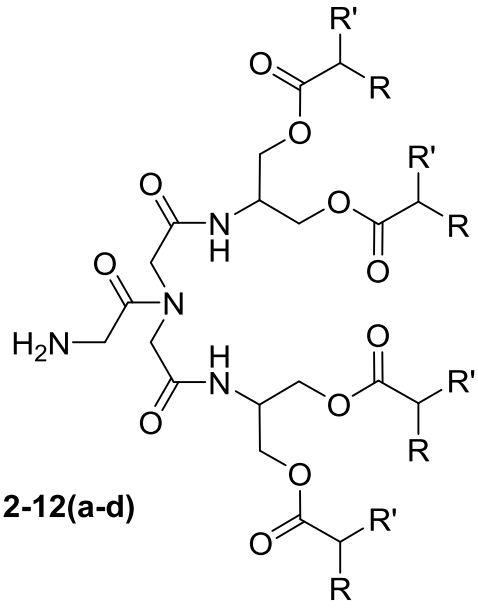

2-12(a-d)

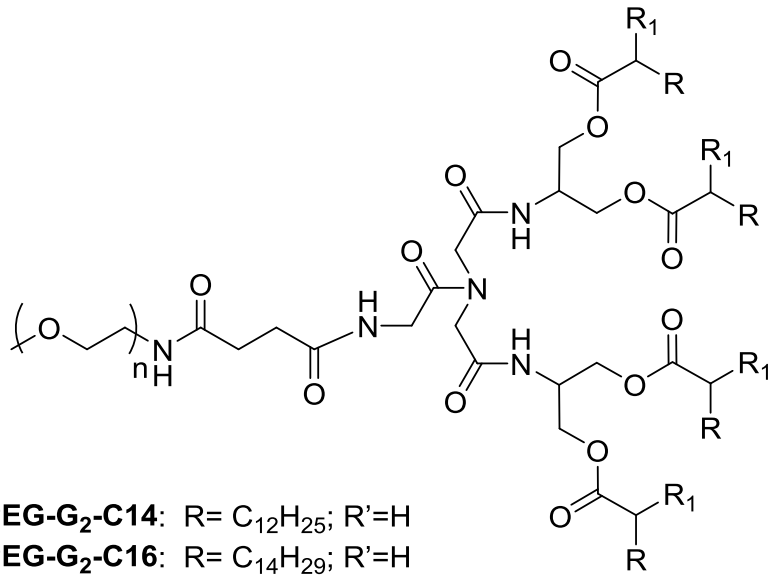

PEG-G$_2$-C14: R= $C_{12}H_{25}$; R'=H
PEG-G$_2$-C16: R= $C_{14}H_{29}$; R'=H
PEG-G$_2$-dC16: R= C_8H_{17}; R'= C_6H_{13}
PEG-G$_2$-C18 R= $C_{16}H_{33}$; R'=H

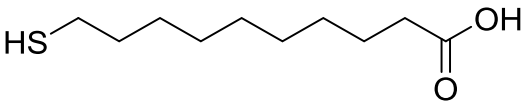

2-13

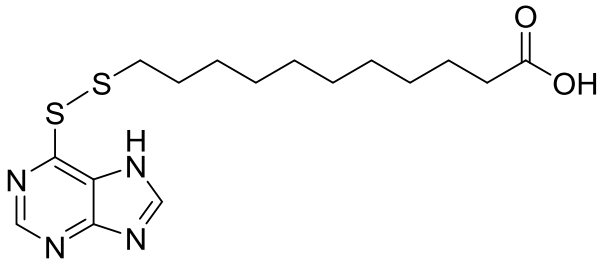

2-14a

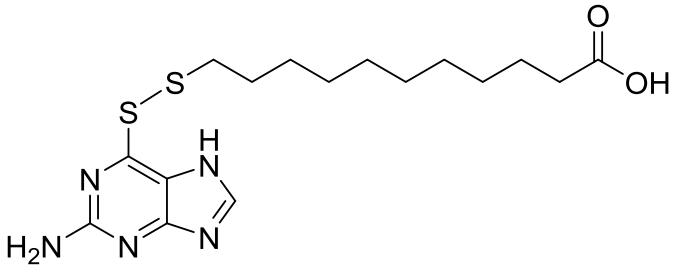

2-14b

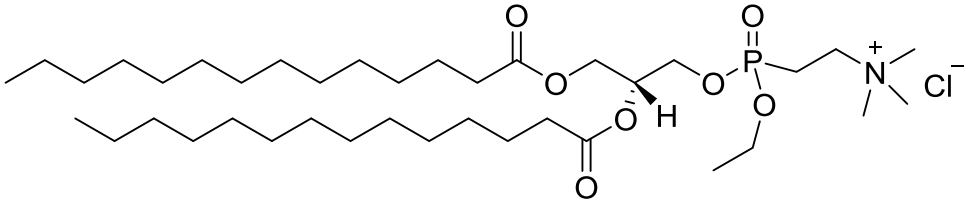

3-1

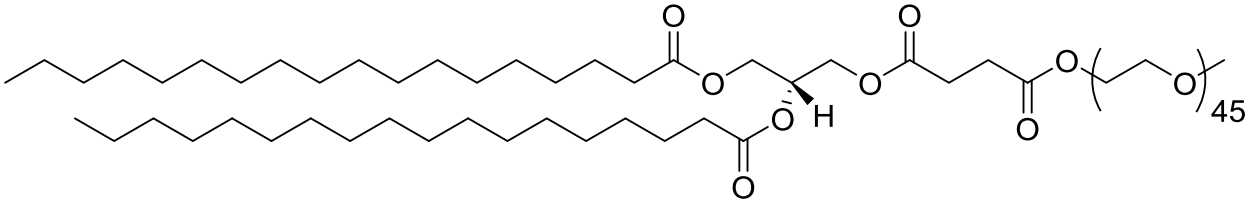

3-2

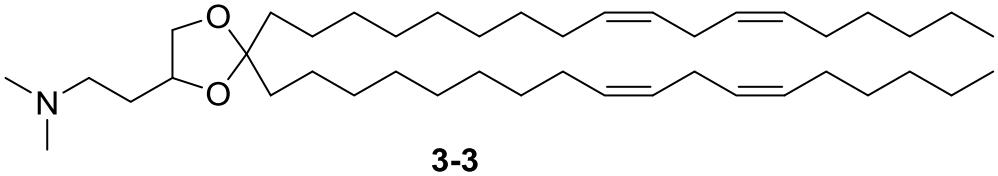

3-3

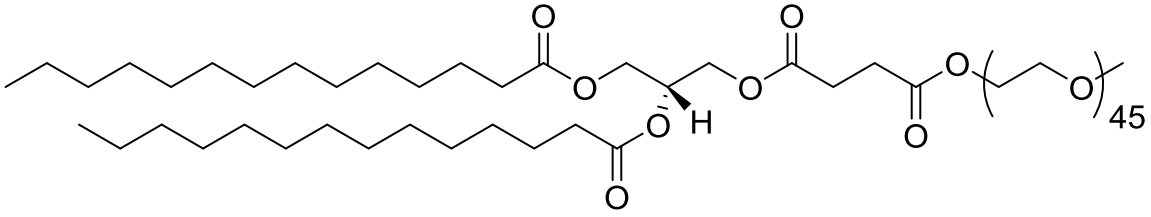

3-4

Acknowledgements

What I have learned in the lab over the past year will soon prove its value several times over. Despite this, it is the other lessons outside the classroom that will lend the immeasurable gains in my life. Mental fortitude, wisdom, and patience are not so easily learnt as the appropriate teacher can be very hard to find. It is these three attributes that I will value most from what Tom has taught me. His guidance along with my family's irreplaceable love and support was all that was needed to get this done.

Chapter 1: Introduction

1.1: Lipid Nanoparticles for Drug Delivery

The development of effective drug delivery vectors has come to the forefront of therapeutic efforts in recent years.[1,2] Such vectors, including dendrimers, viruses, and lipid nanoparticles, have been used to deliver nucleic acids and a broad range of different drugs.[3] While each system has its advantages, recent literature findings support that lipid nanoparticles (LNPs) are the most promising of these drug delivery systems.

Formulating a drug into a delivery vector is a very drug dependent process. Optimization of physiochemical properties, storage and *in vivo* stability, pharmacokinetics, and toxicity of the formulations can take significant effort and often lead to little success. Developing and optimizing a more generalized approach for drug vector formulations would be a huge step forward in improving therapeutics. Given that drugs rarely possess unifying characteristics, such a delivery system would need to be designed to address drugs from a very general perspective. For instance, delivery of nucleic acids and delivery of small hydrophilic drugs could represent two categories in which different, but related, vectors can be used. Lipid nanoparticles (LNPs) are a drug delivery system that has potential for such diversity. In general, LNPs are colloidal carriers composed of a mixture of different lipids that stabilize the drug load. Variation of the lipids and their ratios allows for modifications to suit different categories of drugs and still follow the overall concept of a generalized drug delivery vector.

Lipid-Drug conjugates (LDCs), liposomes, solid lipid nanoparticles (SLNPs), and lipoplexes all fall under the LNP classification. LDCs consist of a hydrophobic moiety linked, either through a covalent or ionic bond, to a polar drug and are primarily used in the delivery of hydrophilic drugs – the hydrophobic component of the LDC allows for the drug to self-assemble into a nanocarrier.[19] Liposomes consist of an aqueous inner compartment where the drug is

solubilized – this compartment is bordered by a lipid bilayer. Among the issues with liposomal delivery is drug leakage, and stability in the aqueous compartment as some drugs are readily hydrolyzed.[1] SLNPs and lipoplexes both represent alternatives to viral delivery in gene therapy. SLNPs possess a solidified lipid core that protects the nucleic acid – this core is then solubilized in aqueous media by a lipid-based surfactant.[16] Lipoplexes on the other hand, rely upon the cationic, or ionisable, lipids to complex with the nucleic acid and it is this complex that is stable during circulation.[20]

Current work on LNPs spans a broad range of potential applications from chemotherapy to central nervous system delivery to gene therapy – such a robust drug delivery system has long been the target of medicinal research. However; LNPs have yet to emerge as the predominant therapeutic for patient treatment. It has been identified that drug delivery systems with therapeutic potential possess these unique features: 1) the ability to deliver cargo with efficiency and efficacy, 2) the ability to target specific organs and tissues, 3) the ability to maintain stable structures in serum and in storage, and 4) have low toxicity.[4] LNPs have not yet successfully met all of these requirements. In modifying the individual components that make up the LNPs, it would be possible to improve on these characteristics.

1.2: Solid Lipid Nanoparticles

Viral vectors had long been thought as the ideal delivery system in gene therapy; however, these have since been shown to be ineffective in many cases.[21] Early clinical trials yielded mostly negative results where one patient death and two cases of the vector causing the onset of leukemia have been reported.[21] Results since then have been more promising; however, concerns remain regarding viral vectors with their potential scale-up and purification.[27] Solid lipid nanoparticles (SLNPs) represent an emerging alternative in delivering nucleic acids to cells.

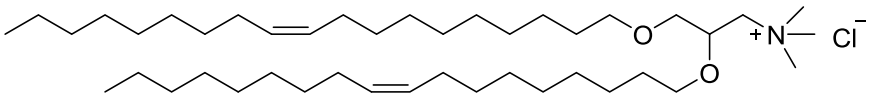

1-1 (Cationic Lipid)

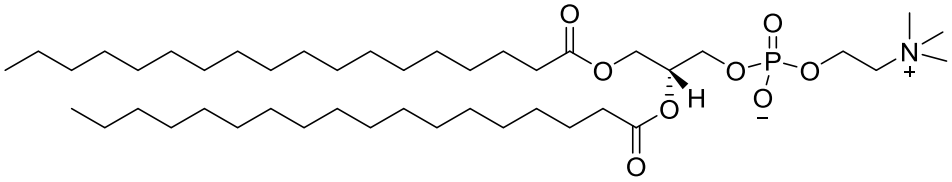

1-2 (Neutral Phospholipid)

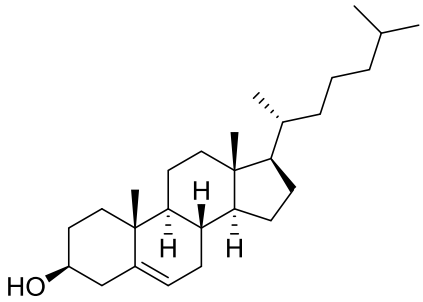

1-3

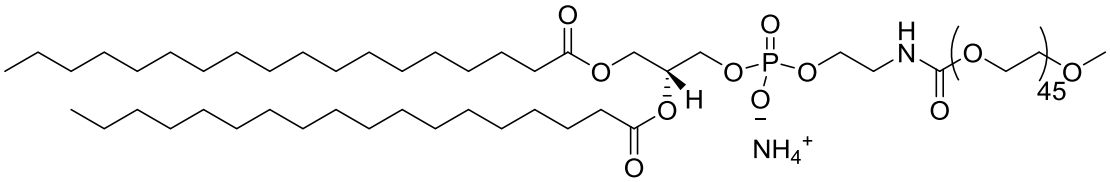

1-4 (PEG-Lipid)

Figure 1.1: Examples of the four lipid components of solid lipid nanoparticles

SLNPs are composed of four lipid components (Figure 1.1); cationic lipid (or ionisable lipid), neutral phospholipid, cholesterol, and PEG (polyethylene glycol)-lipid. The hydrophobic core of the SLNP is thought of as an amorphous solid composed of the ionisable lipid, the neutral phospholipid, and cholesterol. PEG-lipids are used to solubilize and stabilize this core in an aqueous medium

such as the blood. Until recently, it was not well understood how the individual components come together to form the SLNP.[16] For oligonucleic acid cargo e.g. siRNA, the siRNA drug load forms a complex with the cationic lipid within the hydrophobic core – the ratio of cationic lipid's cationic groups to the siRNA's anionic groups is known as the charge ratio.[16] In general the smaller this charge ratio is, the greater the drug loading will be as a fraction of the total particle mass. The PEG-lipid is anchored onto the hydrophobic core by aliphatic chains of the lipid anchors. Literature readings suggest that a composition consisting mainly of ionisable lipid and cholesterol will most likely lead to the formation of stable SLNPs.[16] The SLNP composition, the drug loading, as well as the identity of the lipids themselves, will greatly affect the particles' physiochemical properties and stability. [8, 17]

First generation targeted drug delivery vectors, such as SLNPs, do not have ligands attached for binding to specific cell surfaces, moreover; these particles depend on the enhanced permeability retention (EPR) effect. In order to get the full therapeutic result of the EPR effect the nanocarriers need to have sufficiently long circulation times – this is related to the physiochemical properties of the particle. Size, lipid composition, surface charge, and surface coatings have all been demonstrated to affect biodistribution and pharmacokinetics.[5,6] SLNPs that have sizes within the range of 10-100nm can avoid clearance by the kidneys and the reticuloendothelial system (RES) leading to extended circulation times and increased drug accumulation at target sites.[7] It has been established charged species are readily bound to serum proteins resulting in rapid removal by phagocytic cells.[7] Pegylation, a process by which the outer surface of a particle is covered with PEG, represents a general approach for preventing clearance of drug delivery vectors.[6]

PEG has a number of roles in both the formulation and circulation stability of SLNPs. When formulating SLNPs the PEG prevents aggregation and contributes to obtaining stable, small, mono-disperse nanoparticles.[8] Lipid anchors that sufficiently anchor the PEG to the hydrophobic core result in

formulations that give greater stability under both storage and physiological conditions. While providing a steric barrier for the SLNP, the hydrophilic polymer also serves to significantly decrease the surface charge. Together, this is generally assumed to prevent the SLNPs from associating with serum proteins and ultimately leads to extended circulation times compared to their non-pegylated counterparts.[6, 8] Current commercially available PEG-lipids have been found to insufficiently anchor the polymer to the SLNP resulting in limited circulation times.[8] There has been little work done to develop PEG-lipids that improve the therapeutic efficacy of lipid nanoparticles.

1.3: Lipid-Drug Conjugates

Hydrophilic drugs represent a large portion of available therapeutics in chemotherapy. Non-targeted drug delivery systems have resulted in harmful side effects during cancer treatment as the cancer drugs accumulate non-specifically in all regions of the body.[5] Although some recent success has given passive targeting delivery vectors for anticancer agents doxorubicin and paclitaxel, there remains a significant need for further development of such nanocarriers.[5]

Lipid-Drug Conjugates (LDCs) represent a novel carrier that has yet to be used in chemotherapy. The basic concept is well developed in the use of pro-drugs to assist polar molecules to transverse membranes followed by metabolic processing to release the drug inside the cell. The LDC concept involves linking a polar drug to a hydrophobic component, where this linkage can be either covalent or ionic. Ultimately, this will result in a moiety that overall is hydrophobic and thus is capable to self-assemble into a lipid nanoparticle. Following LDC uptake into the cell, cellular mechanisms will expose the drug inside the cell. As outlined previously, lipid nanoparticles have the potential to avert toxic side effects seen with nonspecific drug delivery.[5] Effective nanocarriers must be stable under both storage and physiological conditions, and more importantly, be able to avoid clearance by the kidneys and the RES (which implies a particle size

ranging from 10-100nm). A higher drug loading would possibly lead to fewer side effects as the exposure to the amount of non-drug components can then be reduced. Incorporation of a disulfide bond within the LDC can lead to improved release kinetics. It is well noted that the interior environment of tumor cells is considerably more reducing than that of the blood plasma; therefore meaning that the active form of the drug is more readily released within the cell.[22] Using an ester linkage instead, which is what is commonly used in the majority of pro-drugs, would not give such favorable release kinetics as esters are non-specifically hydrolyzed by esterases throughout the body.

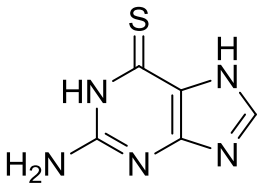

1-5

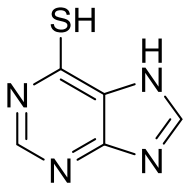

1-6

Figure 1.2: Thiopurine drugs 6-thioguanine and 6-mercaptopurine

1-5 and **1-6** are the thiopurines used as frontline drugs in the treatment of acute lymphoblastic leukemia (ALL). 70% of all people diagnosed with ALL (cancer of the bone marrow) will survive for five or more years. Despite these encouraging results, complications associated with systemic non-specific drug delivery have been found to lead to harmful and sometimes deadly side effects.[10] In some cases, ALL can spread into the central nervous system (CNS) where thiopurine drugs are unable to penetrate the blood brain barrier (BBB).[9,11] A nanocarrier system would have the potential to address the effects associated with nonspecific delivery as well as the BBB impermeability of these thiopurine drugs.[12] A variable oral bioavailability and short half-life are also among the issues that would be resolved.

1.4: Lipid Nanoparticle Formation and Characterization:

A number of high pressure homogenization techniques and emulsification methods are used to promote individual components to self-assemble into LNPs.[23] In order to have therapeutic potential, the method must be able to form LNPs with reproducible physiochemical properties and, at the same time, not require significant time or effort to perform. Current methods do not offer such properties.

The Precision Nanosystems (PNI) microfluidic mixer (NanoAssemblr™) represents a new technology that has been proven to give efficiently reproducible LNP formulations. It relies on herringbone grooved mixing channels – this allows for rapid, rotational mixing of two fluids that eventually lead to the formation of LNPs. Organic solvents in the final products (such as ethanol, and small molecules) are readily removed by dialysis. Particle size can easily be determined by dynamic light scattering (DLS) and the surface charge can also be determined by a zeta potential analyzer. Further characterization using transmission electron microscopy (TEM) allows to visualization of these nanoparticles.

1.5: Goals of the Thesis

In order to have therapeutic potential, LNPs must have the following properties: 1) high drug loading; 2) particle sizes in the range of 10-100nm; 3) low polydispersity (monodisperse); 4) low toxicity; 5) target specific cells for delivery of cargo; 6) deliver cargo with high efficiency and efficacy; and 7) stable in storage and under physiological conditions.[4, 5] Narrowing down a composition space for each LNP to the point that all of these conditions are satisfied has proven to be a difficult task. Determining the identity and ratios of the lipids that go into making these particles takes significant time and effort – rather it would be better to develop and optimize individual components separately and evaluate their effects based upon already established compositions. This approach has

been used in regard to the cationic lipids and the PEG-lipids in SLNPs which eventually lead to particles with much improved physiochemical properties.[8, 17] It would be possible to further develop different PEG-lipids for SLNPs by varying the branching sequences of the lipid anchors as well by exploring different backbone structures. By doing so, one could arrive at structures that specifically address the storage stability and short circulation time issues associated with SLNPs.

The basic concept of LDCs is to make polar drugs more hydrophobic by linking them to a lipid moiety. Different branching sequences and chain lengths will determine how hydrophobic the LDC becomes. Too much hydrophobicity could result in crystallization or very poor processibility. By exploring a range of synthetic lipids, it would be possible to develop an effective nanocarrier.

Novel PEG-Lipids

PEG-lipids that have the potential to improve SLNP stability under storage and physiological conditions would represent a great step forward in developing more effective delivery vectors. Current lipid anchors have been found to insufficiently anchor the PEG to the SLNP's hydrophobic core resulting in poor circulation times.[8] By investigating different backbone structures with different aliphatic branching sequences, it would be possible to arrive at better lipid anchors. The candidate designs explored in this project are given in Figure 1.3.

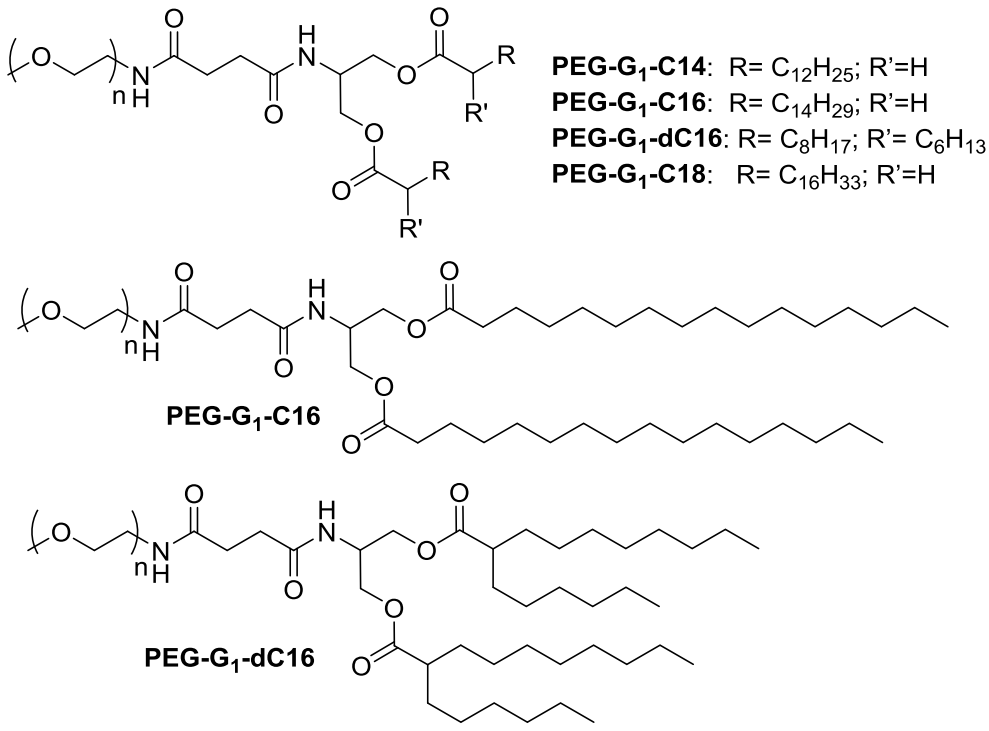

Figure 1.3: First generation novel PEG-Lipids where the number of repeating ethyleneoxy monomers, n, is approximately 45. The C16 isomers are drawn to illustrate different branching sequences.

Incorporating a serinol backbone rather than the glycerol backbone commonly used in commercial PEG-lipids, led to the first generation structures in Figure 1.3. Admittedly, these PEG-lipids are quite similar to those currently available, however; there remain some meaningful differences. The **PEG-G$_1$-dC16** analogue is the first PEG-lipid to possess branched aliphatic chains while the remaining novel PEG-lipids explored the effect of increasing chain length. The amide linkage that connects the PEG to the lipid replaced the phosphodiester bond of other PEG-lipids – this results in an overall neutral compound which avoids potential problems with anionic nucleic acid cargos.

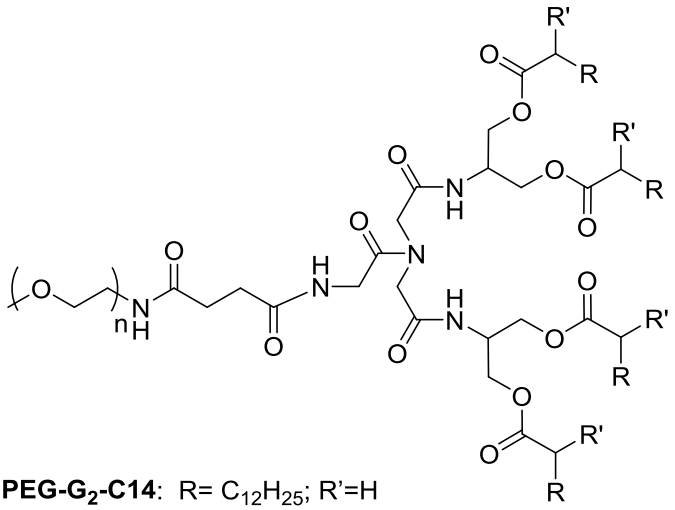

PEG-G_2-C14: R= $C_{12}H_{25}$; R'=H
PEG-G_2-C16: R= $C_{14}H_{29}$; R'=H
PEG-G_2-dC16: R= C_8H_{17}; R'= C_6H_{13}
PEG-G_2-C18 R= $C_{16}H_{33}$; R'=H

Figure 1.4: Second generation PEG-lipids where the number of repeating ethyleneoxy monomers is approximately 45.

Second generation structures based on an iminodiacetic acid backbone, as shown in Fig 1.4, have an interesting element. Both commercial and other novel PEG-lipids utilize one lipid anchor, however; each of the second generation analogues have two lipid anchors per PEG chain. This increase in the amount of "grease" should result in PEG chains which are better anchored to the hydrophobic core. Similar to the 1st generation, branching and chain length variation of the aliphatic chains were investigated. Following characterization with ^{1}H-NMR, ESI-MS was used to further determine the number of repeating ethyleneoxy monomers in the PEG.

The goals of these projects were to; 1) develop chemistry to synthesize the above lipids, 2) prepare SLNPs using the microfluidic mixer while investigating different formulation variables, 3) Characterize the particles by size, polydispersity, and TEM imaging, and 4) evaluate stability under both storage and physiological conditions. The purpose is to establish what sort of effects the different branching sequences and backbones have on the stability of the particles. These studies are in direct comparison to commercial PEG-lipids.

LDCs for Thiopurine Drugs

A nanocarrier system would help resolve several challenges associated with the thiopurine drugs as well as represent a significant advancement in chemotherapy.

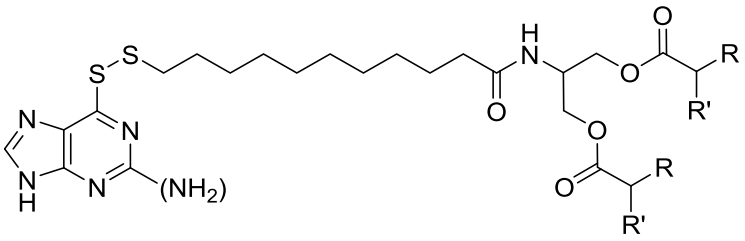

6MP-C14: R= $C_{12}H_{25}$; R'= H
6MP-C16: R= $C_{14}H_{29}$; R'= H
6MP-dC16: R= C_8H_{17}; R'=C_6H_{13}
6MP-C18: R= $C_{16}H_{33}$; R' = H
6TG-C14: R= $C_{12}H_{25}$; R'= H
6TG-C16: R= $C_{14}H_{29}$; R'= H
6TG-dC16: R= C_8H_{17}; R'=C_6H_{13}

Figure 1.5: Structures of the LDCs for 6-mercaptopurine and 6-thioguanine

A disulfide linkage between the lipid and the thiopurine was chosen to form the LDC monomers. In removing the free thiol group, the LDC monomers become less polar and are better candidates for assembly into nanocarriers. The remaining part of the molecule exists to increase the hydrophobicity of the entire compound.

The goals of these projects were; 1) develop chemistry to synthesize the above lipids, 2) prepare LDCs using the microfluidic mixer while investigating different formulation variables, 3) Characterize the particles by size and polydispersity and 4) evaluate stability under both storage and physiological conditions. The purpose is to establish what effects the different branching sequences have on the stability of the particles.

Chapter 2: Synthesis of Synthetic Lipids

2.1: Synthesis of PEG-Lipids

In total eight PEG-lipids were synthesized to evaluate the different backbones and branching sequences of the lipid anchors – their synthesis is discussed here. Full experimental details can be found in Appendix 1, and NMR spectra can be found in Appendix 3. Schemes 2.1.1 (1st generation) and 2.1.2 (2nd generation) provide a general overview for the synthesis of the PEG-lipids.

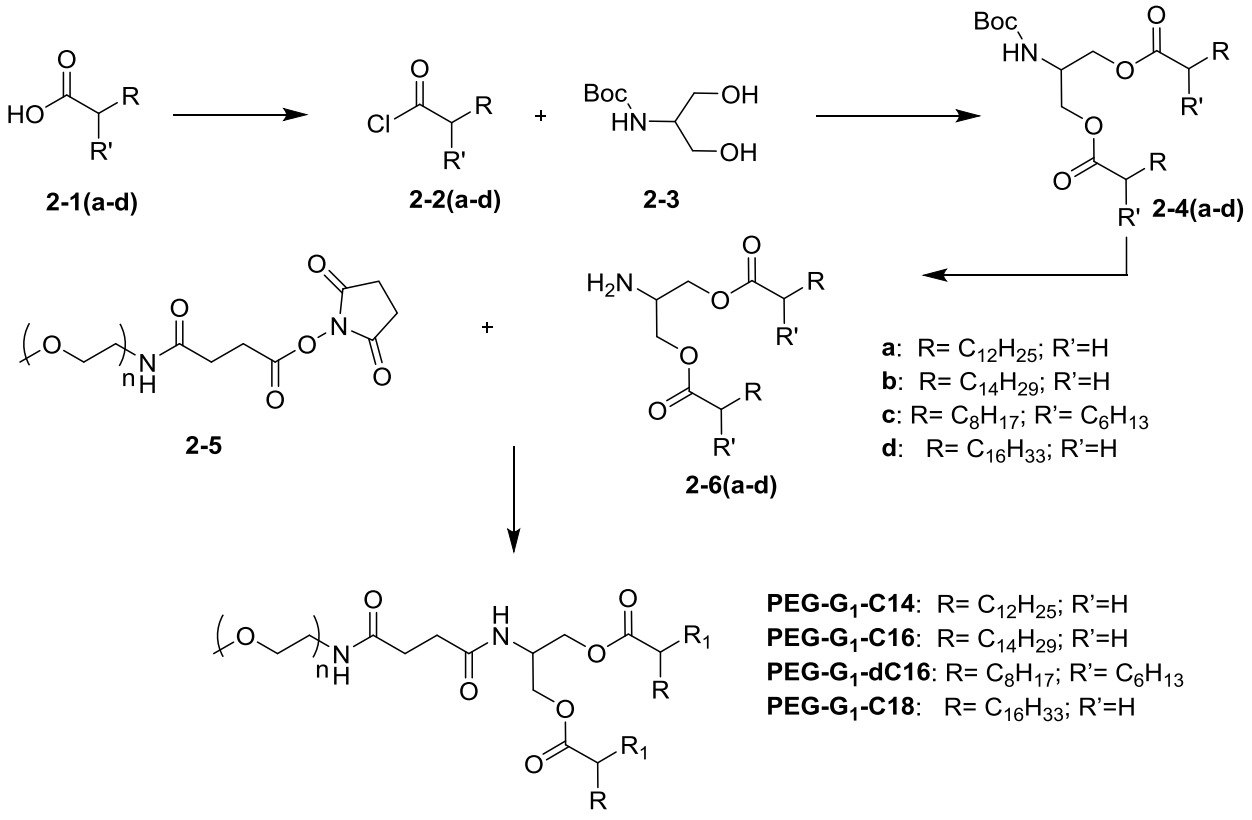

Scheme 2.1.1: Synthesis outline of 1st generation PEG-Lipids

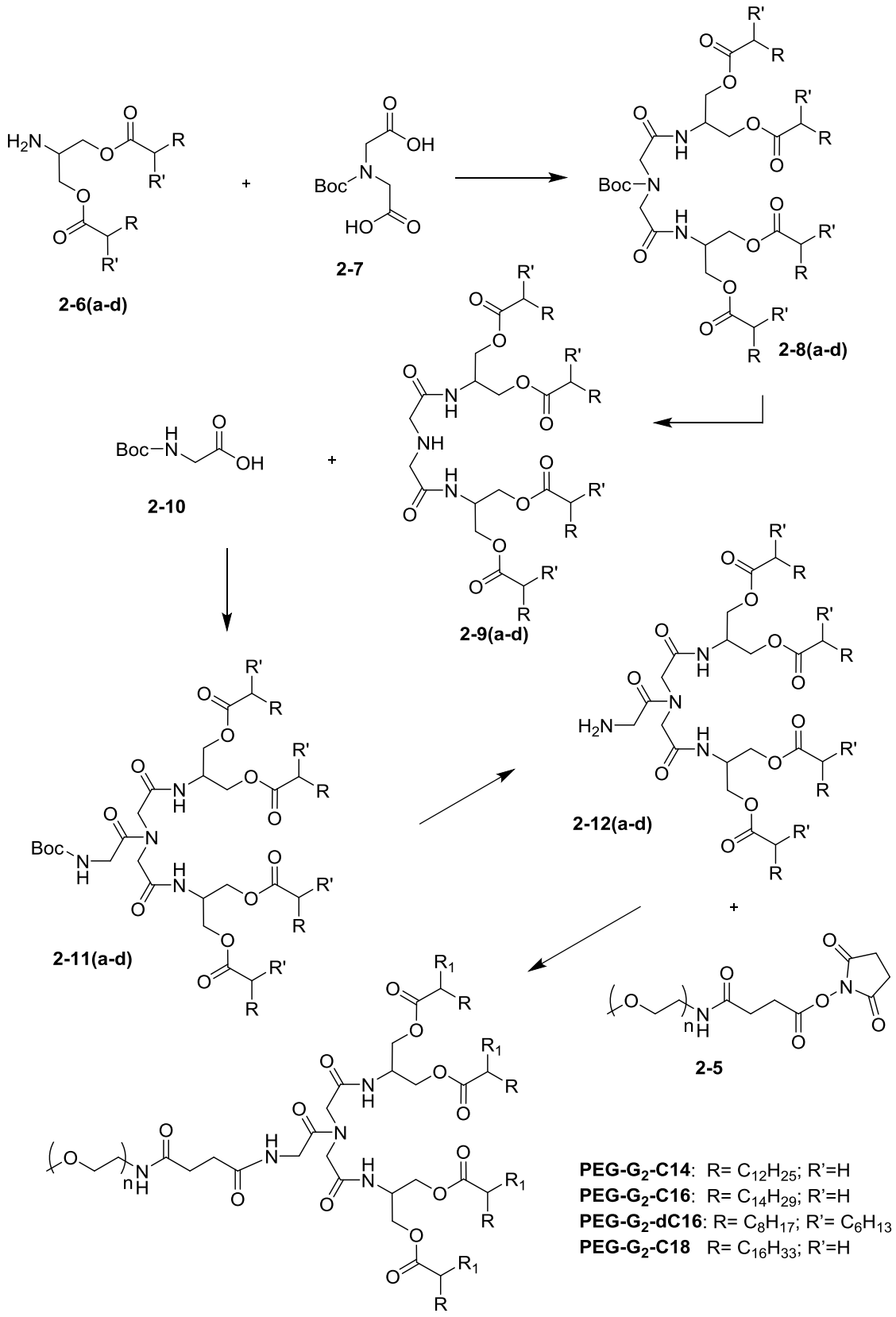

Scheme 2.1.2: Synthesis outline of 2nd generation PEG-Lipids

2.2: Synthesis of 1st Generation PEG-Lipids

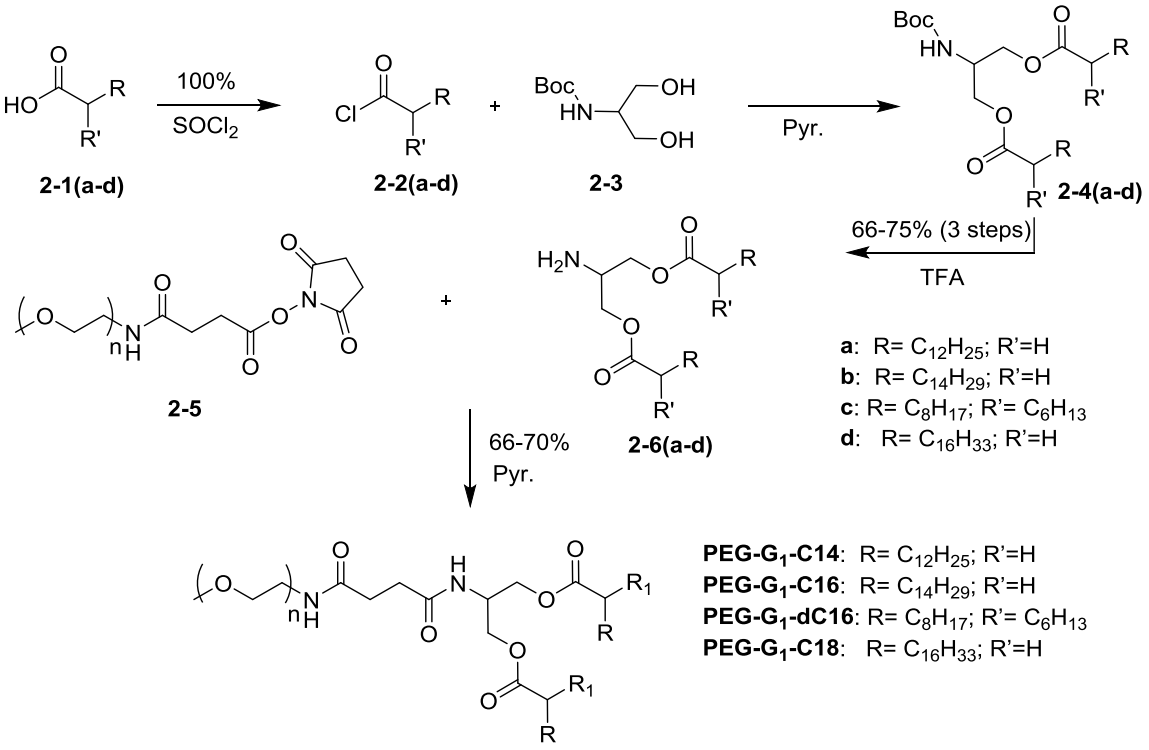

Scheme 2.2.1: Synthesis of the 1st generation PEG-lipids. Synthetic details in Appendix 1, NMR in Appendix 3.

The first step in the synthesis of the 1st generation PEG-lipids was to make the 1st generation lipid anchor. This starts with converting fatty acids **2-1(a-d)** to their respective acid chlorides **2-2(a-d)** by dissolving **2-1(a-d)** in excess thionyl chloride while heating. ^{1}H-NMR monitored the downfield shift of the α-proton(s) signal from 2.35 (2H) ppm to 2.70 ppm (2H) – this was expected given that chlorine electrons donate less readily into the $\pi^*_{c=o}$ orbital. In order to ensure the complete removal of thionyl chloride, **2-2(a-d)** was left overnight on the high vacuum. Yields were assumed to be quantitative.

Initial attempts to synthesize **2-4(a-d)** were unsuccessful. Residual thionyl chloride reacted with the boc-N-serinol hydroxyl groups leading to a mixture of undesired products. Room temperature conditions, where pyridine functioned as the solvent and the sacrificial base, gave a reaction time of 3 days but eventually

produced the desired products. ^{1}H-NMR revealed an upfield shift from 2.70 ppm (2H) to 2.36 ppm (2H) of the carbonyl alpha protons. The methylene protons on the serinol backbone shifted from 3.82 ppm (4H) to 4.15 ppm (4H) and the singlet at 1.45 ppm (9H) confirmed the stability of boc protecting group. Disappearance of the signal at 3.82 ppm established complete conversion to the di-ester. Though acyl chlorides readily form esters with primary alcohols, the steric hindrance of the aliphatic chains and the close proximity of the alcohol groups led to slower reaction rates. Moderate heating yielded **2-4(a-d)** within two hours. The boc deprotection of **2-4(a-d)** with TFA gave the pure 1st generation lipid anchors in yields varying from 66-75% over 3 steps.

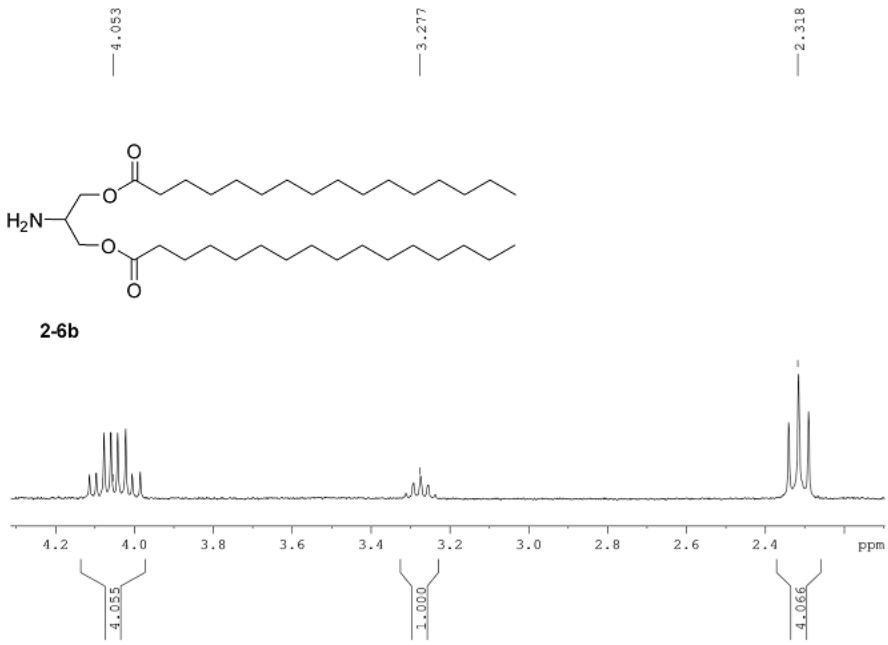

Figure 2.1: ^{1}H-NMR ($CDCl_3$, 300 MHz) of **2-6b**. The protons on the serinol backbone are in an AA'BB'XY_2 spin system.

The isolated products gave ^{1}H-NMR spectra that were generally in line with expectations. However, due to conformational preference within the serinol-derived fragment, the methylene protons are in different chemical environments. ^{1}H-^{1}H COSY showed there was a correlation within the 4.05 ppm multiplet supporting that two chemically inequivalent protons contributed to the signal. The

methine proton was identified at 3.28 ppm (1H) with ^{1}H-^{1}H COSY revealing correlations between this and the 4.05 ppm multiplet. The triplet at 2.32 ppm (4H) corresponds to the carbonyl α-protons. The absence of a singlet at 1.45 ppm confirms a successful boc-deprotection. ESI-MS showed the singly charged species (2-6(a-d) + H)$^{+}$ with required mass/charge ratio for the assigned structures in all cases.

Linkage of the PEG to the lipid anchor proved to be difficult. The first few iterations of this reaction were done at room temperature failed to link the two moieties as detected by thin-layer chromatography analysis. NHS-activated esters are quite reactive such that r.t.[25] reactions with free primary amines proceed to give the desired products; however, the PEG chain hinders the accessibility of the activated carbonyl carbon for nucleophilic attack. Moderate heating over 48 hours in pyridine afforded PEG-lipids in yields of 66-70% following chromatographic purification.

To characterize these PEG-lipids both ESI-MS and ^{1}H-NMR were used. For formulation purposes, it was necessary to accurately determine n – the number of repeating ethylene monomers in the PEG chain. Unfortunately, integration of the signal for ethylene protons from the ^{1}H-NMR was inconclusive. PEG-lipids have a high sensitivity to ESI-MS since the ethylene chains possess a high affinity towards positively charged species such as protons, potassium or sodium ions. Information obtained from the ESI-MS spectra allowed for the determination of n.

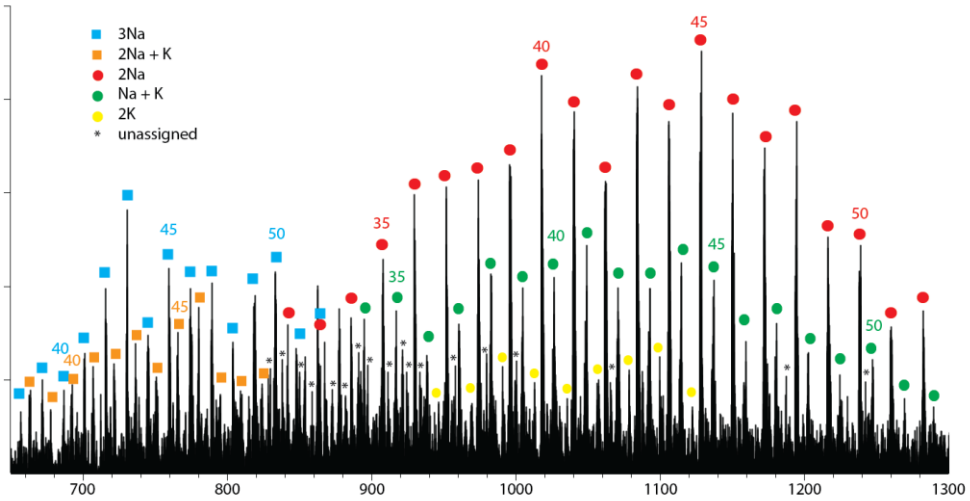

Figure 2.2: Mass spectrum generated from ESI-MS of the starting material NHS-PEG. The sample was treated with 0.1% TFA and 0.1% NaCl. This compound shows the 3Na, 2Na+K, 2Na, Na+K, and 2K ion series where 74 of the 87 ion clusters are accounted for.

ESI-MS of the NHS-PEG starting material shows five different series for multiply-charged species (Figure 2.2). Given the instrument's m/z range does not extend beyond m/z =2000, the singly charged species was not observed. Sigma-Aldrich the supplier reported that n ~ 45 for the commercial sample of NHS-PEG used, so it was expected that the triply charged species would appear around m/z = 700-800. There exists two triply charged series in the mass spectrum; one corresponding to ionization by two sodium ions and another to one potassium (orange squares) and another to ionization by three sodium ions (blue squares). Here, the blue squares indicate the more intense series. Together, these form the 3+ cluster which was identifiable by the peak spacing of m/z = 14.7 between consecutive peaks in the same series and relates to the different degrees of polymerization of the ethylene oxide. The series themselves were readily differentiated based simply on the fact that each has unique mass-to-charge ratios due to being ionized by different ions. Series belonging to the 2+ cluster were identified by having a peak spacing of m/z = 22.0 between consecutive peaks of the same series that also relate to the different degrees of polymerization of the ethylene oxide. Three doubly charged series appeared with

mass-to-charge ratios around 1000; one corresponding to ionization by two sodium ions (red dots), one showing the dipotassium ion series (yellow dots), and another corresponding to ionization by one sodium and one potassium (green dots). Once again, each series within the 2+ cluster was identified based upon unique mass-to-charge ratios. Here, red indicates the most intense series while yellow shows the least intense one.

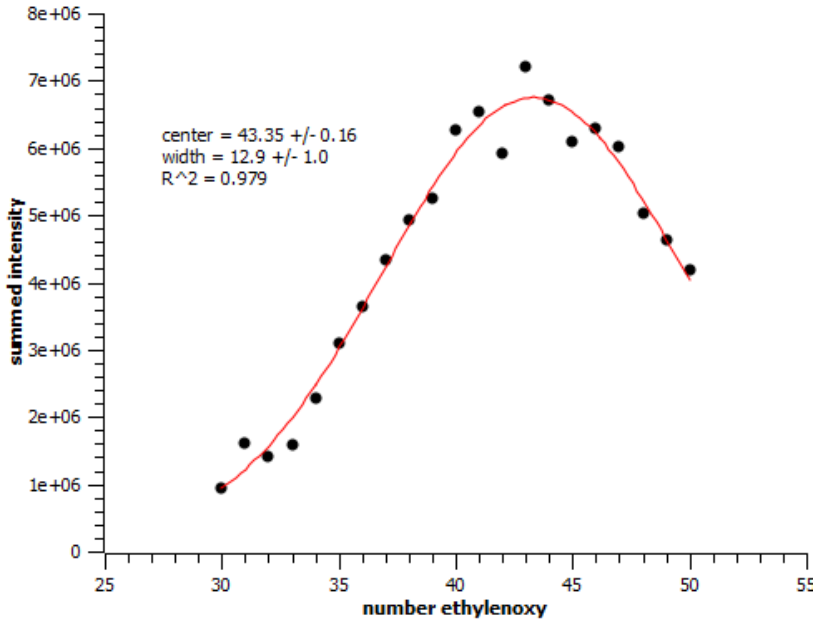

Figure 2.3: The intensities of a given n were summed and plotted versus n for the NHS-PEG. The plot was then fitted to a Gaussian distribution.

Within each series, n = 45 was present and indicated on the spectrum – so for the single species with n = 45 there were five mass-to-charge ratios at which this appears. Once the peaks were assigned, the intensities for a given n can then be summed, and the summed intensities plotted versus n with the data fit to a Gaussian with a high reliability. The center of the Gaussian is 43 which is consistent with a polymeric structure. Commercial samples are quoted as n = 45, though this may just be an approximation by the suppliers. Regardless, the ESI-MS proves that the NHS-PEG is the starting material where 85% of the peaks were assigned.

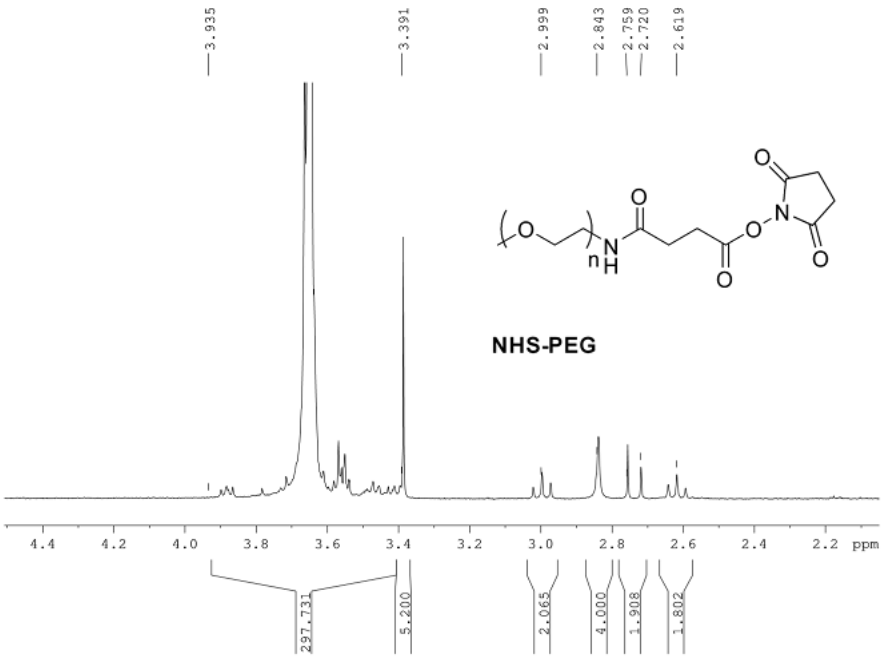

Figure 2.4: The integration of the methylene protons in the ^{1}H NMR (300 MHz) of NHS-PEG, in $CDCl_3$, was significantly different than the expected values.

The singlets observed in the ^{1}H-NMR of the NHS-PEG (Figure 2.4) at 2.72 ppm and 2.76 ppm gave evidence that the starting material contained impurities. The expected integration of the ethylene protons should be ~ 174 H; however, the observed integration was 297 H indicating that there may be polymeric impurities present. Although there were unassigned peaks in the ESI-MS (Figure 2.2), these peaks were not found to correspond to a polymeric series. The impurity was unable to be confidently identified. The singlet for the terminal methoxy shows at 3.39 ppm with an integration of 5.2 H which is considerably greater than the expected 3 H. This indicates that the polymeric impurity is at least terminated in methoxy at one end. In fact when working through the integrations it is most likely that both ends terminate with methoxy groups – suggesting an OMe-PEG-OMe like structure. Qualitative purity calculations based on the ethylene proton signal and methoxy proton signal give mol % purities of 58 % and 63 %, respectively. Averaging of these two approximations gives 61 % purity for the NHS-PEG starting material.

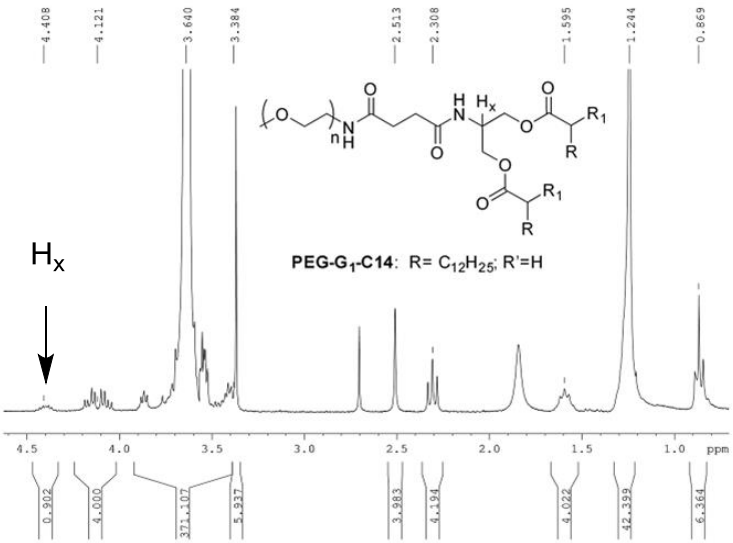

Figure 2.5: ^{1}H-NMR ($CDCl_3$, 300 MHz) of **PEG-G$_1$-C14**. The downfield shift of H_X from 3.28 ppm to 4.41 ppm was indicative of amide formation.

Significant effort was invested in the characterization of the synthesized PEG-lipids. ^{1}H-NMR of **PEG-G$_1$-C14** (Figure 2.5) showed the conversion of the amine in **2-6(a-d)** to the amide linkage which was supported by the downfield shift of the methine proton on the serinol backbone from 3.28 ppm to 4.41 ppm (Figure 2.5 shows **PEG-G$_1$-C14** as an example). Furthermore, due to lack of free bond rotation at the amide, the methylene protons on the serinol backbone experience a greater difference in chemical environment – thus resulting in a more observable difference in their chemical shifts (4.12 ppm) than in the starting amines. Integration of the ethylene protons at 3.64 ppm highlight that there may be polymeric impurities contributing to this signal. The expected integration should be ~ 174 H but in the ^{1}H-NMR this comes out to be 371 H. A similar purity as done with the NHS-PEG can be used here. The mol % purity based on the ethylene proton signal and the methoxy proton signal was 47 % and 51 %, respectively. The average of these two approximations gives a mol % purity of 49 %. Additionally, the singlet observed at 2.71 ppm was unable to be assigned and likely corresponds to the same impurity present in the starting material. These same impurities were observed in the ^{1}H-NMR of the other PEG-lipids.

The mol % purities for the remaining 1st generation PEG-lipids were found to be 84 % (**PEG-G$_1$-dC16**), 54 % (**PEG-G$_1$-C18**), and 69 % (**PEG-G$_1$-C16**).

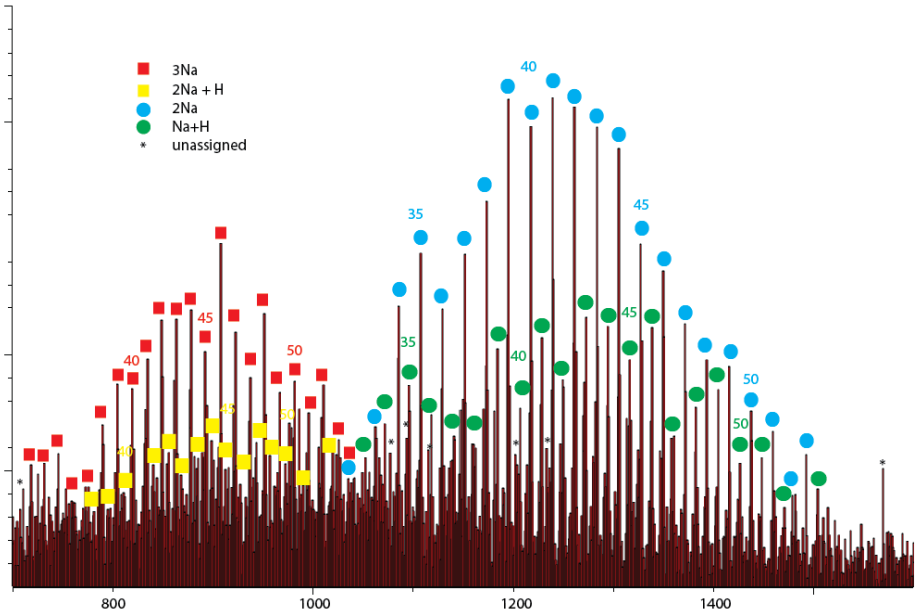

Figure 2.6: Mass spectrum generated from ESI-MS of **PEG-G$_1$-C14**. Sample was treated with 0.1% TFA and 0.1% NaCl. The compound shows 3Na, 2Na+H, 2Na, and Na+H ion series where 78 of the 85 ion clusters are assigned.

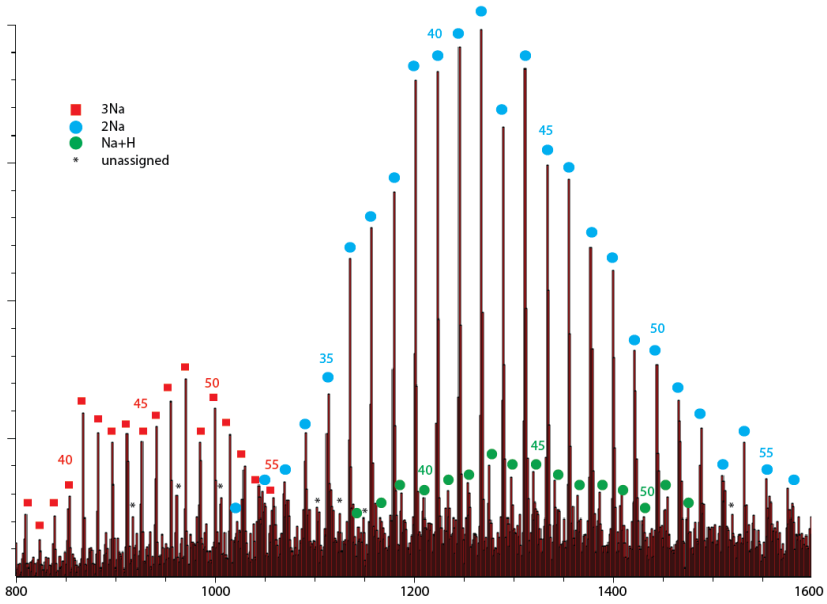

Figure 2.7: Mass spectrum generated from ESI-MS of **PEG-G$_1$-C16**. Sample was treated with 0.1% TFA and 0.1% NaCl. The compound shows 3Na, 2Na, and Na+H ion series where 60 of the 67 ion clusters are assigned.

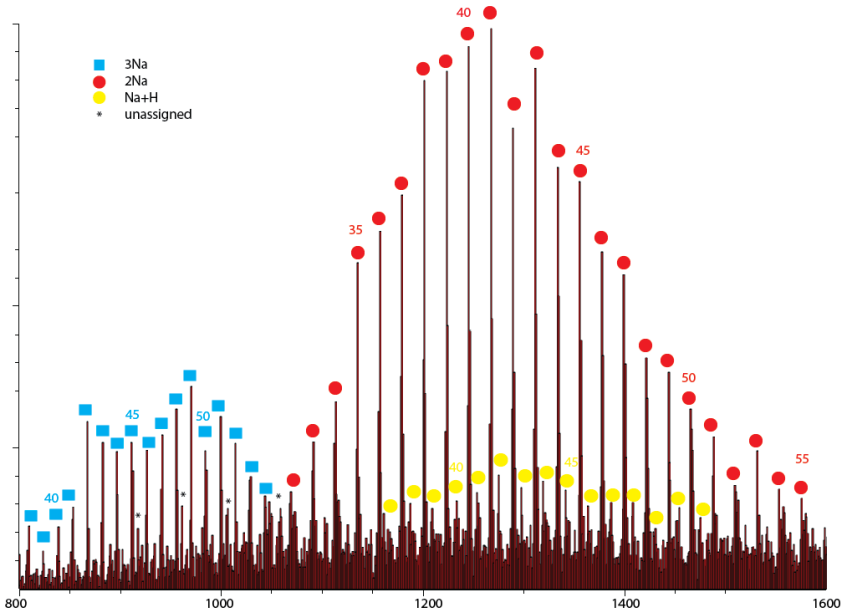

Figure 2.8: Mass spectrum generated from ESI-MS of **PEG-G$_1$-dC16**. Sample was treated with 0.1% TFA and 0.1% NaCl. The compound shows 3Na, 2Na, and Na+H ion series where 56 of the 60 ion clusters are assigned.

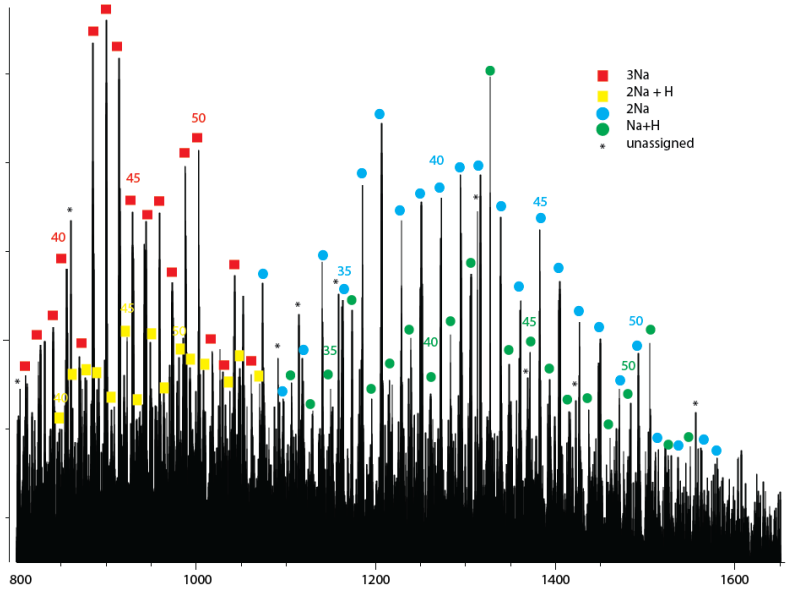

Figure 2.9: Mass spectrum generated from ESI-MS of **PEG-G$_1$-C18**. Sample was treated with 0.1% TFA and 0.1% NaCl. The compound shows 3Na, 2Na+H, 2Na, and Na+H ion series where 79 of the 87 ion clusters are assigned.

Structural confirmation based solely on ^{1}H-NMR proved to be difficult because of the prominence of the signal due to the ethylene protons. Therefore, the integration data was relatively unreliable due the presence of polymeric impurities. PEG-lipids have a high sensitivity to ESI-MS. Figures 2.6-2.10 are the mass spectra for the first generation PEG-lipids. In each case, there exists a 2+ cluster and a 3+ cluster which are identifiable by their peak spacing of m/z =22 and m/z =14.7 respectively. Within the clusters are different series depending on which ion is picked up during ionization. The 3Na, 2Na+H, 2Na, and Na+H ion series were observed in the mass spectra of **PEG-G$_1$-C14** and **PEG-G$_1$-C18** (Figures 2.6 + 2.8) where 92% and 91% of the peaks were assigned respectively. The mass spectra of the **PEG-G$_1$-C16** and **PEG-G$_1$-dC16** (Figures 2.7 + 2.9) showed the 3Na, 2Na, and Na+H ion series in which 90% and 93% of the peaks were assigned respectively. A higher percentage of peaks were assigned in the PEG-lipids than in NHS-PEG. As done with the starting material, the summed intensities were plotted versus n for each PEG-lipid and then fitted to a Gaussian to find n. The centers were found to be at n= 43, 44, 43, and 44 for **PEG-G$_1$-C14**, **PEG=G$_1$-C16**, **PEG-G$_1$-dC16**, and **PEG-G$_1$-C18**, respectively. By averaging

these values, an n value of 43.5 was used for molecular weight determinations. It is unlikely the lower than expected n value can be explained by ESI-MS preferentially ionizing shorter chained polymers. This would require that average distance between positive charges to be closer on the shorter chained polymers – producing some unfavorable electrostatic repulsion.

There were consistently peaks in the PEG-lipids that were unassignable suggesting that there were impurities in the starting material. The mass spectrum of the NHS-PEG, Figure 2.2, shows unassigned sequences. This concurs with what was observed in the ^{1}H NMRs of the PEG-lipids (Appendix 2) and the NHS-PEG starting material. In all cases, the signal for the ethylene protons was significantly greater than expected suggesting that there was an inseparable polymeric impurity present in the starting material contributing to this signal. Though the signal at 2.71 ppm could be N-hydroxysuccinimide, it is also possible that this peak is due to this same impurity. No remaining PEG-NHS starting material was observed in either the ^{1}H NMR or ESI-MS of the lipid products

2.3: Synthesis of 2nd Generation PEG-Lipids

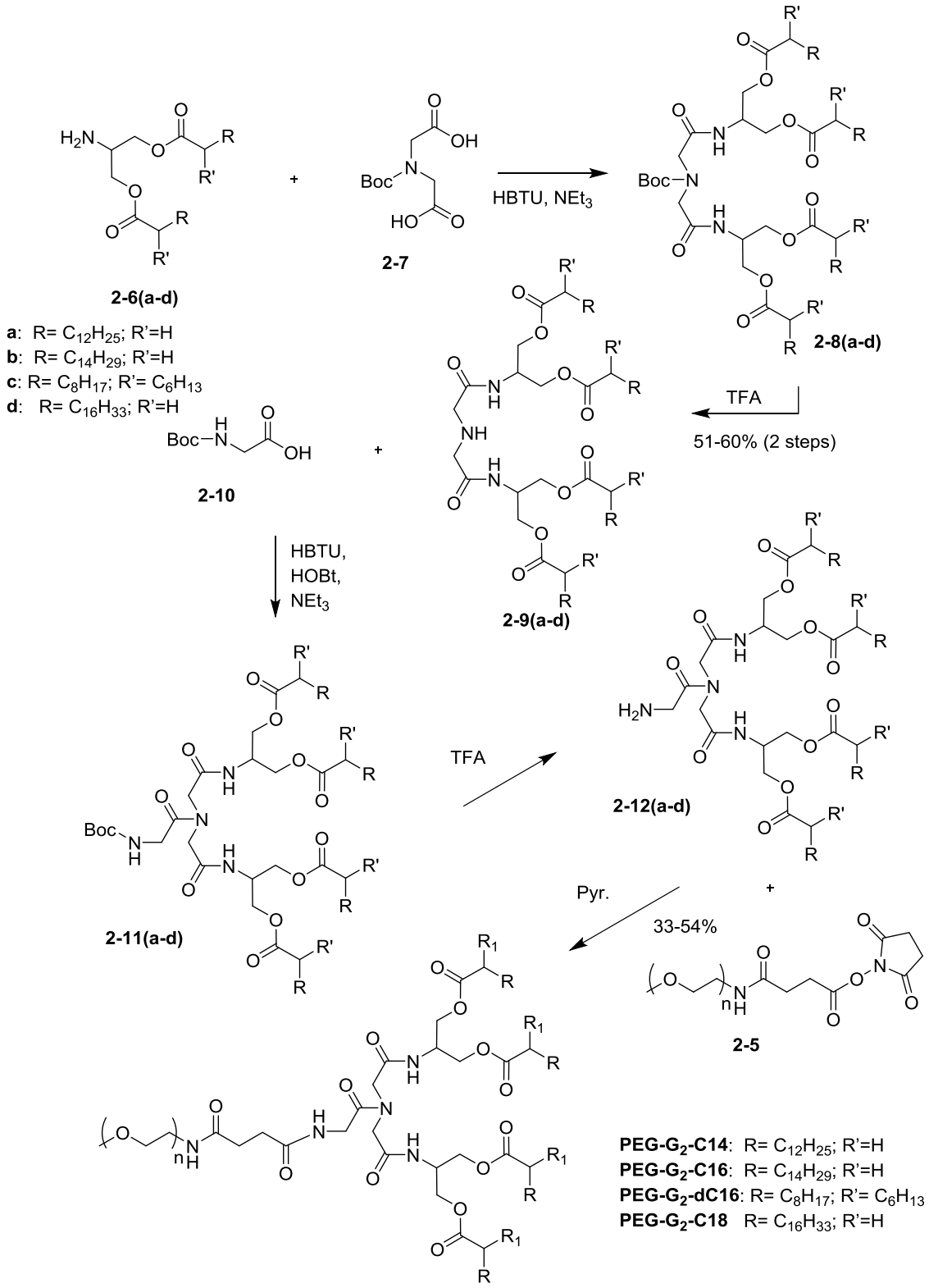

Scheme 2.3.1: Synthesis of the 2nd generation PEG-lipids. Synthetic details in Appendix 1, NMR in Appendix 3.

The second generation lipids are built from the first generation lipids added to an iminodiacetic acid core. Common amide coupling conditions were effective despite the congested iminodiacid backbone. Conversion of the diacid to the diamide was monitored by the downfield shift of the methine proton (1H) in the serinol backbone from 3.28 ppm to 4.47 ppm. Complete conversion was established by a relative integration of 1H (3.28 ppm) to 10H (4.47 ppm) for these methine signals. Following boc deprotection with TFA, pure **2-9(a-d)** were afforded in yields varying from 51-60%.

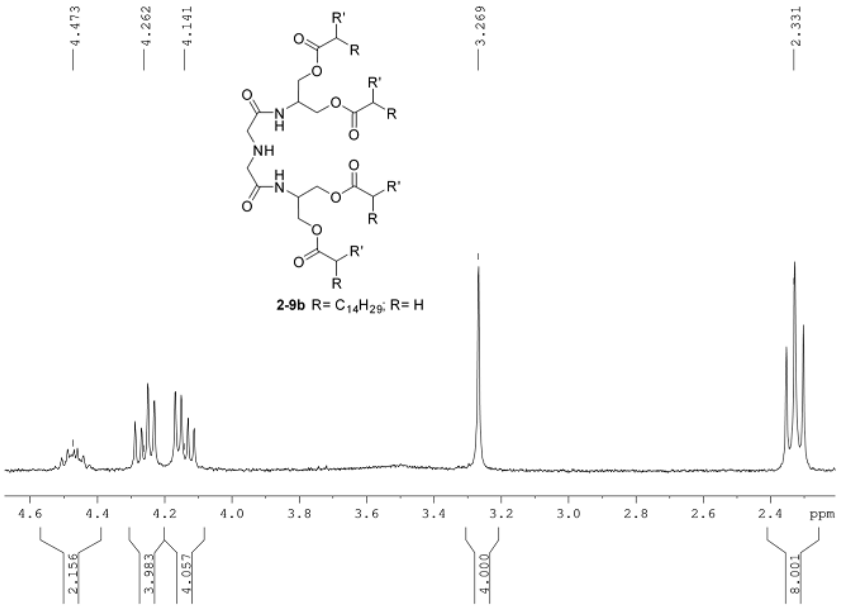

Figure 2.10: ^{1}H-NMR ($CDCl_3$, 300 MHz) of **2-9b**.

^{1}H-NMR supported the isolated products. Due to the lack of free bond rotation at the amides, the methylene protons on the serinol backbone experience a more different chemical environment than previously observed in the 1st generation lipid anchors. This results in the greater difference of chemical shift of these methylene protons as seen at 4.26 ppm (2H) and 4.14 ppm (2H). The methylene protons on the iminodiamide backbone appear as a singlet at 3.27 ppm (4H). Disappearance of the singlet at 1.78 ppm (9H) confirmed a successful boc deprotection. ESI-MS showed the singly charged species (**2-9(a-d)** + H)$^{+}$ with required mass/charge for the assigned structures in all cases.

The initial intent was to use **2-9(a-d)** as the 2nd generation lipid anchor; however, the secondary amine proved to be unreactive towards the NHS-PEG. Heating up to 120 °C in DIPEA, resulted in the decomposition of **2-9(a-d)** as well as an intramolecular cyclization of the NHS-PEG to produce a PEG terminated in an imide as detected in the ESI-MS spectrum of the crude products. Though the electron density on the secondary amine is very similar to that of the primary amine in **2-6(a-d)**, the increased steric bulk on the secondary amine makes the activated carbonyl in the NHS-PEG inaccessible. With the observed lack of reactivity of the secondary amine with NHS-PEG, it was decided to install a primary amine to link to the lipid anchor to the PEG.

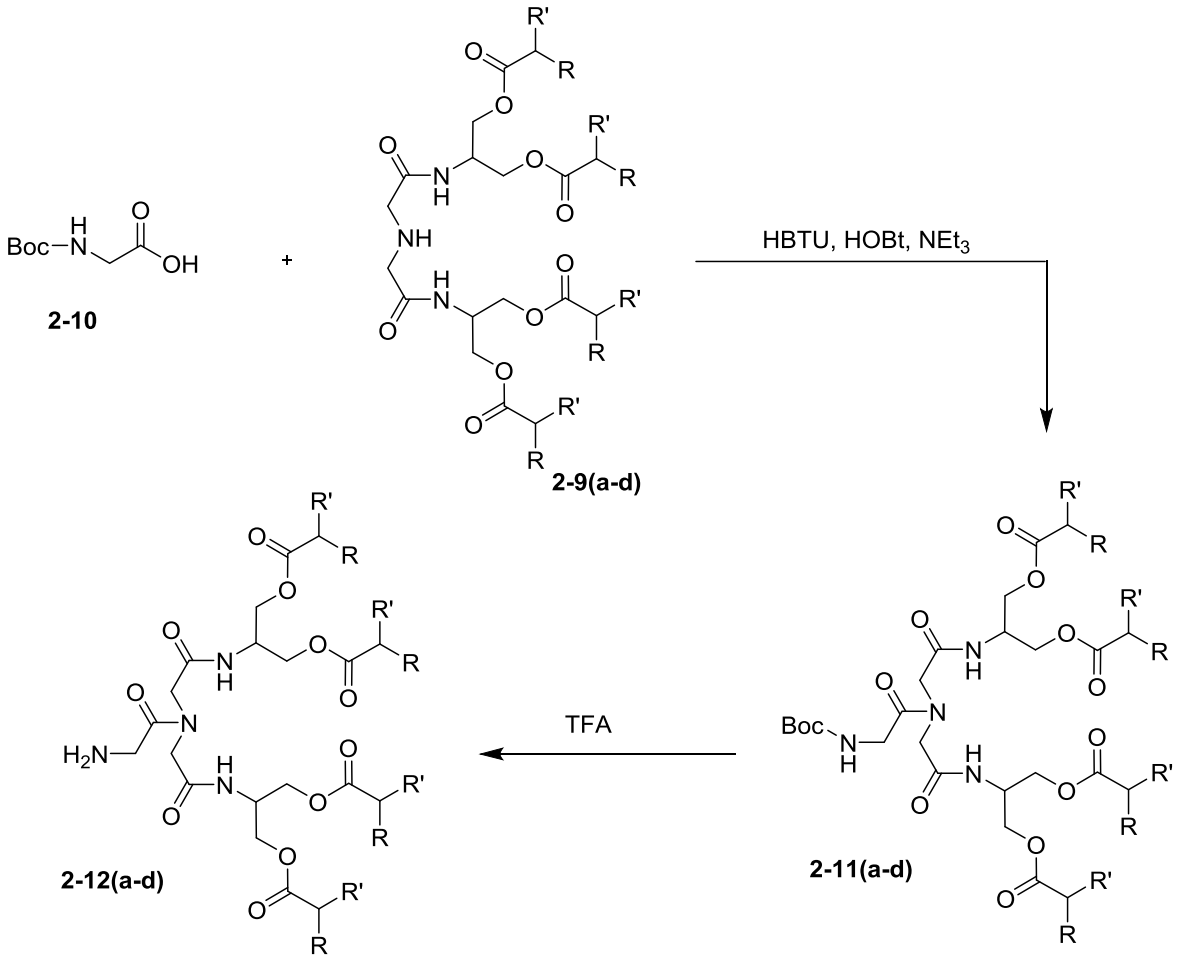

Scheme 2.3.2: Amide coupling of boc-N-glycine with **2-9(a-d)**.

Attempts to couple **2-9(a-d)** to boc-N-glycine with just HBTU were unsuccessful. The reaction proceeded well following the addition of HOBt as indicated in the ^{1}H NMR by the disappearance of the 3.27 ppm singlet for the methylene proton (4H) signal on the iminodiamide backbone. These methylene protons now appear downfield as two separate singlets at 3.91 ppm and 4.00 ppm rather a single signal (3.27 ppm) due to the lack of free rotation at the tertiary amide. The disappearance of the signal at 1.43 ppm indicated a successful boc deprotection. ESI-MS for **2-12b** and **2-12c** gave m/z =1290.00 and m/z=1289.93 respectively. Though from the ^{1}H-NMR it was clear that impurities such as unreacted **2-9(a-d)** were present in the isolated products, the crude products were carried on without purification. As detailed previously, having **2-9(a-d)** present while reacting **2-12(a-d)** with NHS-PEG will not interfere as it was unreactive towards the NHS-PEG. Beyond ^{1}H-NMR, the other analogues were not further characterized with ESI-MS as it was assumed the chemistry should precede the same.

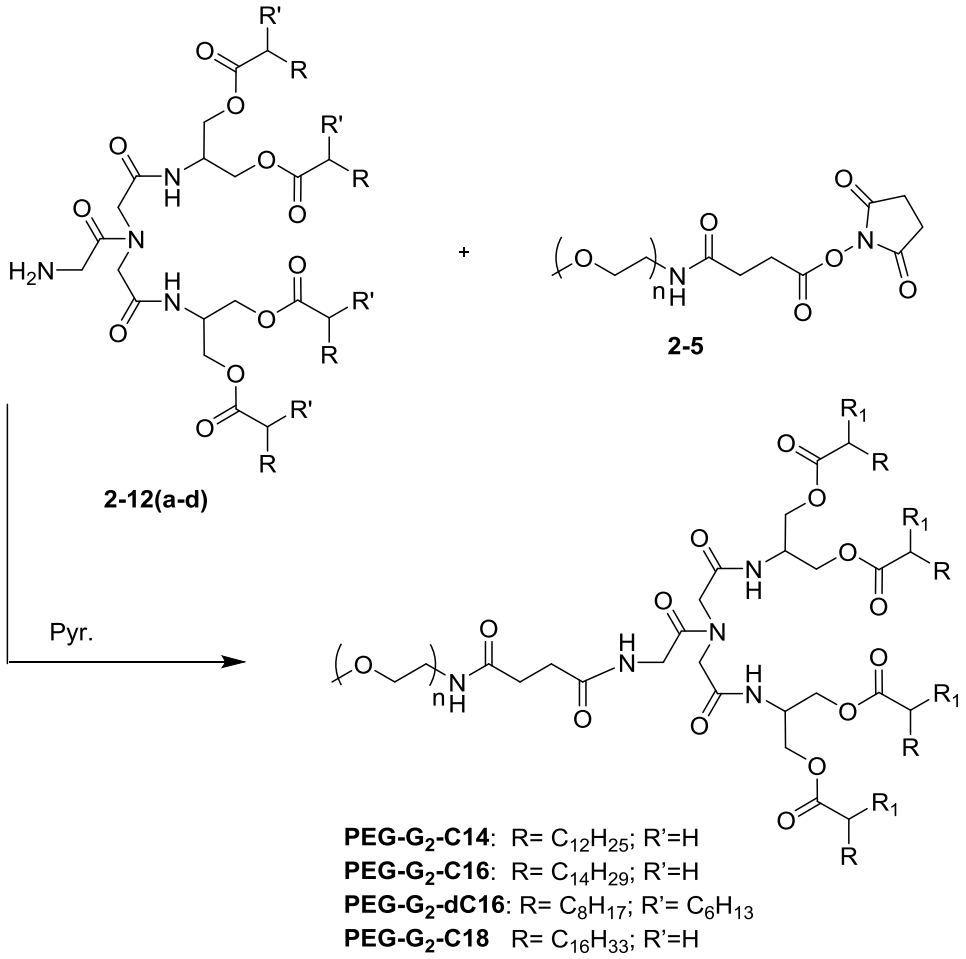

Scheme 2.3.3: Formation of the 2nd generation PEG-lipids

The final step of the 2nd generation PEG-lipid synthesis proceeded under the same conditions used in the linking the 1st generation PEG-lipid to the PEG giving yields from 33-54% after chromatography. ^{1}H-NMR supported that the desired products were isolated. The multiplet at 4.39 ppm (2H) corresponds to the methine protons on the serinol backbone while the cluster of peaks between 3.89 - 4.26 ppm integrated to the expected 14Hs. Chemical inequivalence of the protons on the two lipid anchors was created by the tertiary amide linkage in the iminodiamide backbone – supported by the overlapping triplets at 2.29 ppm (4H) and 2.31 ppm (4H). As was found in the analysis of the first generation PEG-lipids, the integration of the ethylene protons was significantly different than expected and the singlet at 2.71 ppm was also present in the second generation PEG-lipids. The mol % purities were determined to be 80 % (**PEG-G$_2$-C14**), 70 %

(P**EG-G$_2$-C16**), 72 % (**PEG-G$_2$-dC16**), and 59 % (**PEG-G$_2$-C18**). ESI-MS once again was used to confirm the identity of the compounds (Figures 2.11-2.14).

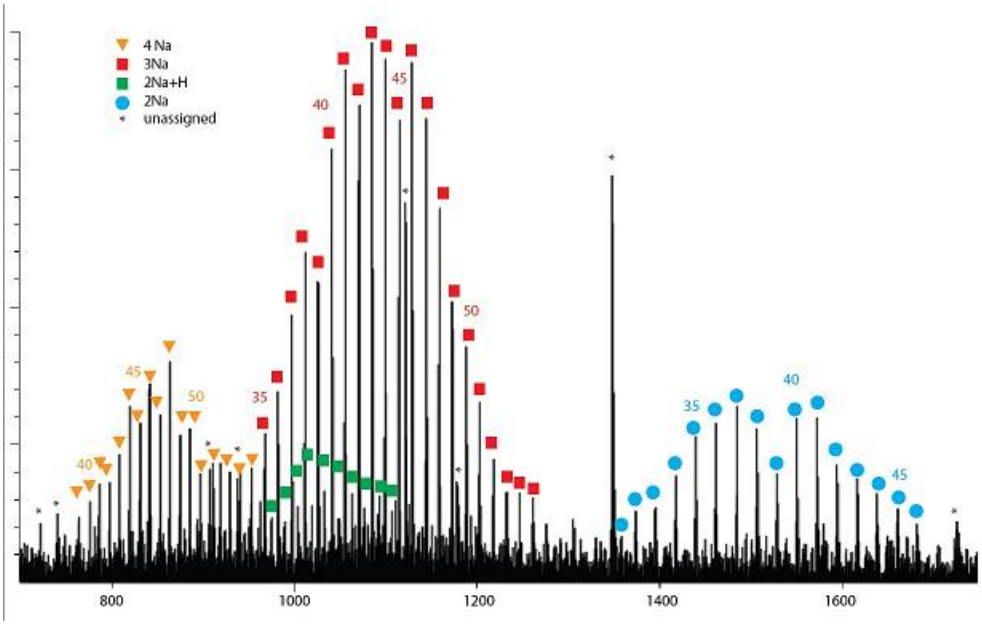

Figure 2.11: Mass spectrum generated from ESI-MS of **PEG-G$_2$-C14**. Sample was treated with 0.1% TFA and 0.1% NaCl. The compound shows 4Na, 3Na, 2Na+H, and 2Na ion series where 64 of the 71 ion clusters are assigned.

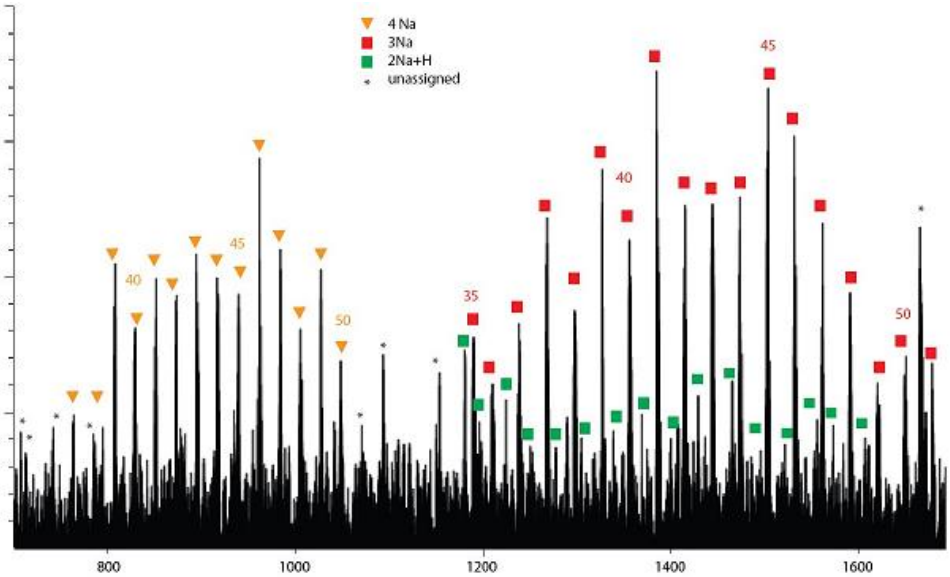

Figure 2.12: Mass spectrum generated from ESI-MS of **PEG-G$_2$-C16**. Sample was treated with 0.1% TFA and 0.1% NaCl. The compound shows 4Na, 3Na, and 2Na+H ion series where 48 of the 56 ion clusters are assigned.

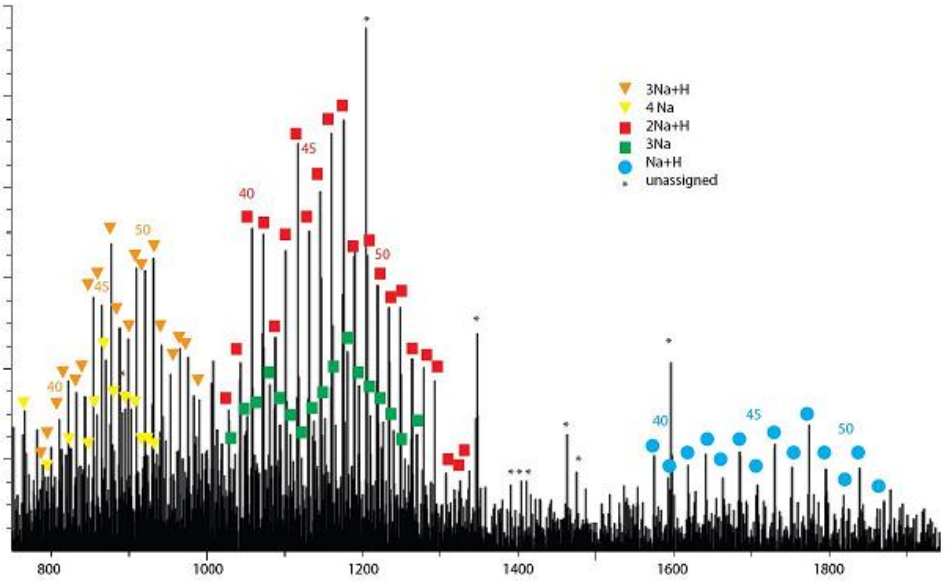

Figure 2.13: Mass spectrum generated from ESI-MS OF **PEG-G$_2$-dC16**. Sample was treated with 0.1% TFA and 0.1% NaCl. The compound shows 3Na+H, 4Na, 2Na+H, 3Na, and Na+H ion series where 83 of the 92 ion clusters are assigned.

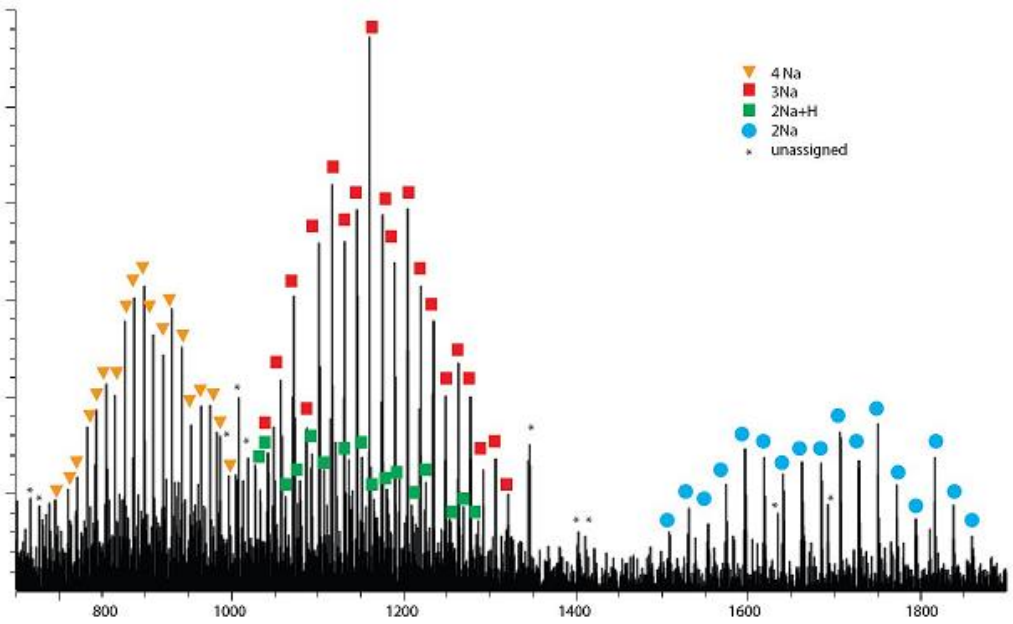

Figure 2.14: Mass spectrum generated from ESI-MS of **PEG-G$_2$-C18**. Sample was treated with 0.1% TFA and 0.1% NaCl. The compound shows 4Na, 3Na, 2Na+H, and 2Na ion series where 73 of the 83 ion clusters ware assigned.

Figures 2.11-2.14 are the mass spectra of the second generation PEG-lipids where the 2+ cluster, 3+ cluster, and 4+ cluster are identifiable by their peak spacing of m/z = 22.0, m/z = 14.7, and m/z = 11.0, respectively. The 4Na, 3Na, 2Na+H, and 2Na ion series are observed in the mass spectrums of **PEG-G_2-C14** and **PEG-G_2-C18** where 90% and 88% of peaks are assigned. From the mass spectrum of **PEG-G_2-C16**, ion series of 4Na, 3Na, and 2Na+H accounted for 86% of all peaks. A Gaussian fit of the summed intensities versus n gave plots centered at n = 43 for both of these PEG-lipids. Five ion series appear in the mass spectrum of **PEG-G_2-dC16**; 3Na+H, 4Na, 2Na+H, 3Na, and Na+H ion series where 90% of the peaks are accounted for. An n value of 47 was determined suggesting that some fractionation of the polymer mixture occurred during column chromatography.

2.4: Synthesis of LDC Monomers

In total seven LDC monomers were synthesized to evaluate the branching chains of the lipid anchors and their ability to self-assemble into LDC nanoparticles – their synthesis is detailed here. Full experimental details can be found in Appendix 1, and NMR spectra can be found in Appendix 2. Scheme 2.4 provides a general overview for the synthesis of the LDC.

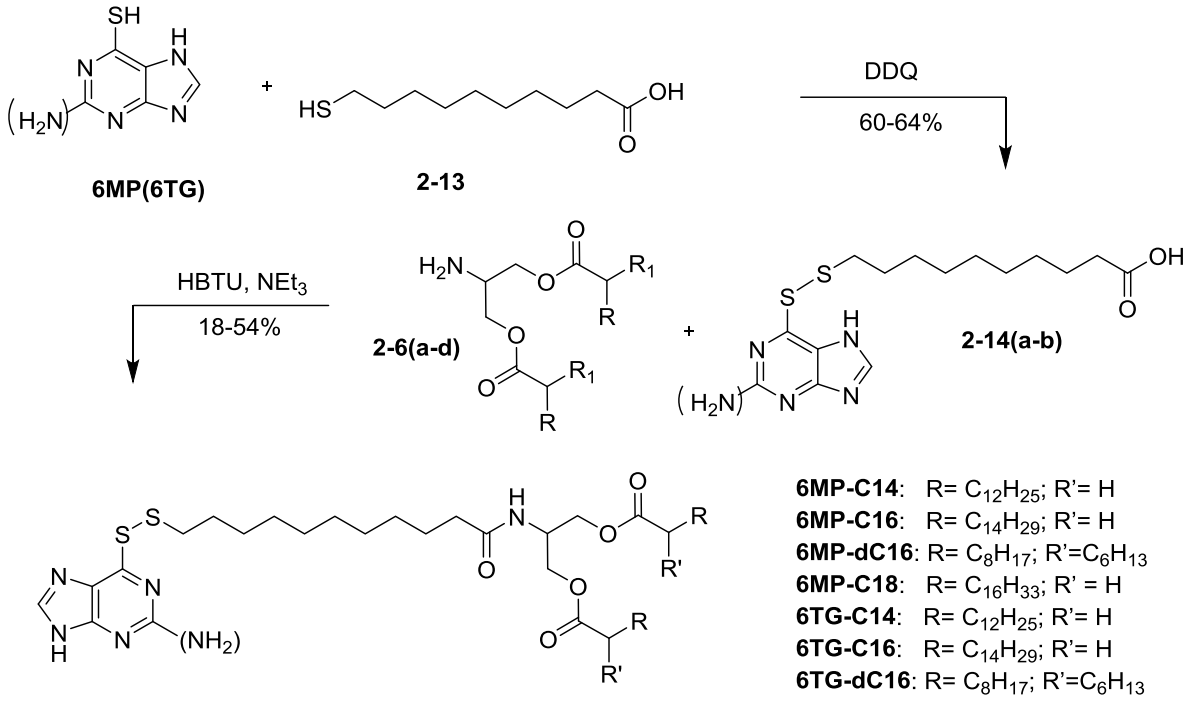

Scheme 2.4.1: Synthesis of LDCs for 6-thioguanine and 6-mercaptopurine. Synthetic details in Appendix 1, NMR in Appendix 3.

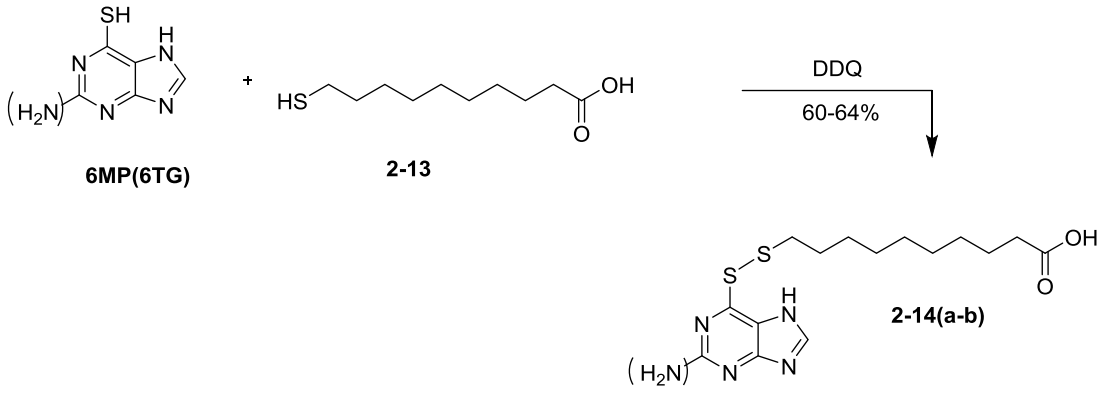

Scheme 2.4.2: Asymmetric disulfide formation of thiopurine drug with 11-mercaptoundecanioc acid

Oxidation with DDQ provides the asymmetric disulfide in surprisingly good selectivity. **2-14(a-b)** was precipitated by adding water to the reaction mixture – the water also reacted with remaining DDQ formally producing HCN athough the pH of the medium was unknown. Workup was delayed (rt) to allow outgassing of

any HCN present. Given that DMSO (as well as the solutes) is readily absorbed by the skin, caution was taken while handling the mixture.

Interestingly, only the asymmetric disulfide was observed in both ^{1}H-NMR and ESI-MS aliquots. This selectively has been well demonstrated for aromatic thiols forming disulfides with alkyl thiols.[15] It is thought that the homo-oxidized alkyl disulfide is formed most readily; however, in the presence of aromatic thiol the alkyl disulfide is subject to a disulfide exchange reaction resulting in the formation of the asymmetric disulfide. Only nucleophilic attack by the aromatic thiol is possible since it is considerably more acidic than the alkyl thiol. At near neutral conditions, only the aromatic thiolate would be present in solution.[18]

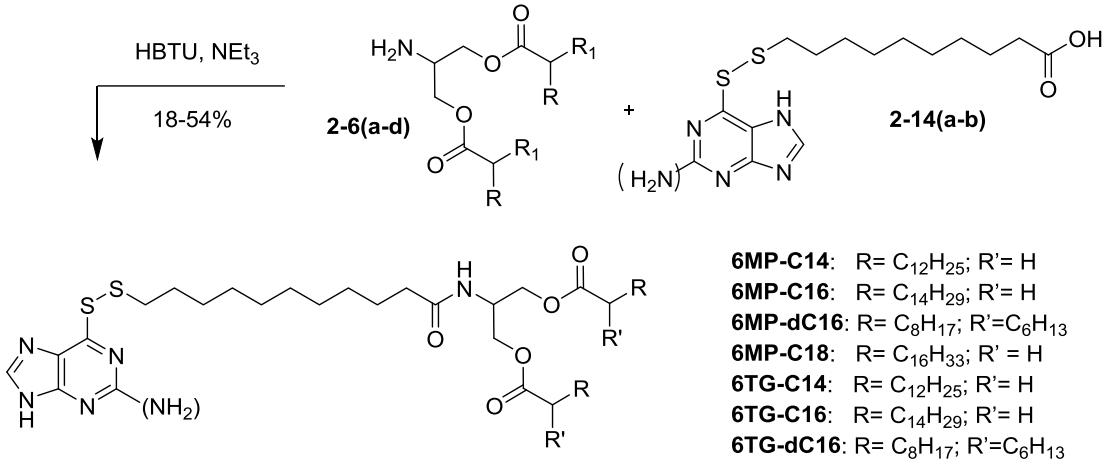

Scheme 2.4.3: Amide coupling of synthetic lipid to **2-14(a-b)**

Amide coupling with HBTU proceeded in poor to moderate yields (18-54%) for the 7 LDC analogues. Though unlikely, the only concern here was the possible amide formation between the aromatic amine (of 6TG) and the lipid anchor. ^{1}H-NMR revealed only one methine proton signal at 4.48 ppm (1H) as well as ESI-MS gave the corresponding expected mass to charge ratios. **6TG-C18** was attempted to be synthesized; however, initial efforts of purification were unsuccessful – it was decided that until the effectiveness of these compounds could be established no further time should be spent on **6TG-C18**.

Chapter 3: Lipid Nanoparticle Formulations and Stability

3.1 Solid Lipid Nanoparticle Formulations

PEG-lipids mainly function to stabilize LNPs under both storage and physiological conditions. LNPs that are unstable tend to aggregate with each other and, under physiological conditions, with serum proteins. In the case of extreme aggregation, precipitation can be observed. PEG-lipids serve to minimize this aggregation and thus allow for the particles to maintain their optimized physiochemical properties. In animal models, SLNPs formulated using commercially available PEG-lipids were rapidly cleared from the circulatory system.[8] It is generally assumed the ability of PEG-lipids to stabilize SLNPs is dependent upon the lipid anchors, and that insufficiently anchored PEG leads to aggregation.[6, 8]

Using these novel synthetic PEG-lipids, it may be possible to show that these compounds are better than their commercial counterparts with respect to particle stability. Furthermore, varying backbone structure and chain length may lead to a correlation between these features and particle stability. To evaluate the stability effects of these PEG-lipids, a suitably stable SLNP composition was first determined by investigating different lipids and their respective ratios. Ideally, these particles would have the following characteristics: be smaller than 100 nm in diameter, be monodisperse, be able to carry a therapeutically relevant drug load, and be stable under storage conditions. Having a stable composition allowed for the variation of the PEG-lipid identity to observe any structure-related stability effects, under a variety of conditions, of different PEG-lipids.

There are five components that constitute a SLNP – all of which can affect a particle's physiochemical properties. It was well established in the literature that the composition needed to be close to 40:11.5:47.5:1 (cationic lipid: DSPC: cholesterol: PEG-lipid) mole composition with a nucleic acid loading of near 6 wt% to obtain stable SLNPs with pharmaceutical potential.[16] Nucleic acid loadings

were calculated based on wt%, that is, the mass of the nucleic acid was divided by the total mass of the entire mixture. The ratio of the positive charge due to the cationic lipid to the negative charge of the nucleic acid is known as the charge ratio – high charge ratios correspond to low nucleic acid loadings. Given this, formulations were carried out to explore the effects of using different nucleic acid loadings and different cationic lipids .

5’-CGC GCG TAT ATA CGC GCG-3’

Figure 3.1: A single strand of the dsDNA used as the nucleic acid load in formulations.

siRNA is unstable at room temperature and requires especially careful handling. All equipment and bench tops must be washed with RNA nuclease denaturing agent and RNA nuclease free water must be used for making buffer solutions. For these reasons, a small oligomer dsDNA was used instead as dsDNA (Figure 3.1) is greatly more stable than siRNA and does not have extensive handling requirements. Given that both siRNA and dsDNA are short oligomers with a helical double stranded structure, it is reasonable to assume that the formulation data gathered from using dsDNA should also be applicable for siRNA.

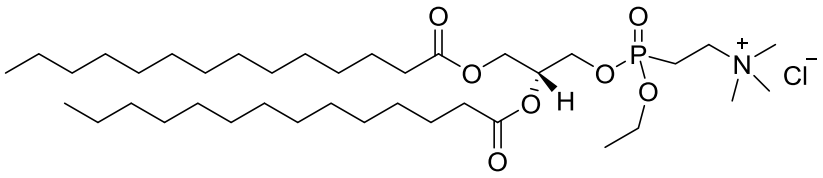

3-1

Figure 3.2: EPC (14:0) (Compound **3-1**)

The major issue here is that commercially available cationic lipids and ionisable lipids have been demonstrated to be rather useless in forming effective SLNPs.[17] Keeping these limitations in mind, initial attempts used EPC(14:0) (Figure 3.2) as the cationic lipids. From a mole composition ratio of 50:10:38.5:1.5 SLNPs were synthesized by microfluidic mixing, and dynamic light scattering was used to measure the particle diameter (see Appendix 1). In

general, formulations containing EPC yielded particles that were monodisperse with sizes ranging from 75 nm to 310 nm. A monodisperse formulation falls under a polydispersity index (PDI) value of less than 0.10. PDI and refers to the breadth of the size distribution of the particles. The smaller this value is, the narrower the distribution and the smaller variation there is between individual particles. Unfortunately, compositions using EPC (14:0) were unable to lead to a general composition for SLNPs as these particles were generally too large to be of therapeutic interest.

PEG-lipid	Particle Diameter (nm)	PDI
PEG-G_1-C14	260.8	0.098
PEG-G_1-C16	306.9	0.102
PEG-G_1-dC16	74.3	0.246
PEG-G_1-C18	268.7	0.094

Table 3.1: Physical characterization of formulations done with a DNA loading of 2.9%, a charge ratio of 9, and a composition of 50:10:38.5:1.5 (EPC(14:0): DSPC: Cholesterol: PEG-lipid)

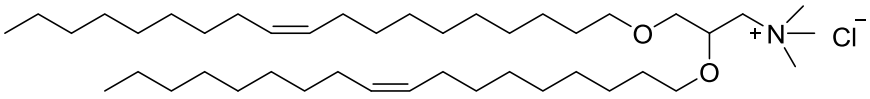

1-1

Figure 3.3: DOTMA (Compound **1-1**)

Formulations using DOTMA (Figure 3.3) as the cationic lipid were more successful in that particles were smaller and were able to hold a higher DNA load. DSPE-PEG (Figure 3.4), a negatively charged PEG-lipid, and DSG-PEG, a neutral PEG-lipid, (Figure 3.5) were used as the two commercial comparisons. See Appendix 2 for details on formulations.

PEG-Lipids	Particle Diameter (nm)	PDI
PEG-G$_1$-C14	104.5	0.288
PEG-G$_1$-C16	76.9	0.259
PEG-G$_1$-dC16	156.1	0.248
PEG-G$_1$-C18	146.1	0.335
PEG-G$_2$-C14	181.4	0.280
PEG-G$_2$-C16	211.1	0.373
PEG-G$_2$-dC16	119.5	0.351
PEG-G$_2$-C18	165.6	0.394
DSG-PEG	80.5	0.268
DSPE-PEG	89.0	0.297

Table 3.2: Physical characterization of formulations done with a DNA loading of 5.1%, a charge ratio of 5, and a composition of 50:10:38.5:1.5 (DOTMA: DSPC: Cholesterol: PEG-lipid)

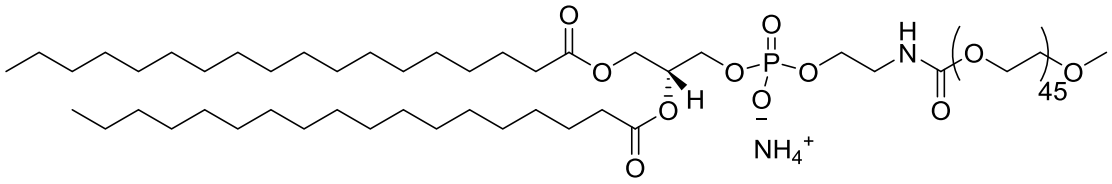

1-4

Figure 3.4: DSPE-PEG2000 (Compound **1-4**)

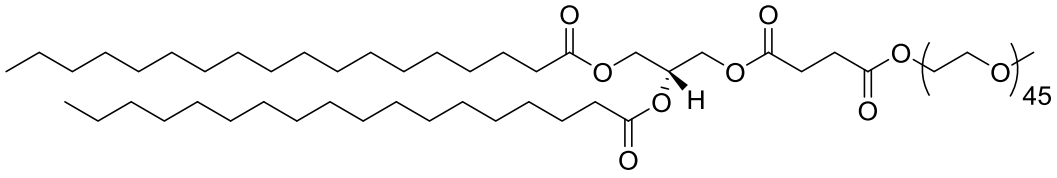

3-2

Figure 3.5: DSG-PEG2000 (Compound **3-2**)

The 1st generation PEG-lipids gave particles that had reasonable diameters and therefore were further evaluated for stability. It is likely that this composition was not well optimized for the 2nd generation PEG-lipids and given the significant structural differences between the 2nd generation PEG-lipids and the other PEG-lipids this was expected. Attempts to optimize the 2nd generation

PEG-lipid formulations by varying the mole ratio of PEG-lipid from 0.75% to 3.0% failed to improve the physiochemical properties of the particles.

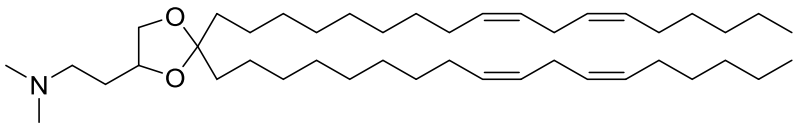

3-3

Figure 3.6: DLin-KC2-DMA (Compound **3-3**)

Eventually an optimized commercial lipid mix (provided by Precision NanoSystems) was used to formulate the dsDNA into SLNPs with the 2nd generation PEG-lipids. Though Precision NanoSystems did not disclose the composition of this commercial lipid mix, it is quite likely it contains the novel ionisable lipid **3-3** (Figure 3.6). **3-3** is commonly used and is among the best ionisable lipids to use for SLNP formulations. [16, 26]

PEG-Lipid	Particle Diameter (nm)	PDI
DMG-PEG	65.2	0.249
PEG-G$_2$-dC16	73.6	0.112
PEG-G$_2$-C16	86.1	0.262

Table 3.3: The physical characterizations of formulations using the commercial lipid mix are shown above. The DNA loading was 5.1% with a corresponding charge ratio of 5. The composition of the commercial mix was 50: 10: 38: 1.5 (Ionisable lipid: DSPC: Cholesterol: PEG-lipid) where the final 0.5 mol% was a fluorescent lipid-marker.

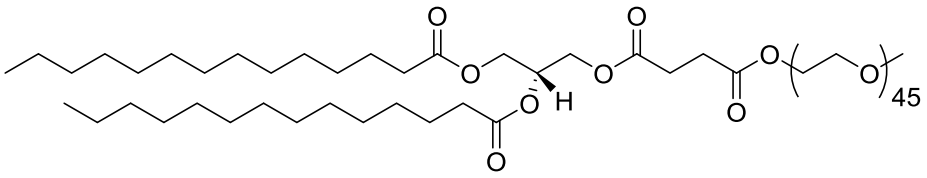

3-4

Figure 3.7: DMG-PEG (Compound **3-4**)

Using this optimized lipid mix and the 2nd generation PEG-lipids, yielded SLNPs with desirable physiochemical properties (Table 3.3). DMG-PEG (Figure

3.7) was provided by PNI and used as the commercial comparison in these experiments. DMG-PEG is structurally very similar to DSG-PEG with only difference being found in the length of their respective aliphatic chains. **PEG-G_2-dC16** gave more promising SLNPs than the commercial DMG-PEG.

Cryo-TEM images (Figures 3.8 -3.9) were prepared by applying the sample, doped with 5 nm gold particles for calibration, to an EM grid. Filter paper was then used to blot the sample and to dehydrate it. This was then frozen in liquid ethane. It was very important to ensure that the sample was consistently kept cool by liquid nitrogen at all times to prevent the formation of ice crystals. This made it difficult to successfully transfer the grid to the grid holder – great care was taken to keep the sample in the liquid nitrogen while doing the transfer. If not handled correctly, the grid can easily be damaged rendering the sample useless. Following imagining with the TEM microscope, it was confirmed spherical particles were formed and the dispersions were moderately polydisperse which concurs with DLS experiments.

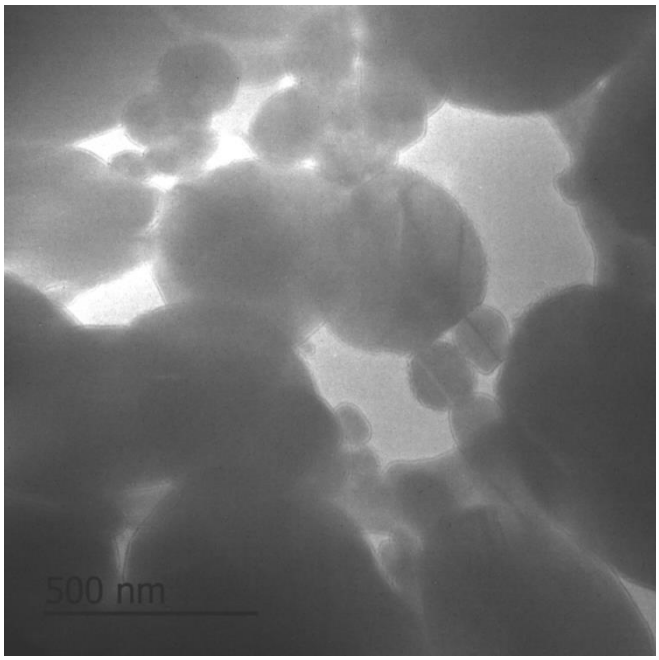

Figure 3.8: Cryo-TEM image of **PEG-G_1-C16** sample showing particles with a generally spherical morphology.

Preparation steps may have damaged the sample – specifically dehydration of the sample likely caused this “flaking” effect observed on the particle’s surface in Figure 3.9. It is possible there was water trapped in the core of the particle that was removed during dehydration leading to this “flaking” effect. Given that the interior of SLNPs are postulated to be solid, the fact that water may be being removed from inside of the particle goes against this idea. It was not possible to conclude that these particles contained a solid interior as some of the TEM images revealed what looked like a lipid bilayer. In Figure 3.9, the white bars indicate 4-10 nm and are centered in regions that could be a lipid bilayer. If confirmed in future imaging, the lipid bilayer would signify the particles are more similar to liposomes rather than SLNPs. However, it is also possible that these regions are a depth-of-field artefact.

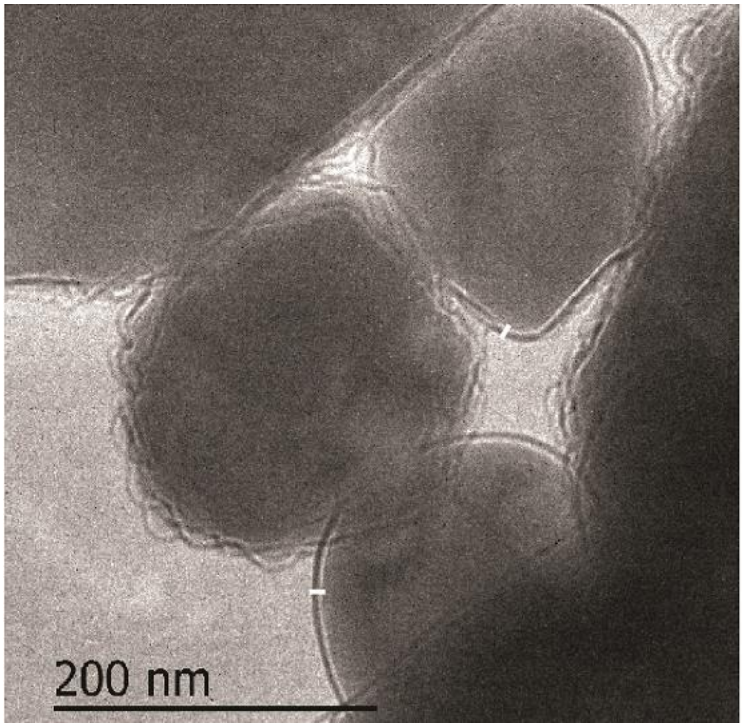

Figure 3.9: Cryo-TEM image of **PEG-G$_1$-C16** sample

3.2 Stability Assay for SLNPs

The effectiveness of the 1st generation PEG-lipids to stabilize the SLNPs was evaluated through a stability assay under 6 different conditions and

compared to DSG-PEG and DSPE-PEG, two commercially available PEG-lipids. The experimental details are documented in Appendix 2.

Commonly, particle stability is evaluated by monitoring particle size and PDI over a time period in PBS buffer. An increase in particle size is indicative of aggregation meaning that when poorly anchored PEG comes off the particle surface the hydrophobic core is exposed to the aqueous medium. These hydrophobic surfaces will associate with each other resulting in an overall increase in particle size. In extreme cases where the PEG was so poorly anchored to the particle, precipitates can be observed in the formulation. In addition to changes in particle size, changes in PDI can indicate aggregation or redistribution within a population of particles. A significant increase in PDI is evidence of particle instability.

Currently, an assay that can assess particle stability under physiological conditions does not exist. Though incubation of formulations at 37 °C in PBS buffer does provide information on thermal stability, it does not take into account the effects associated with serum. Serum contains proteins that can bind and interact with the nanoparticles and, in some cases, cause aggregation. Such aggregation with other particles or with serum proteins will lead to increase in the apparent diameter of particles. The issue with running DLS experiments on media containing 10% serum was that the particles in the serum also scatter light; however, it was still possible to derive meaningful information from these experiments. The reading from the DLS experiments represents a weighted size average between the LNPs and the serum particles. If there was significant increase in the average diameter observed, it would suggest that there was substantial aggregation between serum proteins and the LNPs or between LNPs themselves. In extreme cases, it is possible to observe precipitation of these aggregates.

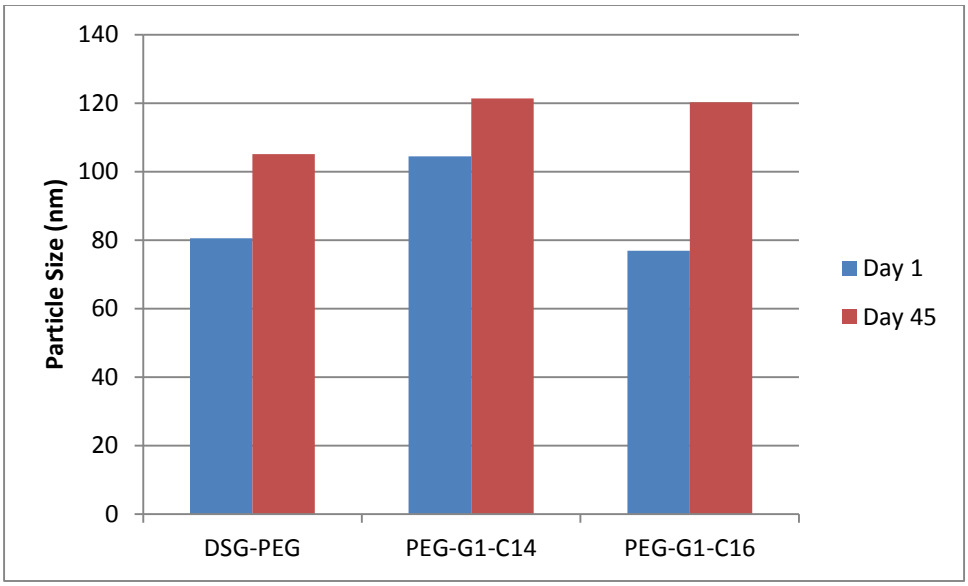

Figure 3.10a: SLNP apparent diameter at 4°C in PBS buffer for 44 days for formulations containing 1.5 mol% of different PEG-lipids. The composition for these SLNPs was 50:10: 38.5: 1.5 (DOTMA: DSPC: Cholesterol: PEG-lipid) with a DNA loading of 5.1 wt%.

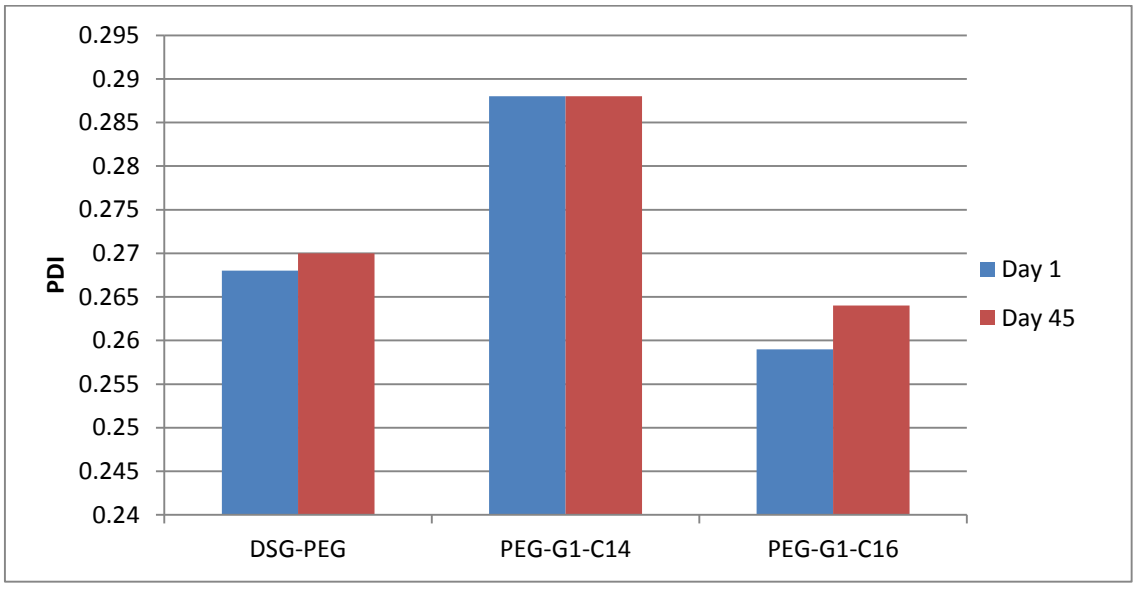

Figure 3.10b: SLNP PDI at 4°C in PBS buffer for 44 days for formulations containing 1.5 mol% of different PEG-lipids. The composition for these SLNPs was 50:10: 38.5: 1.5 (DOTMA: DSPC: Cholesterol: PEG-lipid) with a DNA loading of 5.1 wt%.

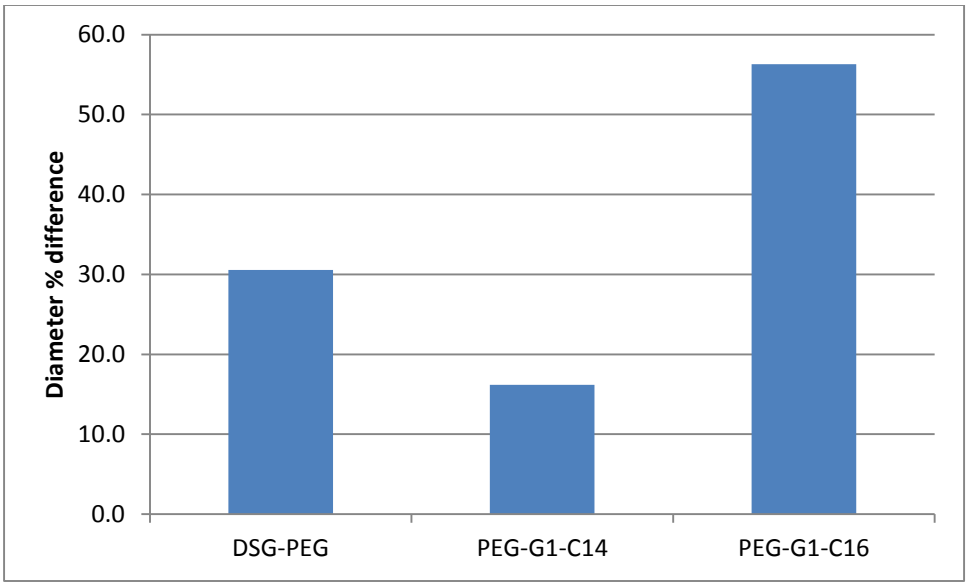

Figure 3.10c: SLNP diameter % difference at 4°C in PBS buffer for 44 days for formulations containing 1.5 mol% of different PEG-lipids. The composition for these SLNPs was 50:10: 38.5: 1.5 (DOTMA: DSPC: Cholesterol: PEG-lipid) with a DNA loading of 5.1 wt%.

Before proceeding with stability test it was first necessary to establish that the SLNPs using DOTMA as the cationic lipid were at least stable at 4°C in PBS buffer. This condition was where it was expected particles to be most stable and thus represented a starting point for whether the determined composition was adequate for further stability tests. In Figure 3.10a is the apparent particle diameter for different formulations monitored over a 44 day period. Clearly, over the course of 44 days the average apparent diameter for each of these formulations has slightly increased. This increase in the average apparent diameter is most evident in **PEG-G$_1$-C16**; moreover, the increase in the PDI observed in Figure 3.10b further signifies instability of the formulation. 16%, 56%, and 31% are the apparent diameter increases shown in Figure 3.10c for **PEG-G$_1$-C14**, **PEG-G$_1$-C16**, and **DSG-PEG**, respectively. In considering the change in the average apparent diameters, it was possible to rank these three formulations in order of highest to lowest stability; **PEG-G$_1$-C14** > DSG-PEG > **PEG-G$_1$-C16**.

Two room temperature storage conditions, as well as physiological stability, were Investigated. Formulations were stored at RT in two different

media; PBS buffer and PBS buffer with 10% serum. Sizes and PDI of the formulations were monitored over one week. To subject the particles to conditions that more resembled physiological conditions, formulations were incubated at 37 °C with and without 10% serum in PBS buffer. Particle sizes and PDIs were recorded over a time of 5 days.

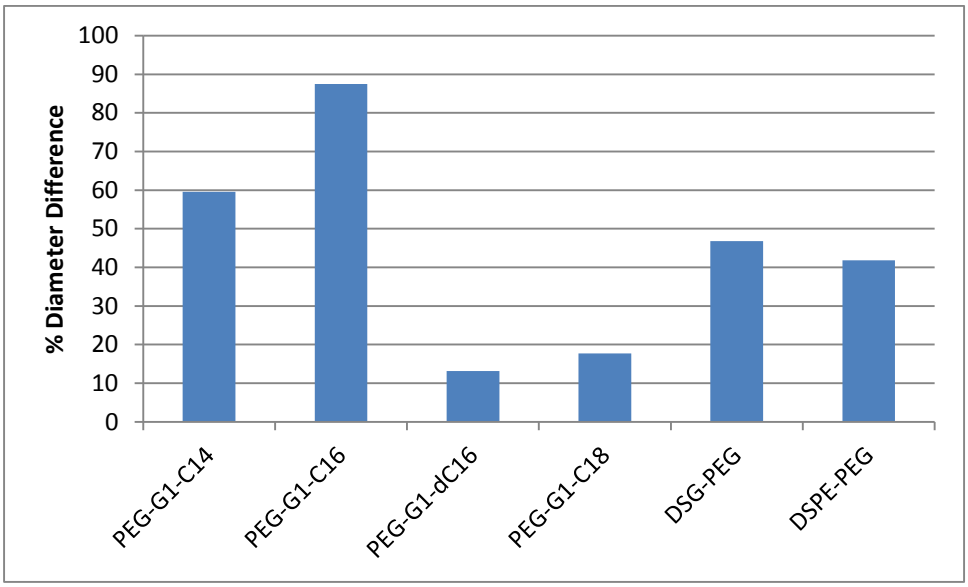

Figure 3.11: SLNP particles incubated at RT in PBS buffer for 7 days for formulations containing 1.5 mol% of different PEG-lipids. The composition for these SLNPs was 50: 10: 38.5: 1.5 (DOTMA: DSPC: Cholesterol: PEG-lipid) with a DNA loading of 5.1 wt%.

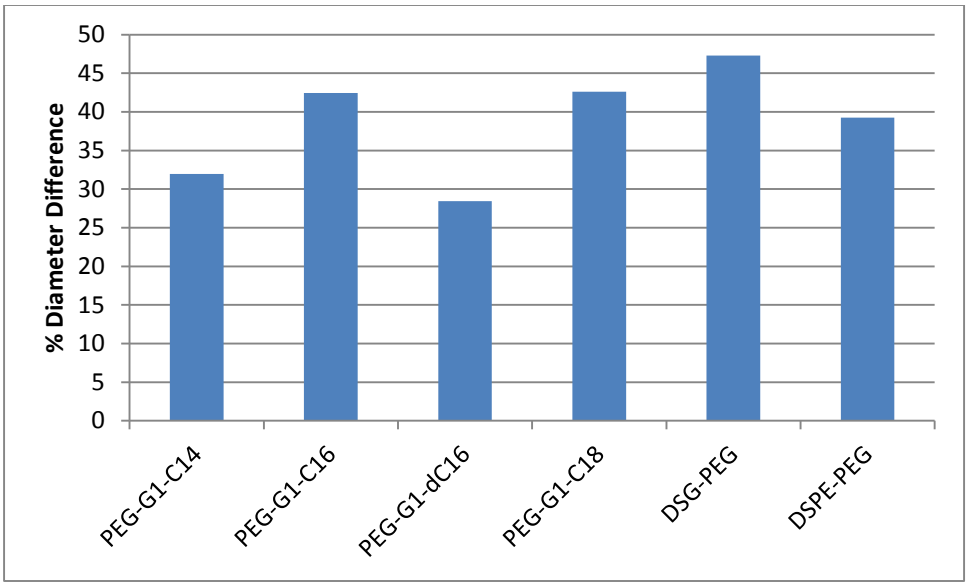

Figure 3.12: SLNPs incubated at RT in PBS buffer and 10% serum for 7 days for formulations containing 1.5 mol% of different PEG-lipids. The composition for these SLNPs was 50: 10: 38.5: 1.5 (DOTMA: DSPC: Cholesterol: PEG-lipid) with a DNA loading of 5.1 wt%.

Despite the best efforts to arrive at a stable SLNP composition, storage at room temperature revealed that even over just 7 days in PBS buffer the particles begin to show aggregation (Figure 3.11). However, it was still possible to deduce the relative stability of these formulations. Under this condition, both **PEG-G_1-dC16** and **PEG-G_1-C18** appeared to be the most stable formulations with respective diameter increases of 13% and 17%. It follows that the relative stability of these formulations from highest to lowest is: **PEG-G_1-dC16** ~ **PEG-G_1-C18** > commercial PEG-lipids > **PEG-G_1-C14** > **PEG-G_1-C16**. When this experiment was done in PBS buffer with 10% serum, the average apparent diameter from DLS experiments represents a weighted average between the serum particles and the SLNPs (Figure 3.12). Also as result of the serum particles, the PDI values were large and, due to this, provide little stability information. **PEG-G_1-dC16** shows the smallest proportional increase in apparent diameter suggesting that it is the most stable formulation in PBS buffer with 10%

serum at room temperature. Overall, **PEG-G$_1$-dC16** appears to produce the most stable formulation.

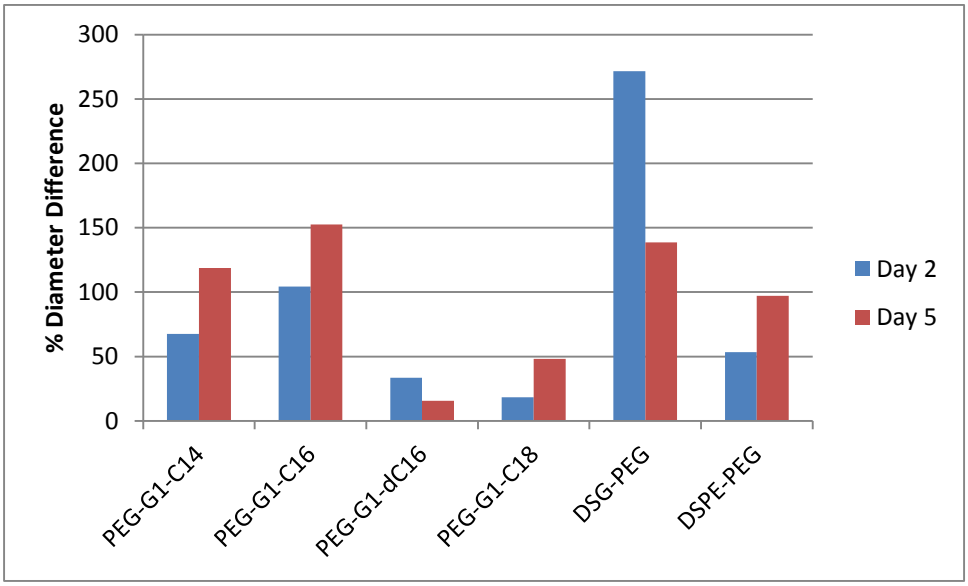

Figure 3.13: SLNPs incubated at 37°C in PBS for 5 days for formulations containing 1.5 mol% of different PEG-lipids. The composition for these SLNPs was 50: 10: 38.5: 1.5 (DOTMA: DSPC: Cholesterol: PEG-lipid) with a DNA loading of 5.1 wt%.

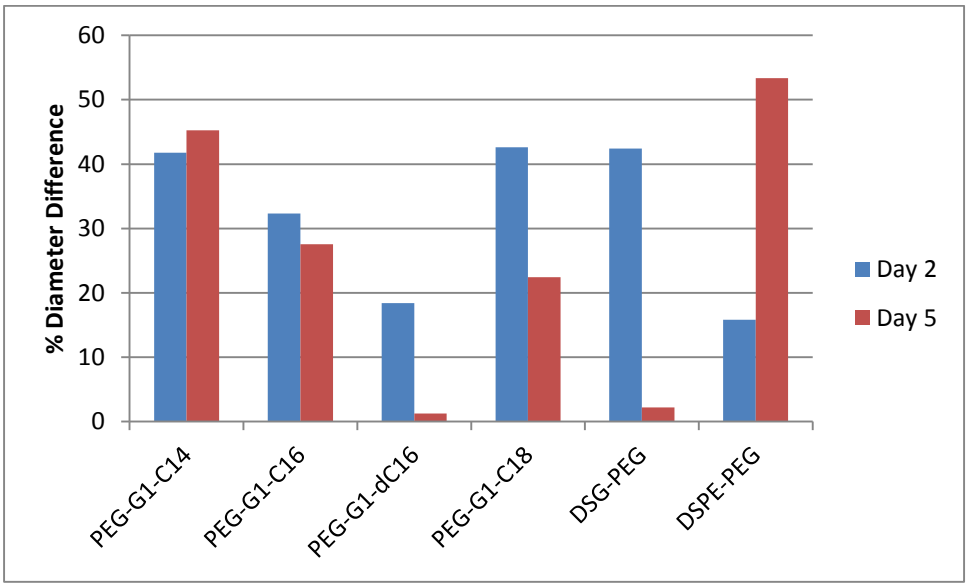

Figure 3.14: SLNPs incubated at 37°C in PBS buffer and 10% serum for 5 days for formulations containing 1.5 mol% of different PEG-lipids. The composition for these SLNPs was 50: 10: 38.5: 1.5 (DOTMA: DSPC: Cholesterol: PEG-lipid) with a DNA loading of 5.1 wt%.

Further experiments at 37°C in PBS buffer and PBS buffer with 10% serum, Figures 3.13-3.14, showed increase the apparent diameter of the SLNPs. Looking at Figure 3.13, it is shown that DSG-PEG SLNPs readily aggregate at 37°C in PBS buffer as both the apparent diameter and the PDI increased significantly over the 5 day incubation period. **PEG-G_1-dC16** and **PEG-G_1-C18** once again appear to be the most stable formulations with apparent diameter increases of 16% and 48% respectively. This however is difficult to see in Figure 3.14 when the SLNPs are incubated at 37°C in PBS buffer with 10% serum. This is explainable by the fact that subtle aggregation is less detectable in these experiments as the serum particles mask this effect. In any case, **PEG-G_1-dC16** shows the smallest proportional increase in diameter – further supporting it as contributing to the most stable formulation.

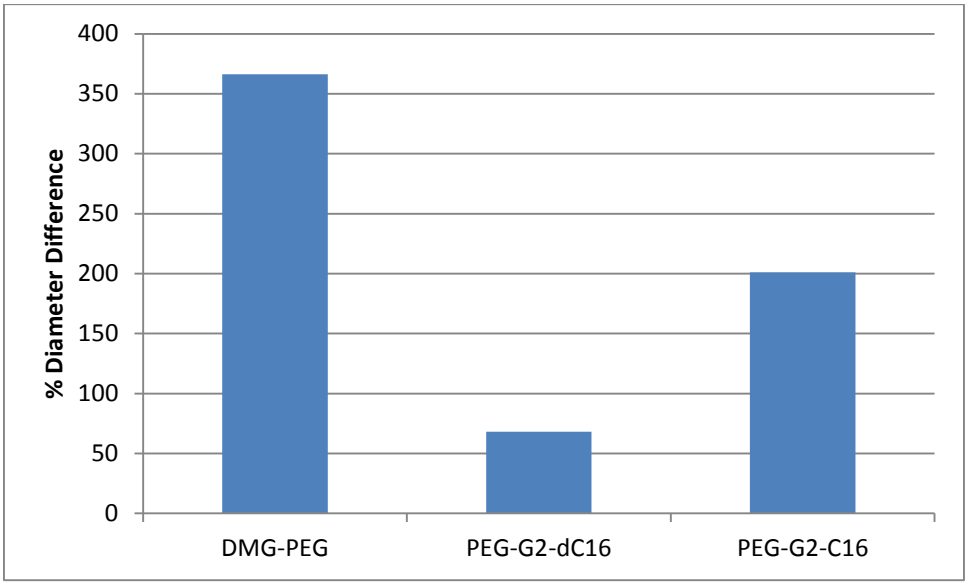

Figure 3.15: SLNPs incubated at 37°C in PBS buffer for 7 days for formulations containing 1.5 mol% of different PEG-lipids. The composition for these SLNPs was 50: 10: 38.5: 1.5 (Ionisable lipid: DSPC: Cholesterol: PEG-lipid) with a DNA loading of 5.1 wt%.

Only a small amount of the commercial lipid mix was available – this limited the number PEG-lipids that were evaluated. A stability experiment was carried out at 37°C in PBS buffer over 7 days. Preliminary results on the 2nd

generation lipids, **PEG-G_2-dC16** and **PEG-G_2-C16**, were compared to the commercial DMG-PEG. Over the incubation period, **PEG-G_2-dC16** showed the smallest proportional increase in apparent diameter at 68% compared to DMG-PEG at 366%. To this point, the **PEG-G_2-dC16** formulation was found to be significantly more stable than both DMG-PEG and **PEG-G_2-C16**. Further stability tests need to done; specifically in regard to PBS with 10% serum at 37°C. This continues to outline branching lipids as a favorable stabilizing factor for SLNPs.

3.3 Lipid-Drug Conjugate Formulations

It was important to first establish a general composition for the formulations. Formulating LDC nanocarriers is fairly unexplored, though there are some evident starting points. Hydrophobic compounds rarely by themselves self-assemble into nanocarriers and usually crystallize or precipitate out of aqueous media. Initial attempts to form the LDC nanocarriers confirmed this as LDC monomers precipitated out of solution. Since the LDC monomers are hydrophobic moieties, it was necessary to incorporate a surfactant into the LDC formulations to improve their solubility. Furthermore, incorporating a co-lipid was thought to stabilize the interior.

LDC	Particle Diameter (nm)	PDI
6MP-C14	489.7	0.343
6MP-C16	216.7	0.288
6MP-dC16	80.9	0.277
6MP-C18	560.3	0.358
6TG-C14	227.5	0.346
6TG-C16	102.2	0.237
6TG-dC16	64.8	0.220

Table 3.4: Physical Characterizations of LDC formulations where the composition was 90: 5: 5 (LDC monomer: DMPC: DSPE-PEG). The drug loading was 15 wt%.

Several different compositions were investigated before arriving at 5% PEG-DSPE, 5% DMPC, and 90% LDC monomer mole ratio. The drug loading for

all of these formulations was 15 wt% calculated from the thiopurine drug mass over the total mass of the mixture. Tween 80 was also evaluated at various mole ratios; however, this surfactant failed to yield LDCs that were stable enough to manipulate over 1-2 days. The particle sizes follow the **C14** > **C16** > **dC16** lipid series. None of the lipids gave any distinct advantage in forming LDCs with low PDIs. Further optimization of the composition may lend to yielding formulations with low PDIs – there exist other surfactants such as DSG-PEG or any of the novel PEG-lipids prepared here that may improve the PDI. Following arrival at this stable composition, the stability of these particles was evaluated over a time period under 6 different conditions.

3.4 Lipid-Drug Conjugate Stability Assay

Identifying stable LDC formulations consistent with eventual therapy application was done as previously described. These were evaluated under 6 different conditions to establish storage stability and physiological stability. The experimental details are documented in Appendix 2.

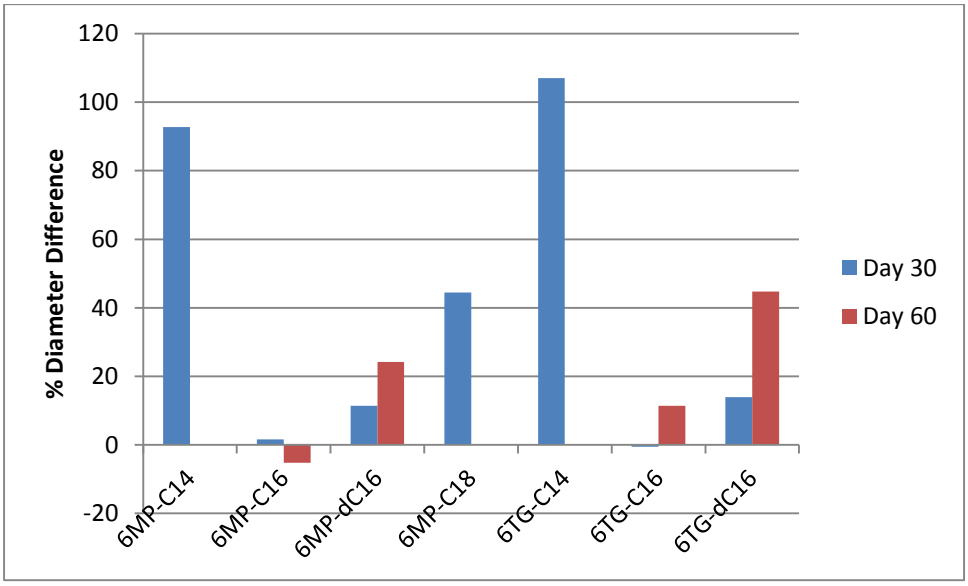

Figure 3.16: LDCs incubated at 4°C in PBS for 60 days formulations where the composition was 90: 5: 5 (LDC monomer: DMPC: DSPE-PEG). The drug loading was 15 wt%.

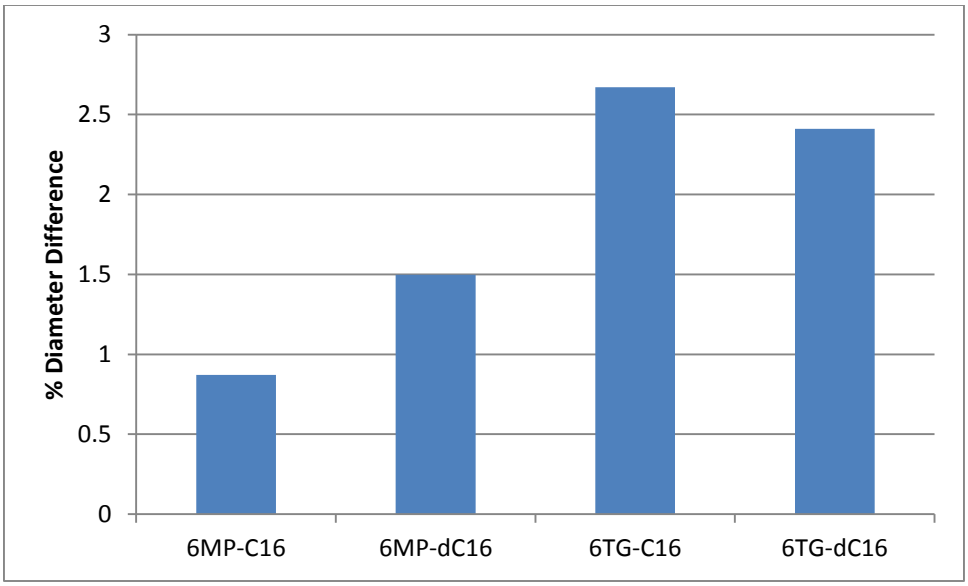

Figure 3.17: LDCs incubated at 4°C in PBS and 10% serum for 30 days where the composition was 90: 5: 5 (LDC monomer: DMPC: DSPE-PEG). The drug loading was 15 wt%.

6MP-C14, **6MP-C18**, and **6TG-C14** were observed to show a greater than 40% apparent diameter increase after 30 days and were concluded to be unstable in PBS buffer at 4 °C (Figure 3.16). **6MP-C16**, **6MP-dC16**, **6TG-C16**, and **6TG-dC16** were shown to maintain their apparent diameters and PDI values – therefore it was concluded that these LDCs were stable under these conditions. These four formulations were then incubated at 4°C in PBS buffer and 10% serum for 30 days (Figure 3.17). The apparent diameters remained constant over this time period and no precipitates were observed meaning that aggregation between particles and serum proteins were relatively low.

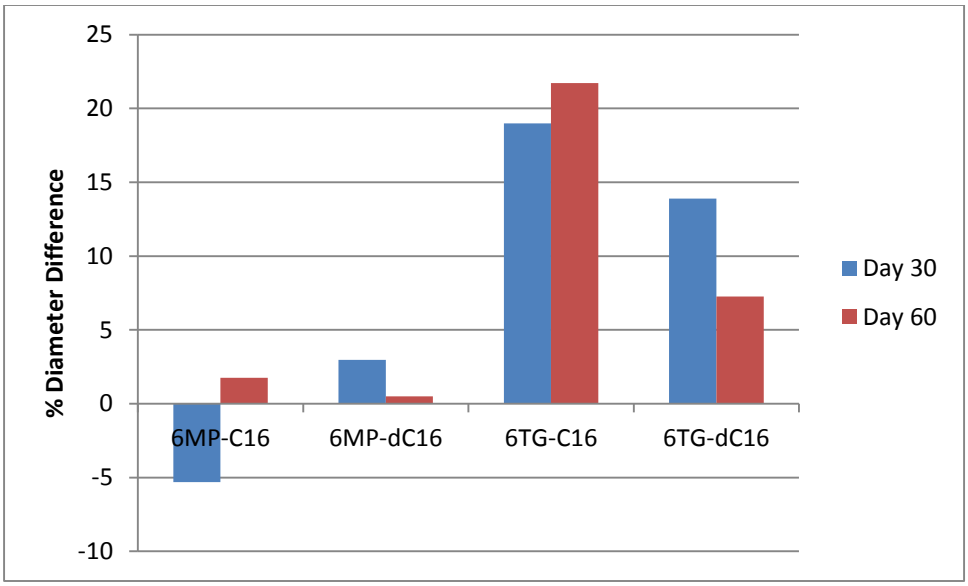

Figure 3.18: LDCs incubated at RT in PBS for 60 days where the composition was 90: 5: 5 (LDC monomer: DMPC: DSPE-PEG). The drug loading was 15 wt%.

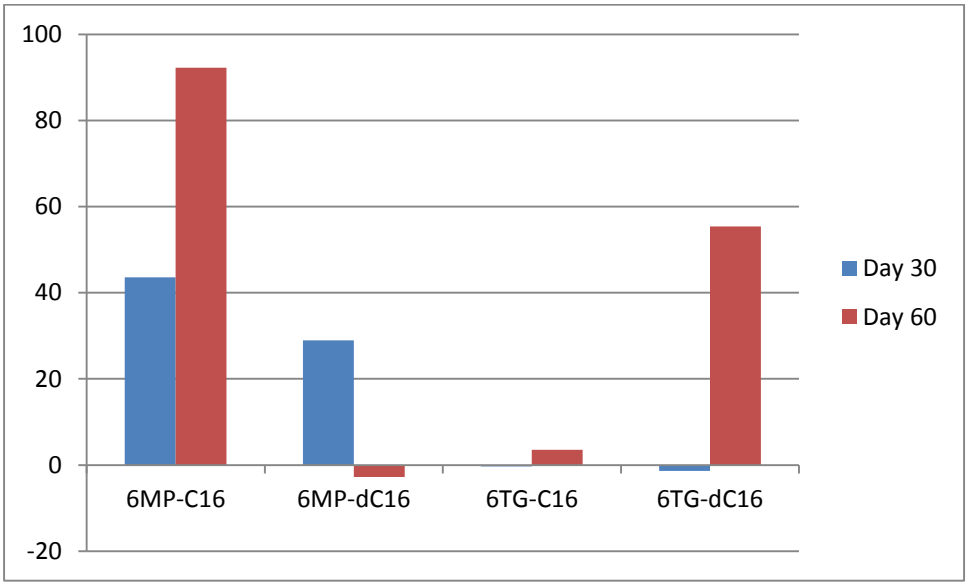

Figure 3.19: LDCs incubated at RT in PBS and 10% serum for 60 days where the composition was 90: 5: 5 (LDC monomer: DMPC: DSPE-PEG). The drug loading was 15 wt%.

Experiments at room temperature in PBS (Figure 3.18) also showed that **6MP-C16**, **6MP-dC16**, **6TG-C16**, and **6TG-dC16** maintained constant apparent diameters. Therefore, these formulations were stable under this condition. The apparent diameter for **6MP-C16** was shown to increase significantly while incubated at room temperature in PBS with 10% serum (Figure 3.19). No precipitates were observed signifying the formulations were relatively stable.

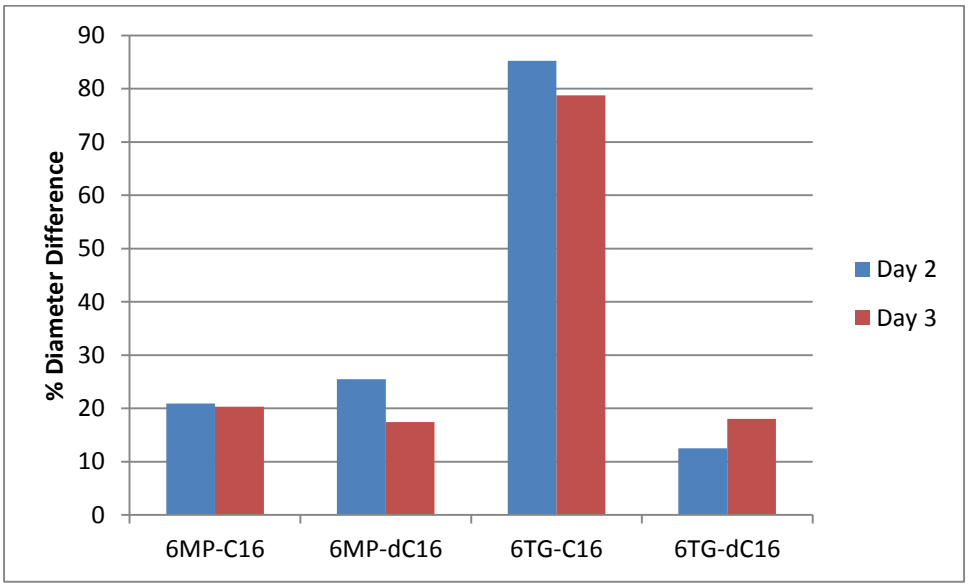

Figure 3.20: LDC incubated at 37°C in PBS for 3 days where the composition was 90: 5: 5 (LDC monomer: DMPC: DSPE-PEG). The drug loading was 15 wt%.

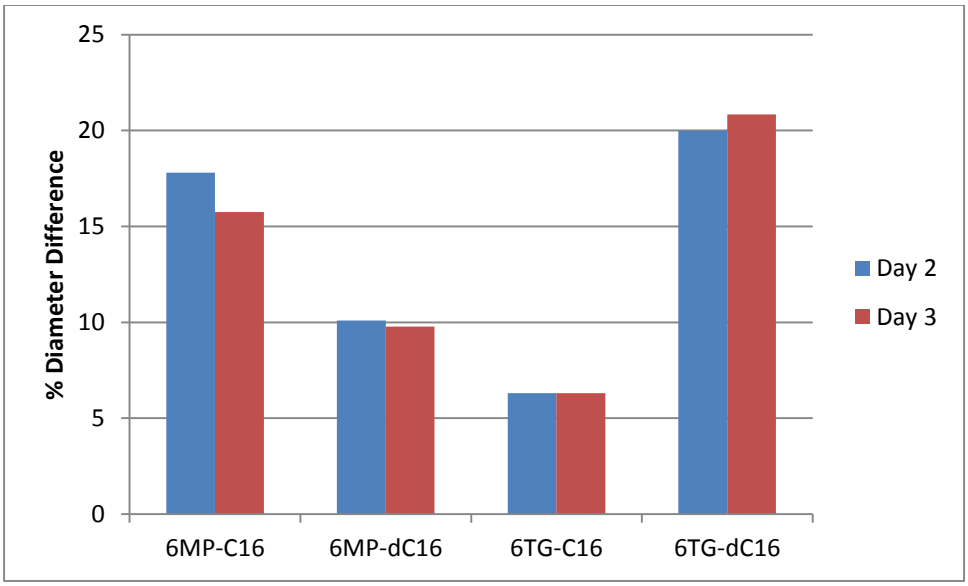

Figure 3.21: LDC incubated at 37°C in PBS and 10% serum for 3 days where the composition was 90: 5: 5 (LDC monomer: DMPC: DSPE-PEG). The drug loading was 15 wt%.

Monitoring stability at 37 °C in PBS buffer over 3 days, Figure 3.20, shows **6MP-dC16** and **6TG-dC16** formulations with constant apparent diameters while a moderate increase of 79% was observed for **6TG-C16**. At 37 °C in PBS buffer with 10% serum (Figure 3.21), the experiment that most closely resembled physiological conditions, no stability differences were discernible between the 4 formulations. Formulations maintained apparent diameters and no precipitates were observed suggesting that all these were stable. **6TG-dC16** and **6MP-dC16** appear to be the most stable and represent the most promising as their particle sizes fall within the 10-100 nm range for high therapeutic potential. The PDI values indicated mildly polydisperse formulations with values between 0.20 - 0.30 – it would be possible to optimize this by investigating different surfactants in the LDC composition at the expense of reduced drug loading.

Chapter 4: Conclusions and Future Work

Eight different PEG-lipids were designed and synthesized for purposes in lipid nanoparticle delivery. These structures explored serinol and iminodiacetic acid backbones as well as different branching sequences in the aliphatic chains. Lipid anchors were linked to PEG by an amide linkage through the reaction of a free primary amine on the lipid anchors with NHS-activated ester PEG. PEG-lipids were isolated in moderate yields. Purification using silica gel in column chromatography was unable to remove some inherent impurities from the NHS-PEG. The synthesis leaves potential for scale-up.

These PEG-lipids were then used to formulate SLNPs through microfluidic mixing. The composition that was determined for these SLNPs was stable enough to not only distinguish stability differences between the novel and commercial PEG-lipids but also provide insight into structural advantages of the synthetic lipids. The relative stability of the first generation PEG-lipids is as follows: **PEG-G$_1$-dC16** > **PEG-G$_1$-C18** > **PEG-G$_1$-C14** > **PEG-G$_1$-C16**. **PEG-G$_1$-dC16** and **PEG-G$_1$-C18** were shown to be more stable than commercial PEG-lipids DSG-PEG and DSPE-PEG. While no stability comparison was able to be done to evaluate stability influences of the different backbone structures, it was evident that branching lipids provides stability advantages over their straight chain counterparts. A commercial lipid mix allowed for comparisons between **PEG-G$_2$-dC16**, **PEG-G$_2$-C16**, and DMG-PEG. Preliminary results indicated that **PEG-G$_2$-dC16** provides the greatest stabilizing effects of these three. With two examples directly comparing branching (dC16) and non-branching (C16) lipids, it appears that branching sequences are better at stabilizing SLNPs.

Moving forward, it is important to further establish branching lipids as a stabilizing feature. There are commercially available C_{20} fatty acids straight and branch chain isomers that can further explore this question. A stable composition for the SLNPs needs to be obtained to compare what stability effects, if any, the different backbone structures have on SLNPs. The 2nd generation PEG-lipids

have much unexplored compositions/applications to be discovered in LNP drug delivery given that they are significantly different from current PEG-lipids.

Once a stable composition is obtained and a correlation between PEG-lipid structure and SLNP stability has been established, it would be possible to investigate the effects PEG-lipid structure has on SLNP transfection ability. SLNP formulations could be done with a short DNA oligomer that is covalently linked to a fluorescent probe. Cells would be treated with these SLNPs, at varying concentrations, and monitored for the amount of fluorescence in the cells following treatment. This experiment only considers the ability of the SLNPs to get into the cells – it does not, however, give any information on whether the nucleic acid is able to be active once inside the cell. A gene knockdown assay would be required to investigate this. This involves formulating SLNPs with siRNA that is covalently linked to a fluorescent probe (to once again track whether the SLNP is getting into the cell). The siRNA must have correct complementary base interactions for the target mRNA to observe a gene knockdown.

Seven different LDC monomers were designed and synthesized for applications in chemotherapy. The asymmetric disulfide was formed to link the thiopurine drugs to synthetic lipids. Pure LDCs were isolated in moderate yields. The reductive environment within the cell would be expected to readily cleave the disulfide – releasing the free drug into the cytoplasm.

LDCs were formulated by microfluidic mixing. Four of the proposed LDCs self-assembled into stable nanocarriers. **6MP-dC16** and **6TG-dC16** formed particles with sizes less than 100 nm while showing the greatest stability under physiological conditions. These nanocarriers may be further optimized to investigate their therapeutic potential by further investigating different compositions – more specifically by considering different surfactants such as DMG-PEG or these novel PEG-lipids. Different formulation buffers may also affect the physiochemical properties of these LDCs. A cell viability assay against HeLa cells, or another cancerous cell-line, would determine whether these LDC

nanocarriers can kill cancerous cells at the same, or better, rate as the thiopurine drugs by themselves.

The toxicity of the LDCs' individual components also needs to be evaluated. Determining this toxicity is not as simple as treating the cells with varying concentrations of each component as this does not take into account the fact that the components are in getting into the cells in different amounts when formulated as a LDC. The best approach to this would be to synthesize an analogue of the LDC monomers that incorporates a known relatively nontoxic component in place of the drug and using this to formulate a pseudo-LDC. Treating cells with this would show whether the remaining components of the LDC as a whole are toxic.

Both the PEG-lipids and LDCs support branching lipids as more stabilizing than their straight chain counterparts. More examples comparing this branching effect needs to be investigated – as mentioned, synthesizing PEG-lipids and LDC monomers starting from the commercial fatty acids C20 for the straight and branch isomers would be an accessible starting point. The stability assay developed for evaluating stability in PBS with 10% serum certainly needs some work and, at this point, remains as a qualitative assay only. Beyond dramatic increases in apparent diameters and observing precipitation, little information can be gathered from this experiment.

Bibliography

1. Allen, T.M. and Cullis, P.R. “Liposomal drug delivery systems: From concept to clinical applications”. *Advanced Drug Delivery Reviews*. 65 (2013) 36-48.
2. Vives, E.; Schmidt, J. and Pelegrin, A. “Cell-penetrating and cell targeting peptides in drug delivery”. *Biochimica et Biophysica Acta.* 1786 (2008) 126-138.
3. Tiwari, G.; Tiwari, R.; Sriwastawa, B.; Bhati, L.; Pandey, S.; Pandey, P. and Bannerjee, S.K.. “Drug delivery systems: An updated review”. *International Journal of Pharmaceutical Investigation.* 2 (2012) 2-11.
4. Zhou, J.; Patel, T.; Fu, M.; Bertram, J.P. and Saltzman, W.M.. “Octa-funtional PLGA nanoparticles for targeted and efficient siRNA delivery to tumors”. *Biomaterials*. 33 (2012) 583-591.
5. Wicki, A.; Witzigmann, D.; Balasubrannanian, V. and Huwyler, J. “Nanomedicine in cancer therapy: Challenges, opportunities, and clinical applications”. *Journal of Controlled Release*. 200 (2015) 138-157.
6. Semple, S.C; Chonn, A. and Cullis, P.R. “Interactions of liposomes and lipid-based carrier systems with blood proteins: Relation to clearance behaviour in vivo”. *Advanced Drug Delivery*. 32 (1998) 3-17.
7. Petros, R. A. and DeSimone, J.M. “Strategies in the design of nanoparticles for therapeutic applications”. *Nature Reviews Drug Discovery*. 9 (2010) 615-627.
8. Heyes, J.; Hall, K.; Tailor, V.; Lenz, R. and MacLachlan, I. “Synthesis and characterization of novel poly(ethylene glycol)-lipid conjugates suitable for use in drug delivery.” *Journal of Controlled Release.* 112 (2006) 280-290.
9. Ohtsuki, S. and Terasaki, T. “Contribution of Carrier-Mediated Transport Systems to the Blood-Brain Barrier as a supporting and protecting Interface for the Brain; Importance for CNS Drug Discovery and Development”. *Pharmaceutical Research*. 24 (2007) 1745-1758.
10. Karran, P. and Attard, N. “Thiopurines in current medical practice: molecular mechanisms and contributions to therapy-related cancer”. *Nature Reviews Cancer.* 8 (2008) 24-36.
11. Mori, S.; Ohtsuki, S.; Takanaga, H.; Kikkawa, T.; Kang, Y. and Terasaki, T. “Organic anion transporter 3 is involved in the brain-to-blood efflux transport of thiopurine nucleobase analogs”. *Journal of Neurochemistry*. 90 (2004) 931-941.
12. Blasi, P.; Giovagnoli, S.; Schoubben, A.; Ricci, M. and Rossi, C. “Solid lipid nanoparticles for targeted brain drug delivery”. *Advanced Drug Delivery Reviews.* 59 (2007) 454-477.

13. Gasparini, G.; Bang, E.; Molimard, G.; Tulumello, D.V.; Ward, S.; Kelley, S.O.; Roux, A.; Sakai, N. and Matile, S. “Cellular uptake of Substrate-initiated Cell-Penetrating Poly(disulfide)s. *J.Am.Chem.Soc.* 136 (2014) 6069-6074.
14. Aubry, S.; Burlina, F.; Dupont, E.; Delarouche, D.; Joliot, A.; Lavielle, S.; Chassaing, G.; and Sagan, S. “Cell-surface thiols affect cell entry of disulfide-conjugated peptides”. *The FASEB Journal*. 23 (2009) 2956-2967.
15. Vandavasi, J.K.; Hu, W.; Chen, C, and Wang, J. “Efficient synthesis of unsymmetrical disulfides”. *Tetrahedron*. 67(2011) 8895-8907.
16. Leung, A.K.K.; Hafez, I.M.; Baoukina, S.; Belliveau, N.M.; Zhigaltsev, I.V.; Afshinmanesh, E.; Tieleman, D.P.; Hansen, C.L.; Hope, M.J., and Cullis, P.R. “Lipid Nanoparticles containing siRNA synthesized by microfluidic mixing exhibit an electron dense nanostructured core”. *The Journal of Physical Chemistry*. 116(2012) 18440-18450.
17. Semple, S.C.; Akinc, A.; Chen, J.; Sandhu, A.P.; Hui, B.L.; Cho, C.K.; Sah, D.W.Y.; Stebbing, D.; Crosley, E.J.; Yaworshi, E.; et al. “Rational design of cationic lipids for siRNA delivery”. *Nature Biotechnology*. 28(2010) 172-178.
18. Houk, J; Singh, R; Whitesides, G.M. “Measurement of thiol-disulfide interchange reactions and thiol pKa values”. *Methods in Enzymology*. 143 (1987) 634-647.
19. Olbrich, C.; Gessner, A.; Schroder, W.; Kayser, O.; and Muller, R. “Lipid-drug conjugate nanoparticles of the hydrophilic drug diminezene-cytotoxicity testing and mouse serum adsorption”. *Journal of Controlled Release*. 96 (2004) 425-435.
20. Tros de llarduya, C.; Sun, Y.; and Duzganes, N. “Gene delivery by lipoplexes and polyplexes”. *European Journal of Pharmaceutical Sciences*. 40 (2010) 159-170.
21. Thomas, C.E.; Ehrhardf, A.; and Kay, M.A. “Progress and Problems with the use of viral vectors for gene therapy”. *Nature Reviews Genetics*. 4 (2003) 346-358.
22. Wang, Y.; Liu, D.; Zheng, Q.; Zhao, Q.; Zhang, H.; Ma, Y.; Fallon, J.; Fu, Q.; Haynes, M.; Lin, G.; Zhang, R.; Wang, D.; Yang, X.; Zhao, L.; He, Z.; and Lin, F. “ Disulfide bond bridge insertion turns hydrophilic anticancer prodrugs into self-assembled Nanomedicines”. *NanoLetters*. 2014.
23. Raziyabegum, S.K.; Mohanvarma, M.; Madan Mohanreddy, M.; Ankarao, E.; Mahidhar reddy, D.; and Jyothirmai, K. “A Novel Review in Nanopharma Technology – Solid lipid Nanoparticles”. *Int.J. Inv. Pharm. Sci.* 1 (2013) 81-84.

24. Williams, M.S.; Longmuir, K.J.; and Yager, P. “A practical guide to staggered herringbone mixer”. *Lab Chip*. 8(2008) 1121-1129.
25. McIlhinney, H. “Determination of N-terminal myristoylation of proteoins using a combined gas chromatographic/ mass spectrometric assay of derived myristoylglycine: Electron impact-induced fragmentation of acylglycine derivatives”. *Journal of Mass Spectrometry*. 30 (1995) 900-910.
26. Jayaraman, M.; Ansell, S.M.; Mui, B.L.; Tam, Y.K.; et al. “Maximizing the Potency of siRNA Lipid Nanoparticles for Hepatic Gene Silencing In Vivo”. *Angew. Chem. Int. Ed.* 51 (2012) 8529-8533.
27. Morenweiser, R. “Downstream processing of viral vectors and vaccines”. *Gene Therapy*. 12 (2005) 103-110.

Appendix 1: Synthetic Experimental Details

General Procedures:

Chemicals and solvents were used as received from known suppliers, except dry DCM which was obtained from a MBRAUN-SPS. NMR spectra were collected on a 300 MHz Bruker instrument. ESI-MS spectra were recorded on a LCQ-Classic instrument.

Synthetic Detail:

2-6: 1st Generation Lipid Anchor Synthesis:

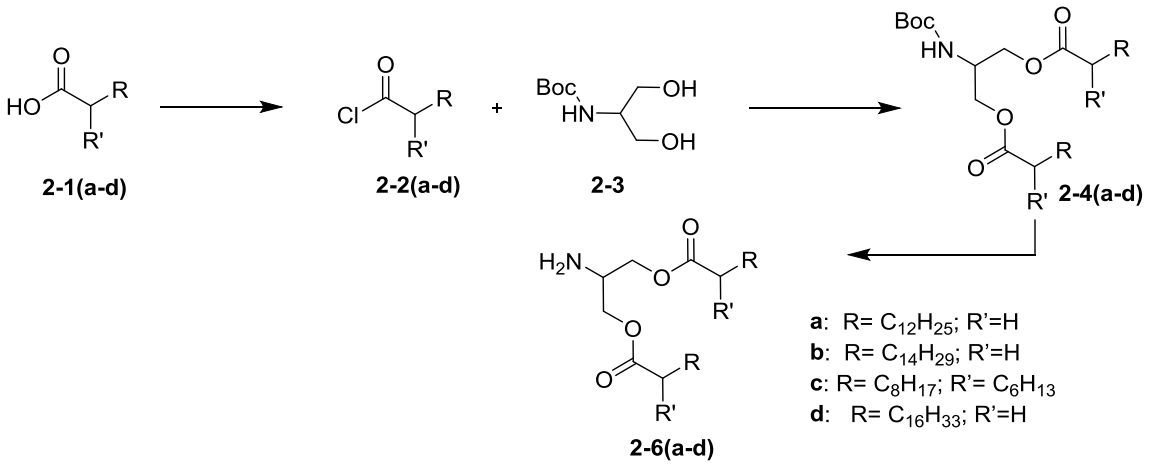

Scheme A1.1: Outline of the synthesis for the 1st generation lipids anchor

General Procedure:

In a round bottom flask a stirred solution of thionyl chloride (10.0 equiv.) and **2-1(a-d)** (1.0 equiv.) was refluxed for 2 hours under a $CaSO_4$ drying tube. The reaction was monitored by ^{1}H-NMR analysis of aliquots. The reaction was allowed to cool and subsequently the thionyl chloride was removed under vacuum on a roto-evaporator to obtain **2-2(a-d)**. In a round bottom flask **2-3** (1.0 equiv.) was dissolved in pyridine (10.0 equiv.) and **2-2(a-d)** (2.5 equiv.) was added dropwise . The mixture was then heated to 70 °C and left to stir for 3 hours

under a $CaSO_4$ drying tube. The reaction was monitored by ^{1}H-NMR analysis of aliquots. Once completed, the reaction was cooled and diluted with DCM. The solution was then washed 3 times with 1 M HCl and 3 times with 1 M NaOH. The organic layer was then dried over anhydrous sodium sulfate and then gravity filtered. The solvent was removed under vacuum to obtain **2-4(a-d)**. Excess TFA was added dropwise to **2-4(a-d)** in a round bottom flask. The reaction was left stirring for 1 hour at room temperature and was monitored by TLC (silica gel, EtOAc/ Hexanes as eluent, visualized by $KMnO_4$). Following completion of the reaction, TFA was removed on a roto-evaporator. NaOH (1 M) was then added and **2-6(a-d)** was extracted with DCM and washed 3 times with 1 M NaOH. The organic layer was dried with anhydrous sodium carbonate and subsequently gravity filtered. DCM was removed on a roto-evaporator yielding **2-6(a-d)**. No chromatography was necessary.

2-6a:

Following the general procedure, **2-2a** was prepared from thionyl chloride (6.35 mL, 87.6 mmol) and **2-1a** (2.000 g, 8.757 mmol) **2-4a** was prepared from **2-3** (0.596 g, 3.13 mmol) in pyridine (2.53 mL, 31.3 mmol) and **2-2a** (1.931 g, 7.835 mmol). **2-6a** was prepared from TFA (5 mL) and **2-4a** affording a waxy yellow solid in a 66% yield (1.06 g). ^{1}H-NMR (300 MHz, $CDCl_3$) δ: 4.07 (m, 2H), 4.05 (m, 2H), 3.28 (m, 1H), 2.33 (t, 4H, 7.7 Hz), 1.62 (m, 4H), 1.48 (s(br), 2H), 1.26 (s, 40H), 0.88 (t, 6H, 7.0 Hz). ^{13}C-NMR (75 MHz, $CDCl_3$): 173.6, 65.8, 49.3, 34.2, 31.9, 29.6, 29.6, 20.4, 29.3, 29.2, 29.1, 24.9, 22.7, 14.1 MS ((+) ESI; Exact mass): calc'd for $C_{31}H_{62}NO_4^+$ = 512.47 amu, obtained = 512.33 amu.

2-6b:

Following the general procedure, **2-2b** was prepared from thionyl chloride (5.61 mL, 78.0 mmol) and **2-1b** (2.000 g, 7.800 mmol). **2-4b** was prepared from **2-3** (0.558 g, 2.92 mmol) in pyridine (2.31 mL, 29.2 mmol) and **2-2b** (2.000 g, 7.299 mmol). **2-6b** was prepared from TFA (5 mL) and **2-4b** affording a waxy white

solid in a 73% yield (1.21 g). ^{1}H-NMR (300 MHz, $CDCl_3$) δ: 4.06 (m, 2H), 4.05 (m, 2H), 3.28 (m, 1H), 2.32 (t, 4H, J=7.8 Hz), 1.61 (m, 4H), 1.24 (s, 48H), 0.87 (t, 6H). ^{13}C-NMR (75 MHz, $CDCl_3$) δ: 173.8, 66.0, 49.5, 34.4, 32.1, 29.9, 29.9, 29.8, 29.7, 29.6, 29.5, 29.4, 25.2, 22.9, 14.3. MS ((+) ESI; Exact mass): calc'd for $C_{35}H_{70}NO_4^+$ = 568.53 amu, obtained = 568.33 amu.

2-6c:

Following the general procedure, **2-2c** was prepared from thionyl chloride (5.66 mL, 78.2 mmol) and **2-1c** (2.30 mL, 7.82 mmol) **2-4c** was prepared from **2-3** (0.488 g, 2.55 mmol) in pyridine (2.46 mL, 30.6 mmol) and **2-2c** (2.10 g, 7.64 mmol) **2-6c** was prepared from TFA (5 mL) and **2-4c** affording a light yellow oil in a 75% yield (1.09 g). ^{1}H-NMR (300 MHz, $CDCl_3$) δ: 4.06 (m, 2H), 4.04 (m, 2H), 3.26 (m, 1 H), 2.34 (m, 2 H), 1.57, 1.44 (m, 8 H), 1.24 (s, 40 H), 0.86 (t, 12 H, J=7.0 Hz). ^{13}C-NMR (75 MHz, $CDCl_3$): 176.2, 65.5, 53.4, 49.4, 45.7, 32.4, 31.8, 31.6, 29.5, 29.4, 29.2, 29.2, 27.4, 27.4, 22.6, 22.6, 14.0, 14.0. MS ((+) ESI; Exact mass): calc'd for $C_{35}H_{70}NO_4^+$ = 568.53 amu, obtained = 568.33 amu.

2-6d:

Following the general procedure, **2-2d** was prepared from thionyl chloride (5.10 mL, 70.3 mmol) and **2-1d** (2.000 g, 7.030 mmol). **2-4d** was prepared from **2-3** (0.510 g, 2.67 mmol) in pyridine (2.15 mL, 26.7 mmol) and **2-2d** (2.020 g, 6.668 mmol) **2-6d** was prepared from TFA (5 mL) and **2-4d** affording a waxy white solid in a 67% yield (1.09 g). ^{1}H-NMR (300 MHz, $CDCl_3$) δ: 4.09 (m, 2H), 4.07 (m, 2H), 3.30 (m, 1H), 2.34 (t, 4H, J=7.5 Hz), 1.63 (m, 4H), 1.26 (s, 56H), 0.89 (t, 6H, J=6.8 Hz). MS ((+) ESI; Exact mass): calc'd for $C_{39}H_{78}NO_4^+$ = 624.59 amu, obtained = 624.53 amu.

2-12(a-d): 2nd Generation Lipid Anchor Synthesis:

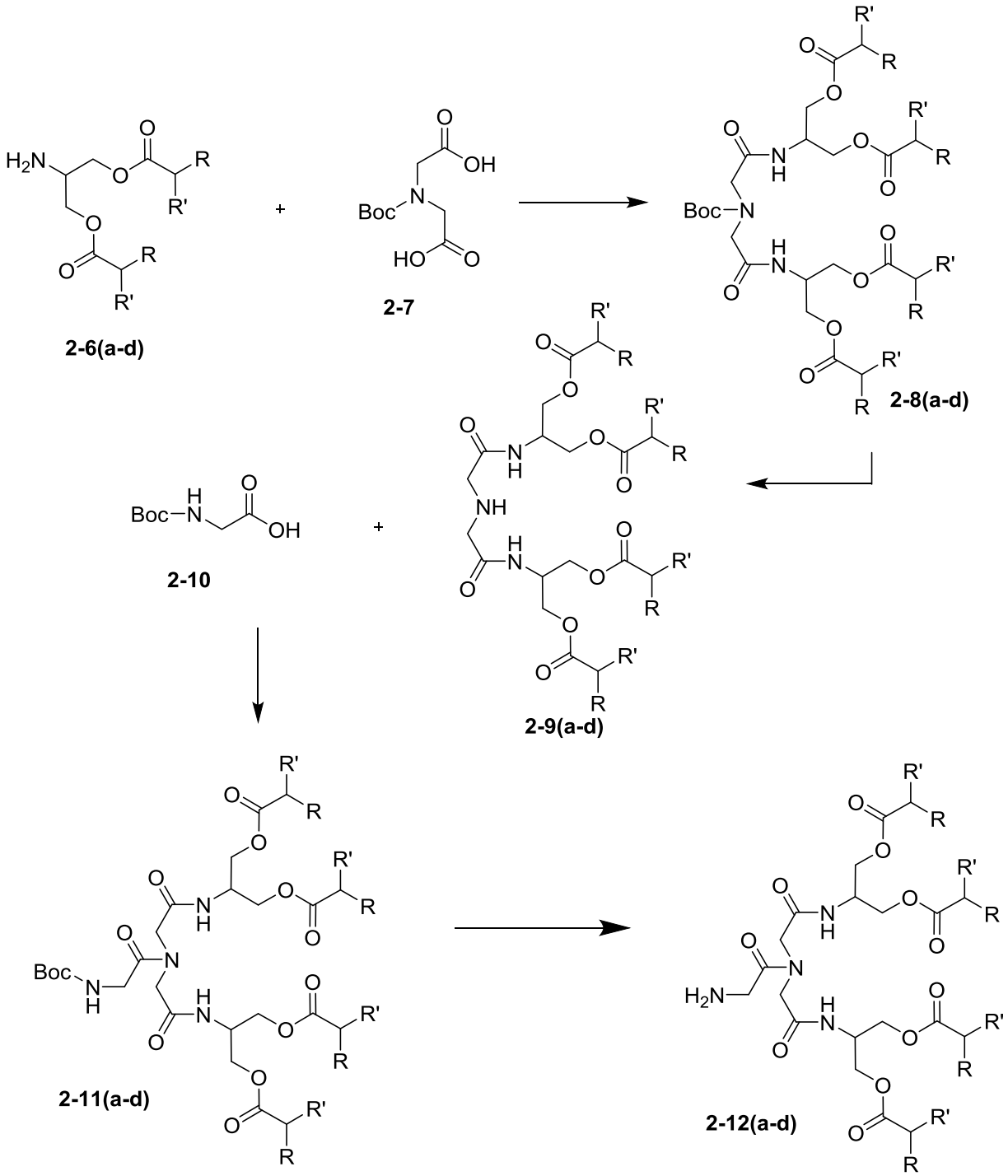

a: R= $C_{12}H_{25}$; R'=H
b: R= $C_{14}H_{29}$; R'=H
c: R= C_8H_{17}; R'= C_6H_{13}
d: R= $C_{16}H_{33}$; R'=H

Scheme A1.2: Outline of the synthesis for the 2nd generation lipid anchors.

General Procedure:

In a round bottom flask was dissolved **2-7** (1.0 equiv.) in dried DCM/DMF (1:1;10mM). HBTU (2.4 equiv.), **2-6(a-d)** (2.2 equiv.) and triethylamine (4.0 equiv.) were subsequently added. The solution was stirred for 20 hours at room temperature and was monitored by ^{1}H-NMR. Once completed, the reaction solution was diluted with EtOAc and washed 3 times with 1M HCl and 3 times with H_2O. The organic layer was then dried over anhydrous sodium sulfate, followed by gravity filtration. EtOAc and DCM were roto-evaporated to yield **2-8(a-d)**. Excess TFA was added dropwise to **2-8(a-d)** in a round bottom flask. The reaction was left to stir for 1 hour and monitored by ^{1}H-NMR. Following completion of the reaction, TFA was removed on roto-evaporator and 1 M NaOH was added to the round bottom flask. **2-9(a-d)** was extracted with DCM and washed 3 times with 1 M NaOH. The organic layer was then dried over sodium carbonate, followed by gravity filtration. DCM was removed on a roto-evaporator and **2-9(a-d)** was isolated. The crude product was subsequently characterized as no purification was necessary. [Characterization- ^{1}H-NMR, ^{13}C-NMR, ESI-MS] In a round bottom flask was dissolved **2-10** (1.1 equiv.) in dried DCM/DMF (1:1;10mM). To this, HOBt (1.2 equiv.), HBTU (1.2 equiv.), **2-9(a-d)** (1.0 equiv.), and triethylamine (3.0 equiv.) were then added and the resulting solution was left stirring at room temperature for 20 hours. When the reaction was complete, visualized by ^{1}H-NMR, the reaction solution was diluted with EtOAc, and washed once with 1 M HCl and 3 times with H_2O. The organic layer was then dried over anhydrous sodium sulfate and then gravity filtered. DCM and EtOAc were removed by roto-evaporation to yield crude **2-11(a-d)**. Excess TFA was added to **2-11(a-d)** in a round bottom flask and the reaction was left for 1 hour. Following completion, as monitored by ^{1}H-NMR, TFA was removed on a roto-evaporator. NaOH (1 M) was added to convert to the amine and **2-12(a-d)** was extracted with diethyl ether and subsequently washed with 3 times with 1 M NaOH. The organic layer was dried with anhydrous sodium carbonate and then gravity filtered. Diethyl ether was removed to obtain the crude product.

2-12a:

Following the general procedure, **2-8a** was prepared from **2-7** (0.104 g, 0.444 mmol) in dried DCM/DMF (22.2 mL/22.2 mL;10 mM). HBTU (0.404 g, 1.066 mmol), **2-6a** (0.500 g, 0.977 mmol) and triethylamine (0.25 mL, 1.8 mmol). **2-9a** was prepared from TFA (5 mL) and **2-8a** affording a waxy light yellow solid in 53% yield (0.264 g). The crude product was subsequently characterized as no chromatography was necessary. ^{1}H-NMR (300 MHz, $CDCl_3$) δ: 7.02 (d, 2H, J=8.6 Hz), 4.46 (m, 2H), 4.24 (m, 4H), 4.12 (m, 4H), 3.25 (s, 4H), 2.31 (t, 8 H, J=7.8 Hz), 1.59 (m, 8H), 1.25 (s, 80H), 0.87 (t, 12H, J=6.9 Hz). ^{13}C-NMR (75 MHz, $CDCl_3$) δ: 174.0, 170.8, 62.9, 52.8, 48.0, 34.3, 32.1, 29.9, 29.9, 29.7, 29.6, 29.5, 29.4, 25.1, 22.9, 14.3. MS ((+) ESI; Exact mass): calc'd for $C_{66}H_{126}N_3O_{10}^+$ = 1120.94 amu, obtained = 1121.00 amu. Following the general procedure, **2-11a** was prepared from **2-10** (0.033g, 0.19 mmol) in dried DCM/DMF (9.0 mL/9.0 mL;10mM). To this, HOBt (0.029 g, 0.21 mmol), HBTU (0.080 g, 0.21 mmol), **2-9a** (0.20 g, 0.179 mmol), and triethylamine (0.075 mL, 0.53 mmol). **2-12a** was prepared from **2-11a** and TFA (5 mL) affording a light brown solid.

2-12b:

Following the general procedure, **2-8b** was prepared from **2-7** (0.093 g, 0.40 mmol) in dried DCM/DMF (20.0 mL/20.0 mL;10 mM). HBTU (0.364 g, 0.960 mmol), **2-6b** (0.500 g, 0.880 mmol) and triethylamine (0.22 mL, 1.6 mmol). **2-9b** was prepared from TFA (5 mL) and **2-8b** affording a light brown waxy solid in 55% yield (0.272 g). The crude product was subsequently characterized as no chromatography was necessary. ^{1}H-NMR (300 MHz, $CDCl_3$) δ: 7.03 (d, 2H, J=8.7 Hz), 4.47 (m, 2H), 4.26 (m, 4H), 4.14 (m, 4H), 3.27 (s, 4H), 2.33 (t, 8H, J=7.3 Hz), 1.60 (m, 8H), 1.27 (s, 96H), 0.89 (t, 12H, J=6.8). ^{13}C-NMR (75 MHz, $CDCl_3$) δ: 174.0, 170.8, 62.8, 52.7, 48.0, 34.31, 32.1, 29.9, 29.7, 29.6, 29.5, 29.4, 25.1, 22.9, 14.3. MS ((+) ESI; Exact mass): calc'd for $C_{74}H_{142}N_3O_{10}^+$ = 1233.07 amu, obtained = 1233.00. Following the general procedure, **2-11b** was prepared from

2-10 (0.030 g, 0.17 mmol) in dried DCM/DMF (8.1 mL/8.1 mL;10mM). To this, HOBt (0.026 g, 0.20 mmol), HBTU (0.074 g, 0.20 mmol), **2-9b** (0.201, 0.162 mmol), and triethylamine (0.068 mL, 0.49 mmol). **2-12b** was prepared from TFA (5 mL) and **2-11b** affording a light brown oil. MS ((+) ESI; Exact mass): calc'd for $C_{76}H_{145}N_4O_{11}^+$ = 1290.09 amu, obtained = 1290.00 amu.

2-12c:

Following the general procedure, **2-8c** was prepared from **2-7** (0.093 g, 0.40 mmol) in dried DMF (20.0 mL). HBTU (0.363 g, 0.960 mmol), **2-6c** (0.500 g, 0.880 mmol) and triethylamine (0.22 mL, 1.6 mmol). **2-9c** was prepared from TFA (5 mL) and **2-8c** affording a colorless oil in 60% yield (0.296 g). The crude product was subsequently characterized as no chromatography was necessary. ^{1}H-NMR (300 MHz, $CDCl_3$) δ: 7.07 (d, 2H, J=8.6 Hz), 4.46 (m, 2H), 4.25 (m, 4H), 4.11 (m, 4H), 3.23 (s, 4H), 2.34 (m, 4H), 1.56, 1.45 (m, 16H), 1.24 (s, 80H), 0.86 (t, 24H, J=7.4 Hz). ^{13}C-NMR (75 MHz, $CDCl_3$) δ: 176.4, 170.4, 62.3, 52.6, 48.0, 45.6, 34.6, 34.4, 32.9, 32.7, 32.5, 32.3, 32.2, 31.8, 31.6, 31.5, 29.6, 29.5, 29.4, 29.2, 29.2, 29.0, 27.4, 27.4, 25.2, 22.6, 22.6, 20.6, 14.0, 14.0, 11.3. MS ((+) ESI; Exact mass): calc'd for $C_{74}H_{142}N_3O_{10}^+$ = 1233.07 amu, obtained = 1232. 87 amu. Following the general procedure, **2-11c** was prepared from **2-10** (0.030 g, 0.17 mmol) in dried DCM (1.62 mL). To this, HOBt (0.026 g, 0.20 mmol), HBTU (0.074 g, 0.20 mmol), **2-9c** (0.200 g, 0.162 mmol), and triethylamine (0.068 mL, 0.49 mmol) **2-12c** was prepared from TFA (5 mL) and **2-11c** affording a light brown oil. MS ((+) ESI; Exact mass): calc'd for $C_{76}H_{145}N_4O_{11}^+$ = 1290.09 amu, obtained = 1289.93 amu.

2-12d:

Following the general procedure, **2-8d** was prepared from **2-7** (0.088 g, 0.36 mmol) in dried DCM/DMF (18.2 mL/18.2 mL;10 mM). HBTU (0.329 g, 0.867 mmol), **2-6d** (0.500 g, 0.801 mmol) and triethylamine (0.20 mL, 1.5 mmol) **2-9d** was prepared from TFA (5 mL) and **2-8d** affording a white waxy solid in a 51%

yield (0.248 g). The crude product was subsequently characterized as no chromatography was necessary.[1]H-NMR (300 MHz, $CDCl_3$) δ: 7.07 (d, 2H, J=8.6 Hz), 4.46 (m, 2H), 4.25 (m, 4H), 4.13 (m, 4H), 3.26 (s, 4H), 2.32 (t, 8H, J=7.8 Hz), 1.60 (m, 8H) 1.25 (s, 112H), 0.87 (t, 12H, J=6.8 Hz). [13]C-NMR (75 MHz, $CDCl_3$) δ: 174.0, 170.8, 62.9, 52.8, 48.1, 34.3, 32.1, 29.9, 29.7, 29.6, 29.5, 29.4, 25.1, 22.9, 14.3. MS ((+) ESI; Exact mass): calc'd for $C_{82}H_{158}N_3O_{10}^+$ = 1345.19 amu, obtained = 1345.07 amu. Following the general procedure, **2-11d** was prepared from **2-10** (0.013 g, 0.074 mmol) in dried DCM/DMF (3.7 mL/ 3.7 mL;10 mM). To this, HOBt (0.012 g, 0.085 mmol), HBTU (0.032 g, 0.085 mmol), **2-9d** (0.0950 g, 0.0706 mmol), and triethylamine (0.030 mL, 0.21 mmol). **2-12d** was prepared from TFA (5 mL) and **2-11d** affording a light brown oil.

Synthesis of PEG-Lipids:

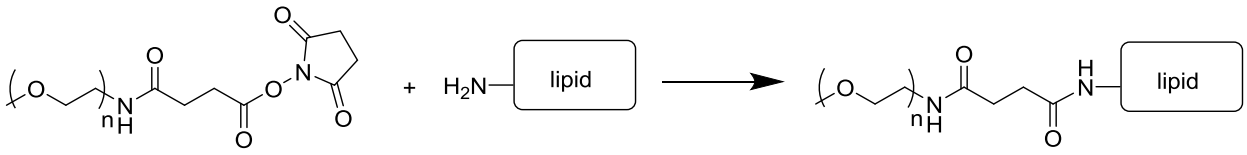

Scheme A1.3: Amide formation between PEG-NHS and the free primary amine on the synthetic lipids

General Procedure:

An equimolar mixture of **2-5** and **2.6(a-d)** was made to a concentration of 0.12M in pyridine in a vial. The vial was then sealed, the solution heated to 55 °C and stirred for 48 hours. Following completion, as monitored by TLC (silica gel, MeOH/DCM as eluent, visualised by iodine), the pyridine was removed on a roto-evaporator and the resulting mixture was purified by flash column chromatography on silica gel, using MeOH/DCM as the eluent.

PEG-G_1-C14:

Prepared following the general procedure from **2-5** (0.111 g, 0.0488 mmol) and **2.6a** (0.025 g, 0.049 mmol). A white solid was isolated in a 70% yield (0.087 g). [1]H-NMR (300 MHz, $CDCl_3$) δ: 4.41 (m, 1H), 4.16 (m, 2H), 4.07 (m, 2H), 3.40-3.90

(m, 174H), 3.38 (s, 3H), 2.51 (s, 4H), 2.31 (t, 4H, 7.8 Hz), 1.59 (m, 4H), 1.24 (s, 40H), 0.87 (t, 6H, J=7.0 Hz). ESI-MS see Figure 2.6.

PEG-G_1-C16:

Prepared following the general procedure from **2-5** (0.100 g, 0.0440 mmol) and **2.6b** (0.025 g, 0.44 mmol). A white solid was isolated in a 66% yield (0.076 g). ^{1}H-NMR (300 MHz, $CDCl_3$) δ: 6.66 (d, 1H, J= 8.3 Hz), 6.53 (m, 1H), 4.40 (m, 1H), 4.16 (m, 2H), 4.07 (m, 2H), 3.38-3.90 (m, 174H), 3.37 (s, 3H), 2.51 (s, 4H), 2.31 (t, 4H, J=7.5 Hz), 1.59 (m, 4H), 1.25 (s, 48H), 0.87 (t, 6H, J=6.8 Hz). ESI-MS see Figure 2.7

PEG-G_1-dC16:

Prepared following the general procedure from **2-5** (0.100 g, 0.0440 mmol) and **2.6c** (0.025 g, 0.044 mmol). A gel-like colorless solid was isolated in a 68% yield (0.087 g). ^{1}H-NMR (300 MHz, $CDCl_3$) δ: 4.40 (m, 1H), 4.19 (m, 2H), 4.04 (m, 2H), 3.39-3.90 (m, 174), 3.38 (s, 3H), 2.51 (s, 4H), 2.34 (m, 2H), 1.57, 1.45 (m, 8H), 1.25 (s, 40H), 0.87 (t, 12H, J=7.2 Hz). ESI-MS see Figure 2.8.

PEG-G_1-C18:

Prepared following the general procedure from **2-5** (0.091 g 0.040 mmol) and **2.6d** (0.025 g, 0.040 mmol). A white solid was isolated in a 67% yield (0.071 g). ^{1}H-NMR (300 MHz, $CDCl_3$) δ: 6.69 (d, 1H, J= 8.9 Hz), 6.61 (m, 1H), 4.41 (m, 1H,), 4.16 (m, 2H), 4.07 (m, 2H), 3.38-3.90 (m, 174H), 3.37 (s, 3H), 2.51 (s, 4H), 2.31 (t, 4H, J=7.8 Hz), 1.61 (m, 4H), 1.24 (s, 56H), 0.87 (t, 6H, J=7 Hz). ESI-MS see Figure 2.9.

PEG-G_2-C14:

Prepared following the general procedure from was added **2-5** (0.098 g, 0.043 mmol) and crude **2.12a** (0.051 g, 0.043 mmol). A white solid was isolated in a 52% yield (0.072 g). ^{1}H-NMR (300 MHz, $CDCl_3$) δ: 4.39 (m, 2H) 3.89-4.26 (m, 14H),

3.37-3.90 (m, 174H), 3.36 (s, 3H), 2.52 (m, 4H), 2.31 (t, 4H, J=7.6 Hz), 2.29 (t, 4H, J=7.6 Hz), 1.24 (s, 80H), 0.86 (t, 12H, 6.8 Hz). ESI-MS see Figure 2.11.

PEG-G_2-C16:

Prepared following the general procedure from **2-5** (0.123 g, 0.054 mmol) and crude **2.12b** (0.070 g, 0.054 mmol). A white solid was afforded in 54% yield (0.096 g) ^{1}H-NMR (300 MHz, $CDCl_3$) δ: 4.38 (m, 2H), 3.88-4.26 (m, 14H), 3.37-3.87 (m, 174H), 3.36 (s, 3H), 2.53 (m, 4H), 2.31 (t, 4H, J=7.6 Hz), 2.29 (t, 4H, J=7.6 Hz), 1.24 (s, 96H), 0.86 (t, 12H, J=7.0 Hz). ESI-MS see Figure 2.12

PEG-G_2-dC16:

Prepared following the general procedure from **2-5** (0.130 g, 0.0572 mmol) and crude **2.12(c)** (0.074 g, 0.057 mmol). A white solid was afforded in 33% yield (0.061 g). ^{1}H-NMR (300 MHz, $CDCl_3$) δ: 6.74 (s, 1H), 6.66 (d, 1H, J= 7.5 H), 6.47 (s, 1H), 4.40 (m, 2H), 3.87-4.22 (m, 14H), 3.36-3.87 (m, 174H), 3.35 (s, 3H), 2.51 (m, 4H), 2.31 (m, 4H), 1.42, 1.53 (m, 16H), 1.22 (s, 80H), 0.85 (t, 24H, J= 7.0 Hz) . ESI-MS see Figure 2.13.

PEG-G_2-C18:

Prepared following the general procedure from **2-5** (0.065 g, 0.029 mmol) and crude **2.12d** (0.040 g, 0.029 mmol, 1.0 equiv.). A gel-like solid was isolated in a 47% yield (0.047 g). ^{1}H-NMR (300 MHz, $CDCl_3$) δ: 4.39 (m, 2H), 3.89-4.27 (m, 14H), 3.38-3.89 (m, 174H), 3.37 (s, 3H), 2.53 (m, 4H), 2.32 (t, 4H, J=7.4 Hz), 2.29 (t, 4H, J=7.4 Hz), 1.24 (s, 112H), 0.87 (t, 12H, J=7.0 Hz) . ESI-MS see Figure 2.14.

2-14a: Asymmetric Disulfide Formation:

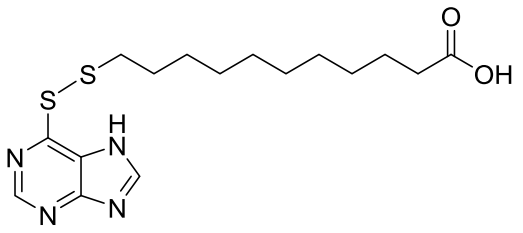

2-14a

In a round bottom flask was dissolved 6-mercaptopurine monohydrate (0.500 g, 2.94 mmol) and **2-13** (0.641 g, 2.94 mmol) in DMSO (9.0 mL; 0.33M). While the reaction was stirred, solid DDQ (0.669 g, 2.94 mmol) was slowly added over 10 minutes and then left at room temperature for 1 hour. The reaction was monitored by TLC (silica gel, MeOH/DCM as eluent, visualized by iodine). Following completion, the product was precipitated by adding 20 mL water to the reaction solution. The resulting mixture was left for 6 hours before being vacuum filtered and isolating a red solid was isolated. The crude product was redissolved in hot methanol and cooled in an ice water bath then vacuum filtered. A white powder was afforded in a 60% yield (0.622 g). ^{1}H-NMR (300 MHz, DMSO-d^{6}) δ: 8.84 (s, 1H), 8.57 (s, 1H), 2.96 (t, 2H, J= 7.0 Hz), 2.21 (t, 2H, J=7.3 Hz), 1.67 (quintet, 2H, J=7.5 Hz), 1.50, 1.40 (m, 4H), 1.25 (s, 10H). ^{13}C-NMR (75 MHz, DMSO-d^{6}) δ: 174.4, 151.7, 38.1, 33.6, 28.8, 28.7, 28.5, 28.1, 27.6, 24.5. (MS ((+) ESI; Exact mass): calc'd for $C_{16}H_{25}N_4O_2S_2^+$ = 369.14 amu, obtained = 369.13 amu.

2-14b: Asymmetric Disulfide Formation:

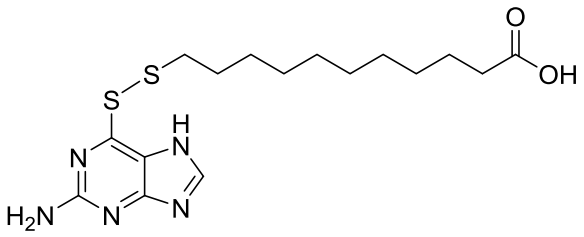

2-14b

In a round bottom flask was dissolved 6-thioguanine (0.500 g, 2.99 mmol) and **2-13** (0.652 g, 2.99 mmol) in DMSO (0.15M). While the reaction was stirred, solid DDQ (0.679 g, 2.99 mmol) was slowly added over 10 minutes and then left at room temperature for 1 hour. The reaction was monitored by TLC (silica gel, MeOH/DCM as eluent, visualized by iodine). Following completion, the product was precipitated by adding water to the reaction solution. The resulting mixture was left for 6 hours before being vacuum filtered and isolating a red solid was isolated. The crude product was redissolved in hot acetone and cooled in an ice water bath then vacuum filtered. A yellowish powder was afforded in 64% yield (0.707 g). ^{1}H-NMR (300 MHz, DMSO-d^{6}) δ: 7.98 (s, 1H), 6.45 (s, 2H), 2.90 (t, 2H, J=7.1 Hz), 2.17 (t, 2H, J=8.4 Hz), 1.62 (quintet, 2H, J=7.0), 1.46, 1.35 (m, 4H), 1.21 (s, 10H). ^{13}C-NMR (75 MHz, $CDCl_3$) δ: 174.5, 159.9 156.9, 140.1, 38.10, 33.6, 28.8, 28.7, 28.5, 28.01, 27.7, 24.5. MS ((+) ESI; Exact mass): calc'd for $C_{16}H_{26}N_5O_2S_2^+$ = 384.15 amu, obtained = 384.27 amu.

LDC: Lipid Coupling:

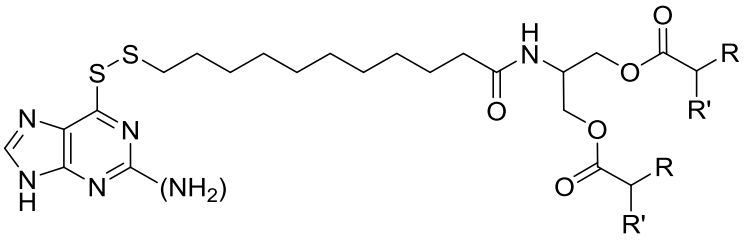

6MP-C14: R= $C_{12}H_{25}$; R'= H
6MP-C16: R= $C_{14}H_{29}$; R'= H
6MP-dC16: R= C_8H_{17}; R'=C_6H_{13}
6MP-C18: R= $C_{16}H_{33}$; R' = H
6TG-C14: R= $C_{12}H_{25}$; R'= H
6TG-C16: R= $C_{14}H_{29}$; R'= H
6TG-dC16: R= C_8H_{17}; R'=C_6H_{13}

General Procedure:

In a round bottom flask was dissolved **2-14(a-b)** (1.1 equiv.) in dried DCM/DMF (1:1;10 mM). To this, HBTU (1.2 equiv.), **2-6(a-d)** (1.0 equiv.), and triethylamine (2.0 equiv.) were then added and the resulting solution was left stirring at room temperature for 20 hours. When the reaction was complete, visualized by ^{1}H-NMR, the reaction solution was diluted with EtOAc, and washed once with 1 M HCl and 3 times with H_2O. The organic layer was then dried over anhydrous sodium sulfate and then gravity filtered. DCM and EtOAc were removed by roto-evaporation. The crude product was purified by flash column chromatography on silica, using EtOAc/Hexanes as the eluent.

6MP-C14:

Prepared following the general procedure, **2-14a** (0.113 g, 0.308 mmol) in dried DCM/DMF (14.6 mL/ 14.6 mL;10 mM), HBTU (0.133 g, 0.352 mmol, 1.20 equiv.), **2-6a** (0.150 g, 0.293 mmol), and triethylamine (0.082 mL, 0.59 mmol). A light yellow solid was afforded in a 28% yield (0.072 g) ^{1}H-NMR (300 MHz, $CDCl_3$) δ: 11.75 (s, 1H), 8.90 (s, 1H), 8.22 (s, 1H), 6.02 (d, 1H, J= 8.3 Hz) 4.52 (m, 1H), 4.30 (m, 2H), 4.11 (m, 2H), 2.91(t, 2H, J=7.0 Hz), 2.32 (t, 4H, J=7.9 Hz), 2.02 (t, 2H, J=7.9 Hz), 1.66 (m, 6H), 1.26, 1.12 (m, 54H), 0.88 (t, 6H, J=7.0). MS ((+) ESI; Exact mass): calc'd for $C_{47}H_{84}N_5O_5S_2^+$ = 862.59 amu, obtained = 862.53 amu.

6MP-C16:

Prepared by the general procedure from **2-14a** (0.0648 g, 0.176 mmol) in dried DCM/DMF (9.0 mL/9.0 mL;10 mM), HBTU (0.112 g, 0.211 mmol), **2-6b** (0.0648 g, 0.176 mmol), and triethylamine (0.076 mL, 0.53 mmol) . A white solid was afforded in a 63% yield (0.102 g) ^{1}H-NMR (300 MHz, $CDCl_3$) δ: 12.88 (s, 1H), 8.91 (s, 1H), 8.29 (s, 1H), 6.05 (d, 1H, J=8.2 Hz), 4.50 (m, 1H), 4.26 (m, 2H), 4.09 (m, 2H), 2.91 (t, 2H, 7.1 Hz), 2.30 (t, 4H, J=7.6 Hz), 2.20 (t, 2H, J=7.1 Hz), 1.65 (m, 6H), 1.24, 1.17 (m, 62H), 0.87 (t, 6H, J=6.9 Hz). ^{13}C-NMR (75 MHz, $CDCl_3$) δ: 174.1, 173.8, 160.5, 152.6, 149.9, 142.0, 131.4, 62.9, 48.0, 39.3, 36.9, 34.3, 32.1, 29.9, 29.9, 29.8, 29.7, 29.6, 29.5, 29.4, 29.1, 28.7, 28.3, 25.9, 25.1, 22.9, 14.3. MS ((+) ESI; Exact mass): calc'd for $C_{51}H_{92}N_5O_5S_2^+$= 918.65 amu, obtained = 918.60 amu.

6MP-dC16:

Prepared by the general procedure from **2-14a** (0.136 g, 0.370 mmol) in dried DCM/DMF (17.5 mL/17.5 mL;10 mM), HBTU (0.160 g, 0.422 mmol), **2-6c** (0.200 g, 0.352 mmol), and triethylamine (0.126 mL, 0.704 mmol). A light yellow oil was afforded in a 42% yield (0.137 g) ^{1}H-NMR (300 MHz, $CDCl_3$) δ: 12.8 (s, 1H), 8.90 (s, 1H), 8.29 (s, 1H), 5.97 (d, 1H, J=8.8 Hz), 4.48 (m, 1H), 4.26 (m, 2H), 4.09 (m, 2H), 2.90 (t, 2H, J=7.3 Hz), 2.32 (m, 2H), 2.2 (m, 2H), 1.68, 1.55, 1.42 (m, 14H), 1.22, 1.16 (m, 50H), 0.85 (t, 12H, J=6.9 Hz). ^{13}C (75 MHz, $CDCl_3$) δ: 176.5, 173.3, 152.2, 142.0, 62.4, 48.0, 45.6, 39.1, 36.7, 32.3, 32.0, 31.8, 31.6, 29.7, 29.5, 29.4, 29.2, 29.2, 28.9, 28.5, 28.2, 27.4, 27.4, 25.6, 22.6, 22.6, 14.0, 14.0. MS ((+) ESI; Exact mass): calc'd for $C_{51}H_{92}N_5O_5S_2^+$= 918.65 amu, obtained = 918.53 amu.

6MP-C18:

Prepared by the general procedure from **2-14a** (0.062g, 0.168 mmol) in dried DCM/DMF (8.0 mL/8.0 mL;10 mM), HBTU (0.073 g, 0.19 mmol), **2-6d** (0.100 g,

0.160 mmol), and triethylamine (0.045 mL, 0.32 mmol). A white solid was afforded in a 32% yield (0.050 g). ^{1}H-NMR (300 MHz, $CDCl_3$) δ: 8.91 (s, 1H), 8.27 (s, 1H), 6.01 (d, 1H, J=8.3 Hz), 4.50 (m, 1H), 4.26 (m, 2H), 4.09 (m, 2H), 2.90 (t, 2H, J=7.2 Hz), 2.30 (t, 4H, J=7.8 Hz), 2.20 (t, 2H, J=7.8 Hz), 1.68, 1.59 (m, 6H), 1.24, 1.15 (m, 70H), 0.87 (t, 6H, J=6.9 Hz). ^{13}C-NMR (75 MHz, $CDCl_3$) δ: 173.8, 173.5, 152.3, 62.7, 47.7, 39.1, 36.7, 34.1, 31.9, 29.7, 29.6, 29.5,, 29.3, 29.2, 29.1, 29.1, 29.0, 28.9, 28.8, 28.4, 28.0, 25.6, 24.9, 22.7, 14.1. MS ((+) ESI; Exact mass): calc'd for $C_{55}H_{100}N_5O_5S_2^+$ = 974.72 amu, obtained = 974.67 amu.

6TG-C14:

Prepared by the general procedure from **2-14b** (0.118 g, 0.308 mmol) in dried DCM/DMF (14.6 mL/ 14.6 mL;10 mM), HBTU (0.133 g, 0.352 mmol), **2-6a** (0.150 g, 0.293 mmol), and triethylamine (0.082 mL, 0.586 mmol). A light yellow solid was afforded in 18% yield (0.047 g) ^{1}H-NMR (300 MHz, $CDCl_3$) δ: 7.92 (s, 1H), 6.10 (d, 1H, J=8.10 Hz), 5.31 (s, 2H), 4.52 (m, 1H), 4.29 (m, 2H), 4.12 (m, 2H), 2.88 (t, 2H, J=7.3 Hz), 2.32 (t, 4H, J=7.3 Hz), 2.18 (t, 2H, J=7.3 Hz), 1.68, 1.59 (m, 6H), 1.25, 1.18 (m, 54H), 0.88 (t, 6H, J=6.9 Hz). ^{13}C-NMR (75 MHz, $CDCl_3$) δ: 174.1, 173.7, 159.7, 139.6, 63.0, 48.0, 39.4, 36.9, 34.3, 32.1, 29.9, 29.9, 29.8, 29.7, 29.6, 29.5, 29.4, 29.4, 29.3, 29.1, 28.7, 28.3, 25.8, 14.3. MS ((+) ESI; Exact mass): calc'd for $C_{47}H_{85}N_6O_5S_2^+$= 877.60 amu, obtained = 877.67 amu.

6TG-C16:

Prepared by the general procedure from **2-14b** (0.068 g, 0.18 mmol) in dried DCM/DMF (8.8 mL/ 8.8 mL;10 mM), HBTU (0.112 g, 0.211 mmol), **2-6b** (0.120 g, 0.18 mmol), and triethylamine (0.076 mL, 0.53 mmol) A light yellow solid was afforded in a 49% yield (0.081 g). ^{1}H-NMR (300 MHz, $CDCl_3$) δ: 11.23 (s, 1H), 7.87 (s, 1H), 6.08 (d, 1H, J=8.4 Hz), 5.24 (s, 2H), 4.51 (m, 1H), 4.29 (m, 2H), 4.11 (m, 2H), 2.87 (t, 2H, J=7.0 Hz), 2.31 (t, 2H, J=7.5 Hz), 2.17 (t, 2H, J=7.6 Hz), 1.68, 1.60 (m, 6H), 1.24, 1.17 (m, 62H), 0.87 (t, 6H, J=7.0 Hz). ^{13}C-NMR (75

MHz, $CDCl_3$): 173.9, 173.5, 159.4, 62.8, 47.7, 39.2, 36.6, 34.1, 31.9, 29.7, 29.6, 29.4, 29.3, 29.2, 29.1, 29.0, 29.0, 28.8, 28.4, 28.1, 25.6, 24.9, 22.7, 14.1. MS ((+) ESI; Exact mass): calc'd for $C_{51}H_{93}N_6O_5S_2^+$ = 933.66 amu, obtained = 933.73 amu.

6TG-dC16:

Prepared by the general procedure from **2-14b** (0.071 g, 0.19 mmol) in dried DCM/DMF (8.8 mL/8.8 mL;10 mM), HBTU (0.080 g, 0.21), **2-6c** (0.100 g, 0.176 mmol), and triethylamine (0.049 mL, 0.35 mmol). A light yellow liquid was afforded in a 37% yield (0.061 g) ^{1}H-NMR (300 MHz, $CDCl_3$) δ: 7.88 (s, 1H), 6.05 (d, 1H, J=8.2 Hz), 5.20 (s, 2H), 4.50 (m, 1H), 4.30 (m, 2H), 4.12 (m, 2H), 2.87 (t, 2H, J=7.1 Hz), 2.35 (m, 2H), 2.15 (t, 2H, J=7.4 Hz), 1.68, 1.57, 1.45 (m, 14H), 1.24, 1.16 (m, 50H) 0.86 (t, 12H, J=6.5 Hz). ^{13}C-NMR (75 MHz, $CDCl_3$) δ: 176.7, 173.3, 159.4, 62.5, 48.0, 45.7, 39.1, 36.6, 32.3, 31.8, 31.6, 29.7, 29.6, 29.4, 29.3, 29.2, 29.1,29.0, 29.0, 28.8, 28.4, 28.0, 27.4, 27.4, 25.5, 22.6, 22.6, 14.1, 14.00. MS ((+) ESI; Exact mass): calc'd for $C_{51}H_{93}N_6O_5S_2^+$ = 933.66 amu, obtained = 933.60 amu.

Appendix 2: Preparation and Stability of Lipid Nanoparticles

A2.1: Lipid Nanoparticle Preparation

SLNP Preparation: SNPs were prepared using a NanoAssemblr™ microfluidic mixer by the controlled mixing of ethanol solutions of lipid mixture with aqueous buffer. The molar composition used in formulating the SNPs was 1.5:10:38.5:50 (PEG-Lipid: Neutral Lipid: Cholesterol: Cationic/Ionizable Lipid) and with a lipid concentration of 12.5 mM. Stock solutions were made up in ethanol and the required amounts were transferred and then made to the required concentration by dilution with ethanol. The lipid mixture was made up in an Eppendorf tube from stock solutions of PEG-lipid (see Table A2.1), DSPC (20 mg/mL; volume added: 27.2 uL), DOTMA (40 mg/mL; volume added: 57.6 uL)), and cholesterol (20 mg/mL; volume added: 51.2 uL).The final volume was made up to a total volume of 0.55 mL with additional ethanol (see Table A2.1). The mixture was then sealed and heated to 43 °C for 5 minutes in the oven. A stock solution of the dsDNA oligomer (50.00 mg/mL) was made up in PBS buffer (10.0 mM Na_3PO_4, 0.154 M NaCl, and made to pH 7.4 using concentrated HCl, in Millipore water). To a glass vial, 6.0 uL of the dsDNA stock solution was added and made up to a volume of 2.244 mL with sodium acetate buffer (25.00 mM; pH 4 using concentrated HCl to adjust the pH).

Prior to each SLNP preparation, the NanoAssembler™ cartridge was washed with the sodium acetate buffer in a 3 mL syringe (left port) and ethanol in a 3 mL syringe (right port) with a 12 mL/min. flow rate and a 1:1 (aqueous:ethanol ratio) flow ratio. A total of 4 mL of wash was collected and discarded. The NanoAssemblr™ microfluidic mixer was then used to make the SNPs. In a 3 mL syringe (left port) was loaded the 2.244 mL aqueous dsDNA solution and in another 3 mL syringe (right port) was loaded the 0.55 mL lipid mixture. The flow rate was set to 12 mL/min., the flow ratio to 3:1 (aqueous: EtOH), and the total

volume collected set to 2 mL with the initial 300 uL at the beginning and 50 uL at the end being discarded. The collected formulation was immediately transferred to a 3 mL Slide-A-Lyzer® Dialysis Cassette G2 (10,000 molecular weight cutoff) and dialyzed against PBS buffer for 6 hours. The PBS was refreshed after 3 hours and the removal of ethanol from the formulation was monitored using potassium dichromate (stable orange colour without greenish reaction indicated EtOH removal).

Diameters of the SNPs were determined by dynamic light scattering (DLS) experiments (on a Brookhaven Instrument, ZetaPALS particle sizing software) The SNPs were then stored at 4 °C.

PEG-Lipid	PEG-Lipids [Stock] (mg/mL)	Volume of PEG-Lipid Added (uL)	Volume of EtOH Added (uL)
PEG-G_1-C14	19.2	13.6	400.4
PEG-G_1-C16	18.6	14.4	399.6
PEG-G_1-dC16	17.4	15.4	398.6
PEG-G_1-C18	17.9	15.3	398.8
PEG-G_2-C14	30.6	10.8	403.3
PEG-G_2-C16	29.6	11.6	402.5
PEG-G_2-dC16	29.0	11.8	402.3
PEG-G_2-C18	30.3	11.7	402.4
DSG-PEG	20.0	13.5	400.5
DSPE-PEG	10.0	28.9	385.1

Table A2.1: Concentrations of PEG-lipid solutions and required volumes for formulations containing 1.5 mol% of different PEG-lipids. The composition for these SLNPs was 50: 10: 38.5: 1.5 (DOTMA: DSPC: Cholesterol: PEG-lipid) with a DNA loading of 5.1 wt%.

PEG-Lipids	SNP Diameter (nm)	Polydispersity
PEG-G_1-C14	104.5 ± 1.5	0.307 ± 0.006
PEG-G_1-C16	76.9 ± 0.7	0.259 ± 0.004
PEG-G_1-dC16	156.1± 1.9	0.248 ± 0.008
PEG-G_1-C18	146.1± 1.4	0.335 ± 0.003
PEG-G_2-C14	181.4 ± 21.4	0.280 ± 0.137
PEG-G_2-C16	211.1± 4.8	0.373 ± 0.016
PEG-G_2-dC16	119.5 ± 7.1	0.351± 0.025
PEG-G_2-C18	165.6 ± 11.3	0.394 ± 0.031
DSG-PEG	80.5 ± 0.9	0.268 ± 0.005
DSPE-PEG	89.0 ± 0.4	0.297± 0.002

Table 3.2: Physical characterization of the SNP formulations immediately following preparation for formulations containing 1.5 mol% of different PEG-lipids. The composition for these SLNPs was 50: 10: 38.5: 1.5 (DOTMA: DSPC: Cholesterol: PEG-lipid) with a DNA loading of 5.1 wt%.

LDC Preparation: Stock solutions of lipids were made up in ethanol with a lipid concentration of ~10 mM (see Table A2.3). In an eppendorf tube, the lipid mixture of PEG-lipid (5.00 mol %), DMPC (5.00 mol %), and LDC (90.00 mol %) was made up to a total volume of 0.25 mL with additional ethanol (see Table A2.3). The mixture was then heated to 43 °C for 5 minutes in the oven.

Prior to using, the NanoAssembler™ cartridge was washed with PBS buffer in a 3 mL syringe (left port) and ethanol in a 3 mL syringe (right port) with a 12 mL/min. flow rate and a 1:1 (aqueous:ethanol ratio) flow ratio. A total of 4 mL of wash was collected and discarded. The NanoAssemblr™ microfluidic mixer was then used to make the LDCs. In a 3 mL syringe (left port) was loaded 2 mL PBS buffer and in another 3 mL syringe (right port) was loaded the 0.25 mL lipid mixture. The flow rate was set to 4 mL/min., the flow ratio to 3:1 (aqueous:EtOH), and the total volume collected 1 mL with the initial 300 uL at the beginning and 50 uL at the end being discarded. An aliquot (0.50 mL) of the collected formulation was then diluted to 0.40 mM (thiopurine) with PBS buffer, transferred to a 3 mL Slide-A-Lyzer® Dialysis Cassette G2 (10,000 molecular weight cutoff) and dialyzed against PBS buffer for 5 hours. The PBS was refreshed after 3 hours and the removal of ethanol from the formulation was monitored using potassium dichromate (VI). Diameters of the SNPs were determined by dynamic

light scattering (DLS) experiments (on a Brookhaven Instrument, ZetaPALS particle sizing software). The results are in Table A2.4. The SNPs were then stored at 4 °C.

LDC	LDC [Stock] (mg/mL)	Volume of LDC Added (uL)	Volume of DSPE-PEG Added (uL)	Volume of DMPC Added (uL)	Volume of EtOH Added (uL)
6MP-C14	10.0	204.0	36.9	8.9	0.0
6MP-C16	10.4	199.0	35.0	8.5	7.9
6MP-dC16	10.0	206.5	35.0	8.5	0.0
6MP-C18	12.4	168.9	33.4	8.1	39.7
6TG-C14	17.7	115.7	36.4	8.8	89.1
6TG-C16	13.7	151.1	34.6	8.4	55.9
6TG-dC16	16.6	124.8	34.6	8.4	82.3

Table A2.2: LDC composition with stock [DSPE-PEG] = 10.0 mg/mL and stock [DMPC] = 10.0 mg/mL where the composition was 90: 5: 5 (LDC monomer: DMPC: DSPE-PEG). The drug loading was 15 wt%.

LDC	LDC Diameter (nm)	Polydispersity (PDI)	Volume of PBS buffer Added (mL)
6MP-C14	489.7 ± 14.1	0.343 ± 0.007	2.59
6MP-C16	216.7 ± 7.7	0.288 ± 0.004	2.44
6MP-dC16	80.9 ± 0.9	0.277 ± 0.003	2.44
6MP-C18	560.3 ± 10.1	0.358 ± 0.010	2.30
6TG-C14	227.5 ± 11.3	0.346 ± 0.009	2.55
6TG-C16	102.2 ± 2.2	0.237 ± 0.006	2.40
6TG-dC16	64.8 ± 1.2	0.220 ± 0.007	2.40

Table A2.3: Physical Characterizations of LDC formulations immediately following dialysis where the composition was 90: 5: 5 (LDC monomer: DMPC: DSPE-PEG). The drug loading was 15 wt%.

A2.2: Lipid Nanoparticle Stability

LNP Stability Assay: The stability of the formulated SNPs was assessed under 6 conditions: LNPs were stored at 3 different temperatures; 4 °C, RT, and 37 °C, and incubated in 2 different media; PBS buffer and PBS buffer with 10% serum (by volume). To a polystyrene cuvette, 200 uL of LNPs solution and 2.30 mL of PBS buffer were added and the diameters measured in a DLS experiment. Cuvettes were then sealed and incubated under the indicated conditions. Diameter measurements were taken regularly. To a polystyrene cuvette, 200 uL of LNPs solution, 2.05 mL of PBS buffer, and 0.25 mL of serum were added and the diameters measured in a DLS experiment. Cuvettes were sealed and incubated under the indicated conditions. Stability results for the SLNPs and the LDCs are in Tables A2.5-A2.8 and Tables A2.9-A2.14, respectively.

Formulation	Day 1 Size (nm); PDI	Day 8 Size (nm); PDI
PEG-G_1-C14	104.5 ± 1.5; 0.307 ± 0.006	166.7 ± 2.4; 0.222 ± 0.004
PEG-G_1-C16	76.9 ± 0.7; 0.259 ± 0.004	144.2 ± 1.3; 0.212 ± 0.003
PEG-G_1-dC16	156.1 ± 1.9; 0.248 ± 0.008	176.6 ± 2.1; 0.232 ± 0.007
PEG-G_1-C18	146.1 ± 1.4; 0.335 ± 0.003	172.0 ± 1.6; 0.280 ± 0.002
DSG-PEG	80.5 ± 0.9; 0.268 ± 0.005	118.2 ± 1.3; 0.268 ± 0.005
DSPE-PEG	89.0 ± 0.4; 0.297 ± 0.002	126.2 ± 0.6; 0.293 ± 0.002

Table A2.4: SLNP storage stability at RT in PBS buffer for formulations containing 1.5 mol% of different PEG-lipids. The composition for these SLNPs was 50: 10: 38.5: 1.5 (DOTMA: DSPC: Cholesterol: PEG-lipid) with a DNA loading of 5.1 wt%.

Formulation	Day 1 Size (nm); PDI	Day 8 Size (nm); PDI
PEG-G$_1$-C14	134.1± 1.1 ; 0.350 ± 0.001	197.1 ± 1.6; 0.345 ± 0.001
PEG-G$_1$-C16	129.6 ± 1.4; 0.340 ± 0.000	225.1 ± 2.4; 0.381 ± 0.005
PEG-G$_1$-dC16	178.3 ± 5.5; 0.337 ± 0.005	249.1 ± 7.7; 0.338 ± 0.005
PEG-G$_1$-C18	166.8 ± 4.4; 0.345 ± 0.003	290.7 ± 7.7; 0.376 ± 0.003
DSG-PEG	117.9 ± 2.2; 0.357 ± 0.004	223.7 ± 4.2; 0.383 ± 0.004
DSPE-PEG	129.0 ± 4.8; 0.349 ± 0.005	212.3 ± 7.9; 0.389 ± 0.006

Table A2.5: SLNP storage stability at RT in PBS buffer with 10% serum for formulations containing 1.5 mol% of different PEG-lipids. The composition for these SLNPs was 50: 10: 38.5: 1.5 (DOTMA: DSPC: Cholesterol: PEG-lipid) with a DNA loading of 5.1 wt%.

Formulation	Day 1 Size (nm); PDI	Day 2 Size (nm); PDI	Day 5 Size (nm); PDI
PEG-G$_1$-C14	104.5 ± 1.5; 0.307 ± 0.006	175.2 ± 1.1; 0.194 ± 0.010	228.6 ± 1.4; 0.164 ± 0.008
PEG-G$_1$-C16	76.9 ± 0.7; 0.259 ± 0.004	157.2 ± 1.4; 0.204 ± 0.002	194.3 ± 1.7; 0.131 ± 0.001
PEG-G$_1$-dC16	156.1± 1.9; 0.248 ± 0.008	198.7 ± 7.5; 0.088 ± 0.042	180.5 ± 6.8; 0.363 ± 0.012
PEG-G$_1$-C18	146.1 ± 1.4; 0.335 ± 0.003	173.0 ± 1.4; 0.245 ± 0.008	216.3 ± 1.8; 0.204 ± 0.007
DSG-PEG	80.5 ± 0.9; 0.268 ± 0.005	299.1± 16.0; 0.230 ± 0.004	192.1 ± 10.3; 0.187 ± 0.003
DSPE-PEG	89.0 ± 0.4; 0.297 ± 0.002	136.5 ± 1.7; 0.255 ± 0.005	175.4 ± 2.2; 0.146 ± 0.003

Table A2.6: SLNP stability at 37°C in PBS buffer for formulations containing 1.5 mol% of different PEG-lipids. The composition for these SLNPs was 50: 10: 38.5: 1.5 (DOTMA: DSPC: Cholesterol: PEG-lipid) with a DNA loading of 5.1 wt%.

Formulation	Day 1 Size (nm); PDI	Day 2 Size (nm); PDI	Day 5 Size (nm); PDI
PEG-G_1-C14	134.1 ± 1.1; 0.350 ± 0.001	190.1± 2.8; 0.291 ± 0.012	194.8 ± 2.9; 0.349 ± 0.014
PEG-G_1-C16	129.6 ± 1.4; 0.340 ± 0.000	171.5 ± 1.9; 0.344 ± 0.005	165.3 ± 1.8; 0.351 ± 0.005
PEG-G_1-dC16	178.3 ± 5.5; 0.337 ± 0.005	211.1 ± 16.8; 0.194 ± 0.069	180.5 ± 14.4; 0.363 ± 0.047
PEG-G_1-C18	166.8 ± 4.4; 0.345 ± 0.003	237.9 ± 23.3; 0.320 ± 0.042	204.2 ± 19.9; 0.363 ± 0.048
DSG-PEG	117.9 ± 2.2; 0.357 ± 0.004	167.9 ± 9.4; 0.366 ± 0.002	120.5 ± 6.7; 0.356 ±0.002
DSPE-PEG	129.0 ± 4.8; 0.349 ± 0.005	149.4 ± 6.0; 0.370 ± 0.005	197.8 ± 7.9; 0.365 ± 0.005

Table A2.7: SLNP stability at 37°C in PBS buffer with 10% serum for formulations containing 1.5 mol% of different PEG-lipids. The composition for these SLNPs was 50: 10: 38.5: 1.5 (DOTMA: DSPC: Cholesterol: PEG-lipid) with a DNA loading of 5.1 wt%.

LDC	Day 1 Size(nm); PDI	Day 30 Size(nm); PDI	Day 60 Size(nm); PDI
6MP-C14	227.5 ± 11.3; 0.346 ± 0.009	1013.7 ± 85.4; 0.427 ± 0.036	--
6MP-C16	216.7 ± 7.7; 0.288 ± 0.004	220.2 ± 2.3; 0.209 ± 0.013	205.4 ± 2.1; 0.231 ± 0.014
6MP-dC16	80.9 ± 0.9; 0.277 ± 0.003	90.1 ± 0.5; 0.284 ± 0.002	100.5 ± 0.6; 0.296 ± 0.002
6MP-C18	560.3 ± 10.1; 0.358 ± 0.010	807.4 ± 10.8; 0.371 ± 0.003	--
6TG-C14	489.7 ± 14.1; 0.343 ± 0.007	438.4 ± 5.4; 0.267 ± 0.004	--
6TG-C16	102.2 ± 2.2; 0.237 ± 0.006	101.6 ± 0.3; 0.215 ± 0.008	113.9 ± 0.3; 0.279 ± 0.010
6TG-dC16	64.8 ± 1.2; 0.220 ± 0.007	73.8 ± 1.3; 0.245 ± 0.009	93.8 ± 1.7; 0.314 ± 0.012

Table A2.8: LDC storage stability at 4 °C in PBS buffer where the composition was 90: 5: 5 (LDC monomer: DMPC: DSPE-PEG). The drug loading was 15 wt%.

LDC	Day 1 Size(nm); PDI	Day 30 Size(nm); PDI
6MP-C16	160.7 ± 3.7; 0.399 ± 0.004	162.1 ± 4.8; 0.401 ± 0.007
6MP-dC16	126.8 ± 2.3; 0.406 ± 0.002	128.7 ± 2.6; 0.396 ± 0.003
6TG-C16	134.8 ± 3.1; 0.408 ± 0.002	138.4 ± 1.7; 0.405 ± 0.004
6TG-dC16	128.6 ± 7.4; 0.413 ± 0.004	131.7 ± 2.5; 0.405 ± 0.003

Table A2.9: LDC storage stability at 4 °C in PBS buffer with 10% serum where the composition was 90: 5: 5 (LDC monomer: DMPC: DSPE-PEG). The drug loading was 15 wt%.

LDC	Day 1 Size(nm); PDI	Day 30 Size (nm); PDI	Day 60 Size (nm); PDI
6MP-C16	216.7 ± 7.7; 0.288 ± 0.004	205.2 ± 7.3; 0.224 ± 0.003	220.5 ± 7.8; 0.212 ± 0.003
6MP-dC16	80.9 ± 0.9; 0.277 ± 0.003	83.3 ± 0.9; 0.259 ± 0.003	81.3 ± 0.9; 0.261 ± 0.003
6TG-C16	102.2 ± 2.2; 0.237 ± 0.006	121.6 ± 2.6; 0.147 ± 0.004	124.4 ± 2.7; 0.164 ± 0.004
6TG-dC16	64.8 ± 1.2; 0.220 ± 0.007	73.8 ± 1.4; 0.275 ± 0.009	69.5 ± 1.3; 0.219 ±0.007

Table A2.10: LDC storage stability at RT in PBS buffer where the composition was 90: 5: 5 (LDC monomer: DMPC: DSPE-PEG). The drug loading was 15 wt%.

LDC	Day 1 Size(nm); PDI	Day 30 Size (nm); PDI	Day 60 Size (nm); PDI
6MP-C16	160.7 ± 3.7; 0.399 ± 0.004	230.8 ± 5.3; 0.413 ± 0.004	309.0 ± 7.1; 0.418 ± 0.004
6MP-dC16	126.8 ± 2.3; 0.406 ± 0.002	163.5 ± 3.0; 0.397 ± 0.002	123.3 ± 2.3; 0.353 ± 0.002
6TG-C16	134.8 ± 3.1; 0.408 ± 0.002	134.4 ± 3.1; 0.407 ± 0.002	139.6 ± 3.2; 0.413 ± 0.002
6TG-dC16	128.6 ± 7.4; 0.413 ± 0.004	126.8 ± 7.3; 0.401 ± 0.004	199.8 ± 11.5; 0.433 ± 0.004

Table A2.11: LDC storage stability at RT in PBS buffer with 10% serum where the composition was 90: 5: 5 (LDC monomer: DMPC: DSPE-PEG). The drug loading was 15 wt%.

LDC	Day 1 Size(nm); PDI	Day 2 Size(nm); PDI	Day 3 Size (nm); PDI
6MP-C16	216.7 ± 7.7; 0.288 ± 0.004	262.1 ± 5.0; 0.208 ± 0.007	260.5 ± 2.5 ; 0.221 ± 0.010
6MP-dC16	80.9 ± 0.9; 0.277 ± 0.003	101.5 ± 4.2; 0.315 ± 0.007	95.0 ± 4.1; 0.309 ± 0.008
6TG-C16	102.2 ± 2.2; 0.237 ± 0.006	189.3 ± 5.7; 0.208 ± 0.011	182.5 ± 0.7; 0.173 ± 0.005
6TG-dC16	64.8 ± 1.2; 0.220 ± 0.007	72.9 ± 1.9; 0.251 ± 0.003	76.3 ± 1.8; 0.258 ± 0.013

Table A2.12: LDC storage stability at 37 °C in PBS buffer where the composition was 90: 5: 5 (LDC monomer: DMPC: DSPE-PEG). The drug loading was 15 wt%.

LDC	Day 1 Size(nm); PDI	Day 2 Size(nm); PDI	Day 3 Size (nm); PDI
6MP-C16	160.7 ± 3.7; 0.399 ± 0.004	189.3 ± 2.3; 0.393 ± 0.003	186.0 ± 1.3; 0.402 ± 0.008
6MP-dC16	126.8 ± 2.3; 0.406 ± 0.002	139.6 ± 16.8; 0.379 ± 0.001	134.4 ± 2.6; 0.388 ± 0.005
6TG-C16	134.8 ± 3.1; 0.408 ± 0.002	143.3 ± 7.1; 0.378 ± 0.008	139.2 ± 3.0; 0.388 ± 0.004
6TG-dC16	128.6 ± 7.4; 0.413 ± 0.004	154.3 ± 15.1; 0.387 ± 0.001	155.4 ± 2.8; 0.375 ± 0.004

Table A2.13: LDC storage stability at 37 °C in PBS buffer with 10% serum where the composition was 90: 5: 5 (LDC monomer: DMPC: DSPE-PEG). The drug loading was 15 wt%.

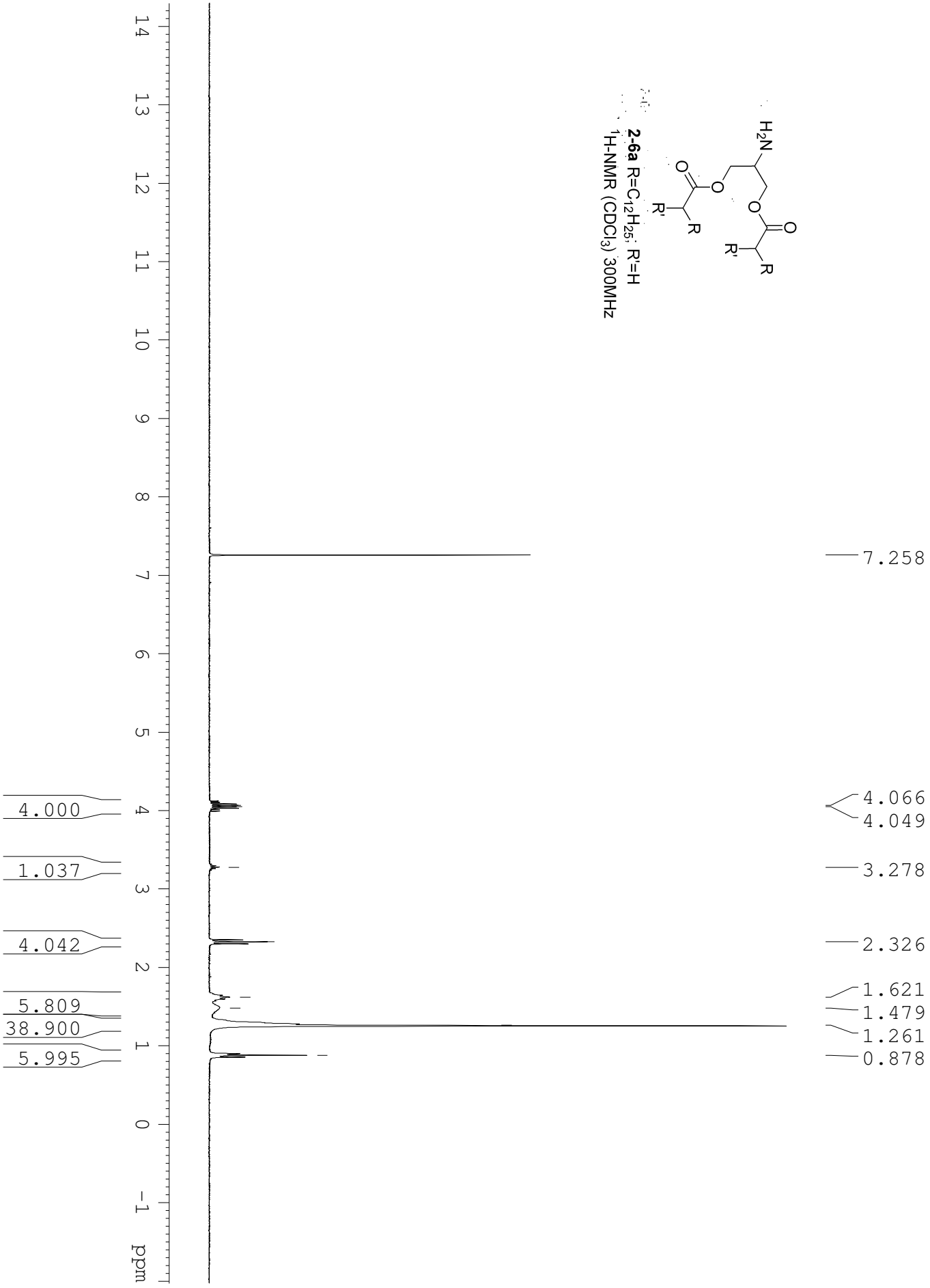
2-6a R=C12H25; R'=H
1H-NMR (CDCl3) 300MHz
H2N
O
R'
R
ppm
14
13
12
11
10
9
8
7
6
5
4
3
2
1
0
-1
7.258
4.066
4.049
3.278
2.326
1.621
1.479
1.261
0.878
4.000
1.037
4.042
5.809
38.900
5.995

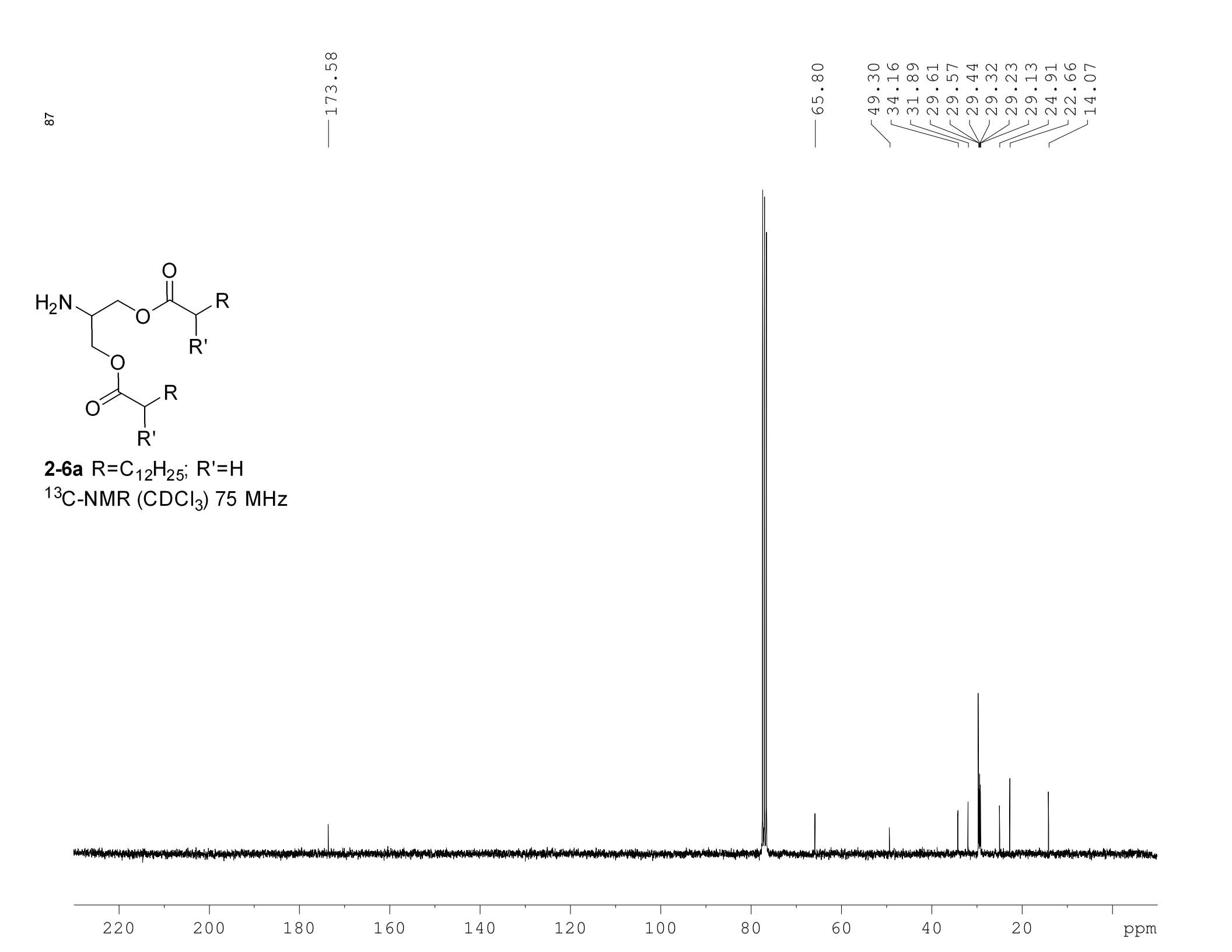

2-6a R=$C_{12}H_{25}$; R'=H

^{13}C-NMR ($CDCl_3$) 75 MHz

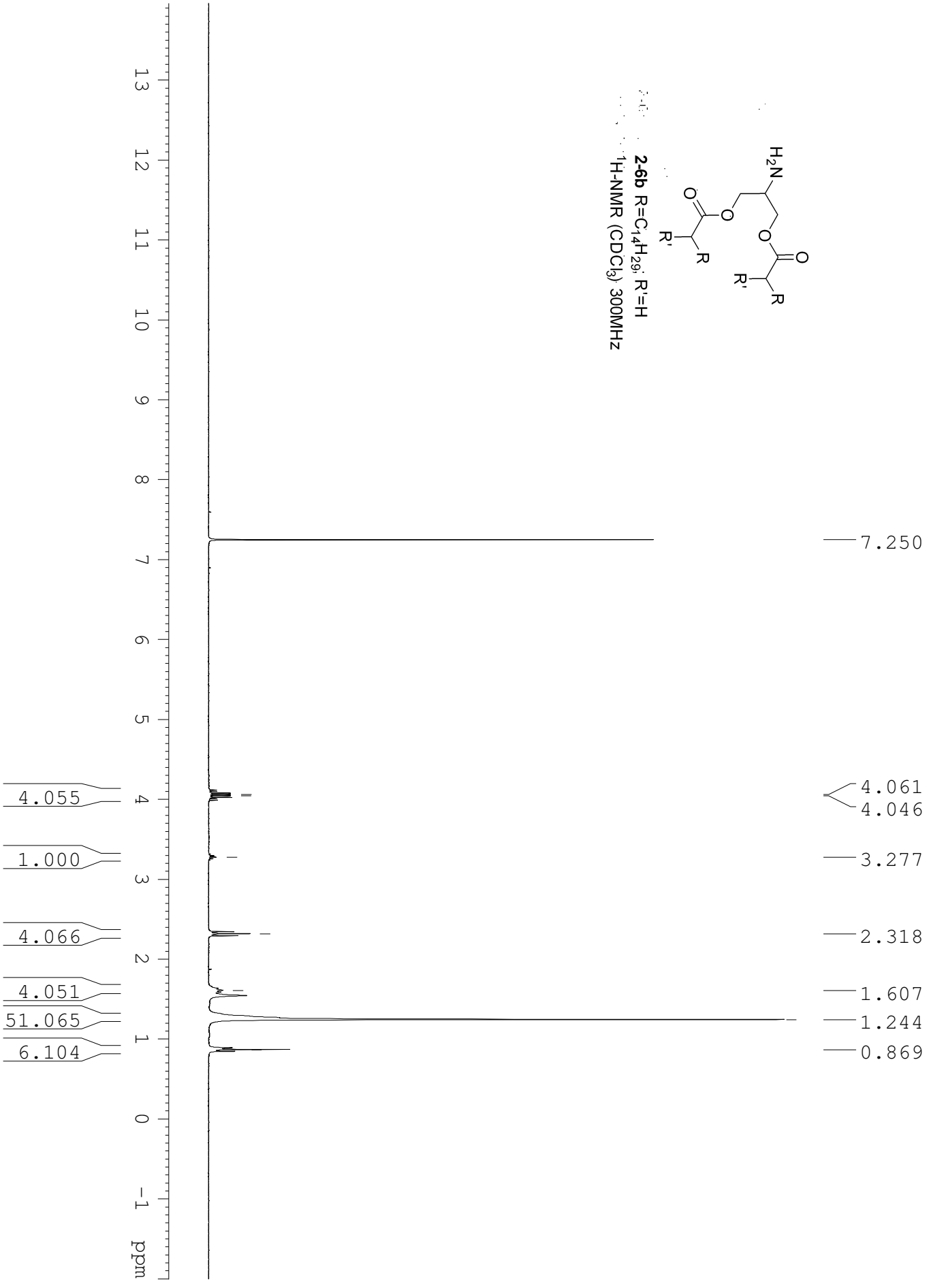
2-6b R=C14H29; R'=H
1H-NMR (CDCl3) 300MHz
H2N
O
R'
R
ppm
13
12
11
10
9
8
7
6
5
4
3
2
1
0
-1
7.250
4.061
4.046
3.277
2.318
1.607
1.244
0.869
4.055
1.000
4.066
4.051
51.065
6.104

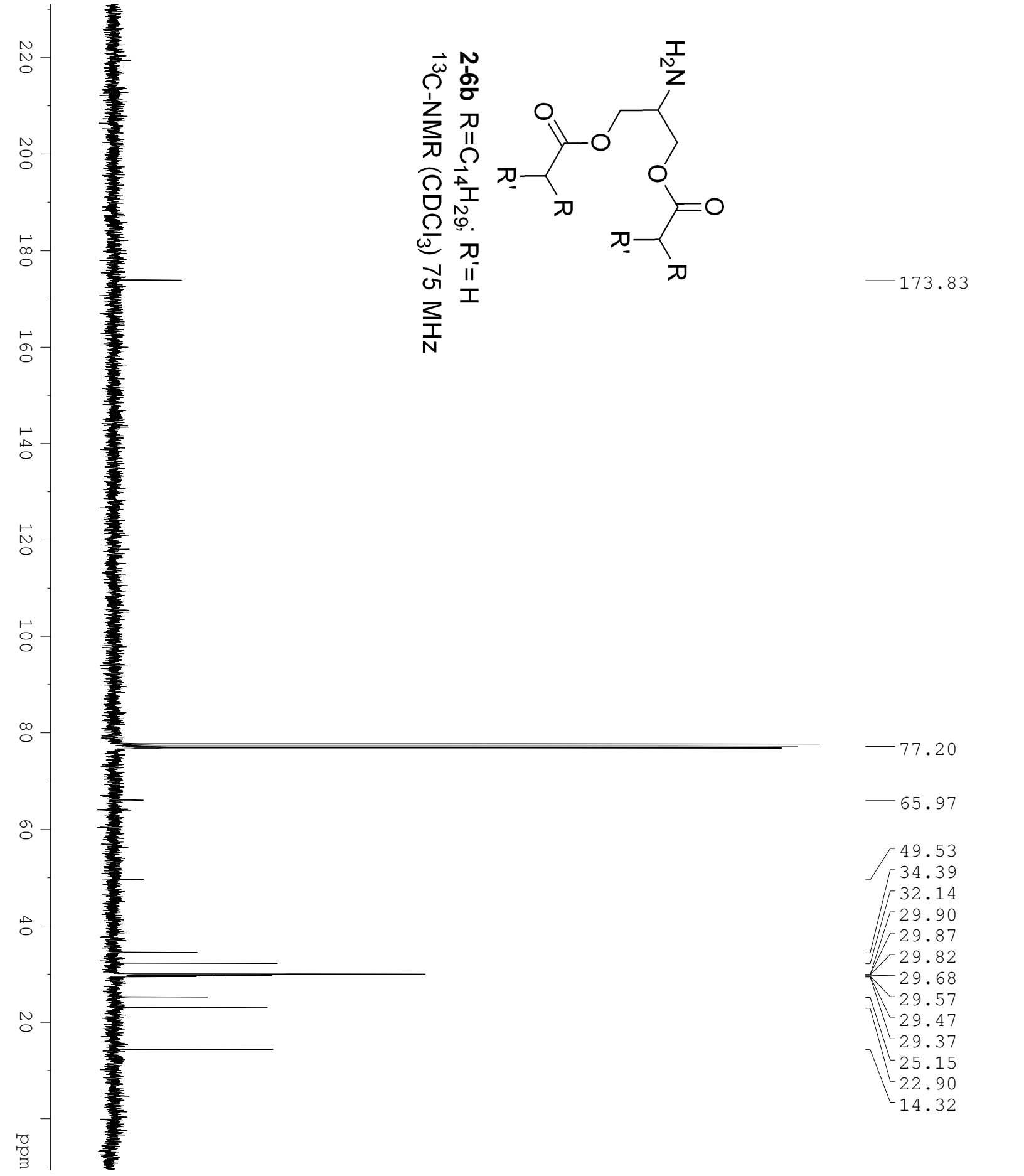
2-6b R=C14H29; R'= H
13C-NMR (CDCl3) 75 MHz
H2N
O
O
O
O
R'
R
R'
R
173.83
77.20
65.97
49.53
34.39
32.14
29.90
29.87
29.82
29.68
29.57
29.47
29.37
25.15
22.90
14.32
220
200
180
160
140
120
100
80
60
40
20
ppm

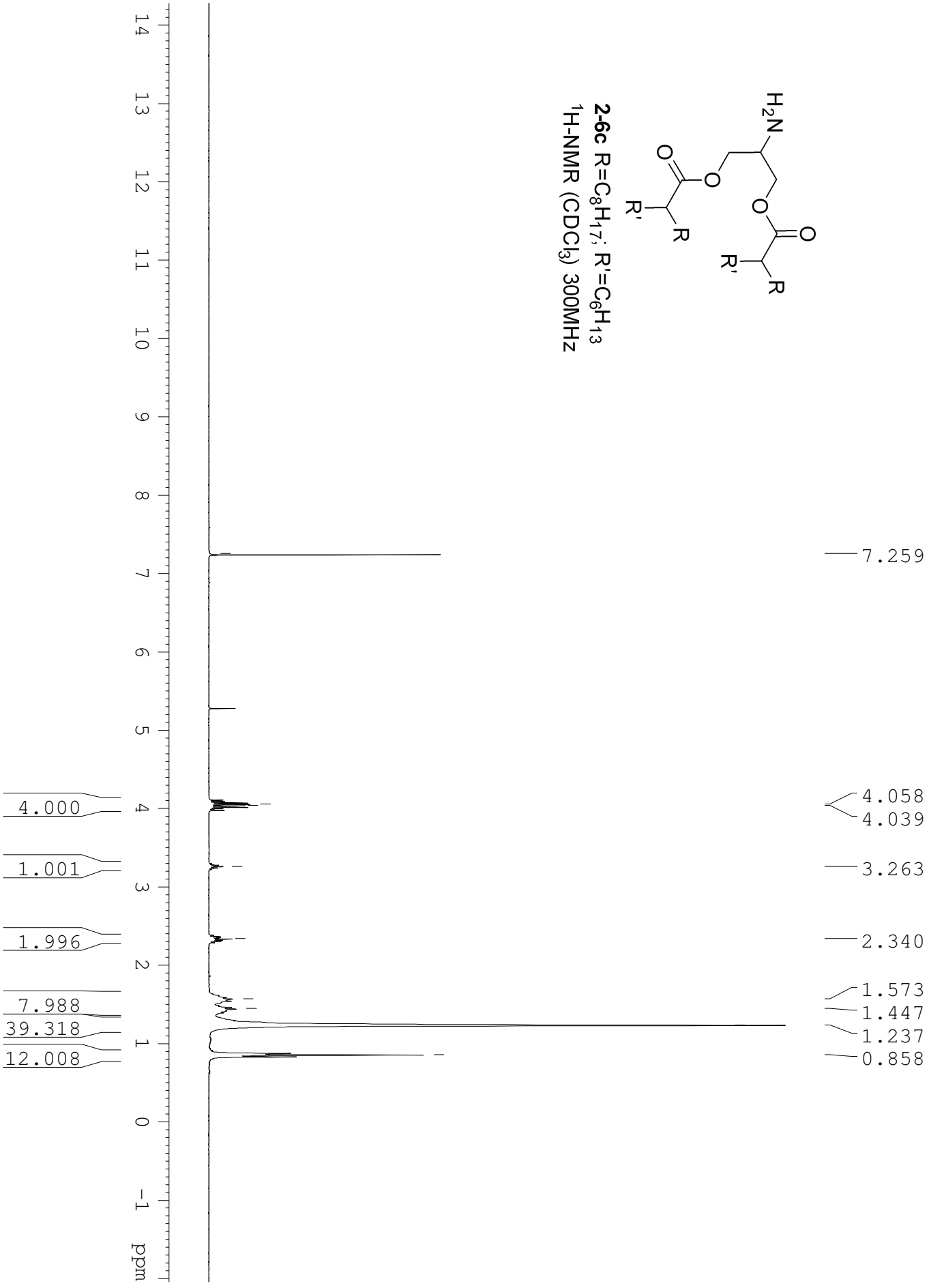
2-6c R=C8H17; R'=C6H13
1H-NMR (CDCl3) 300MHz
H2N
O
R'
R
7.259
4.058
4.039
3.263
2.340
1.573
1.447
1.237
0.858
4.000
1.001
1.996
7.988
39.318
12.008
ppm

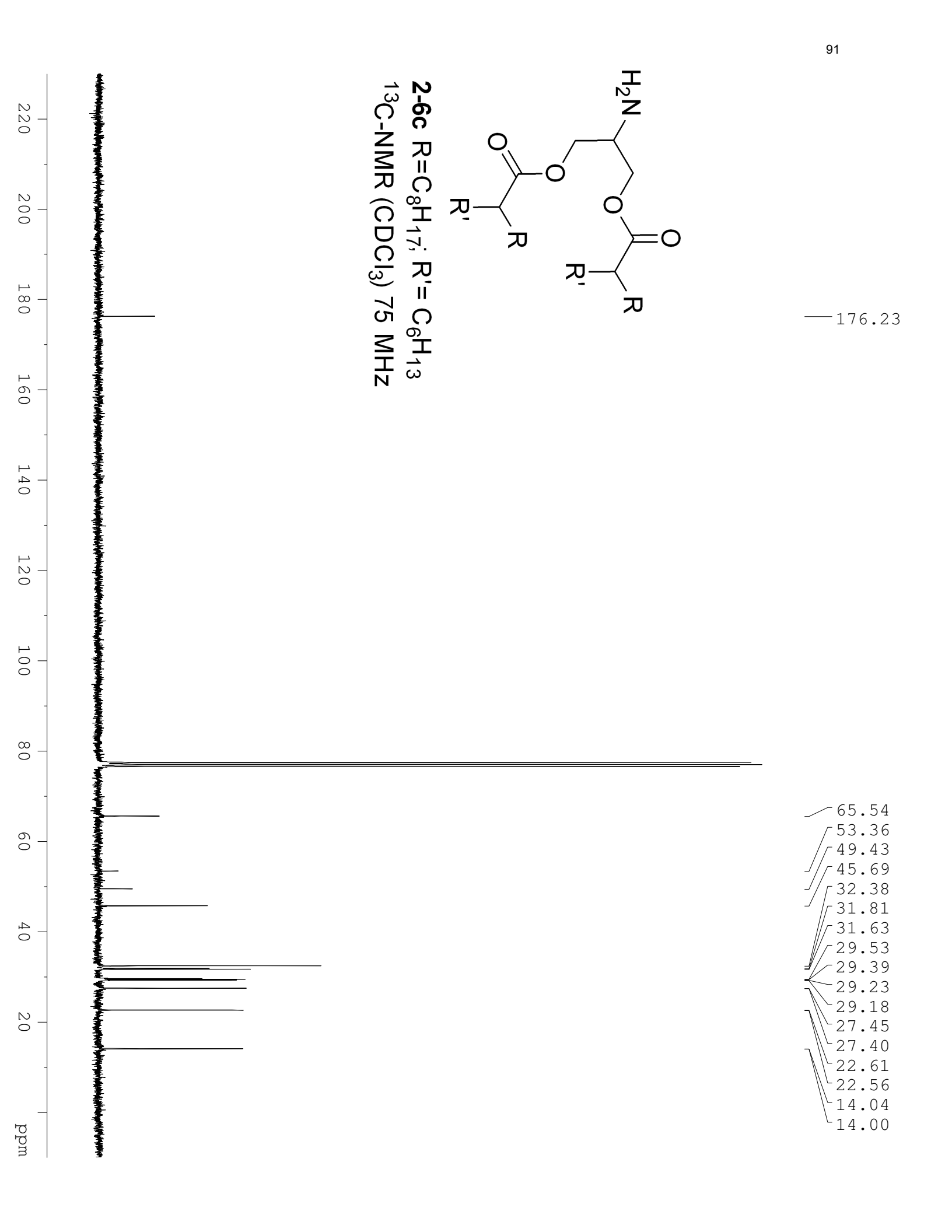
2-6c R=C8H17; R'= C6H13
13C-NMR (CDCl3) 75 MHz
H2N
O
O
O
O
R'
R
R'
R
176.23
65.54
53.36
49.43
45.69
32.38
31.81
31.63
29.53
29.39
29.23
29.18
27.45
27.40
22.61
22.56
14.04
14.00
220
200
180
160
140
120
100
80
60
40
20
ppm

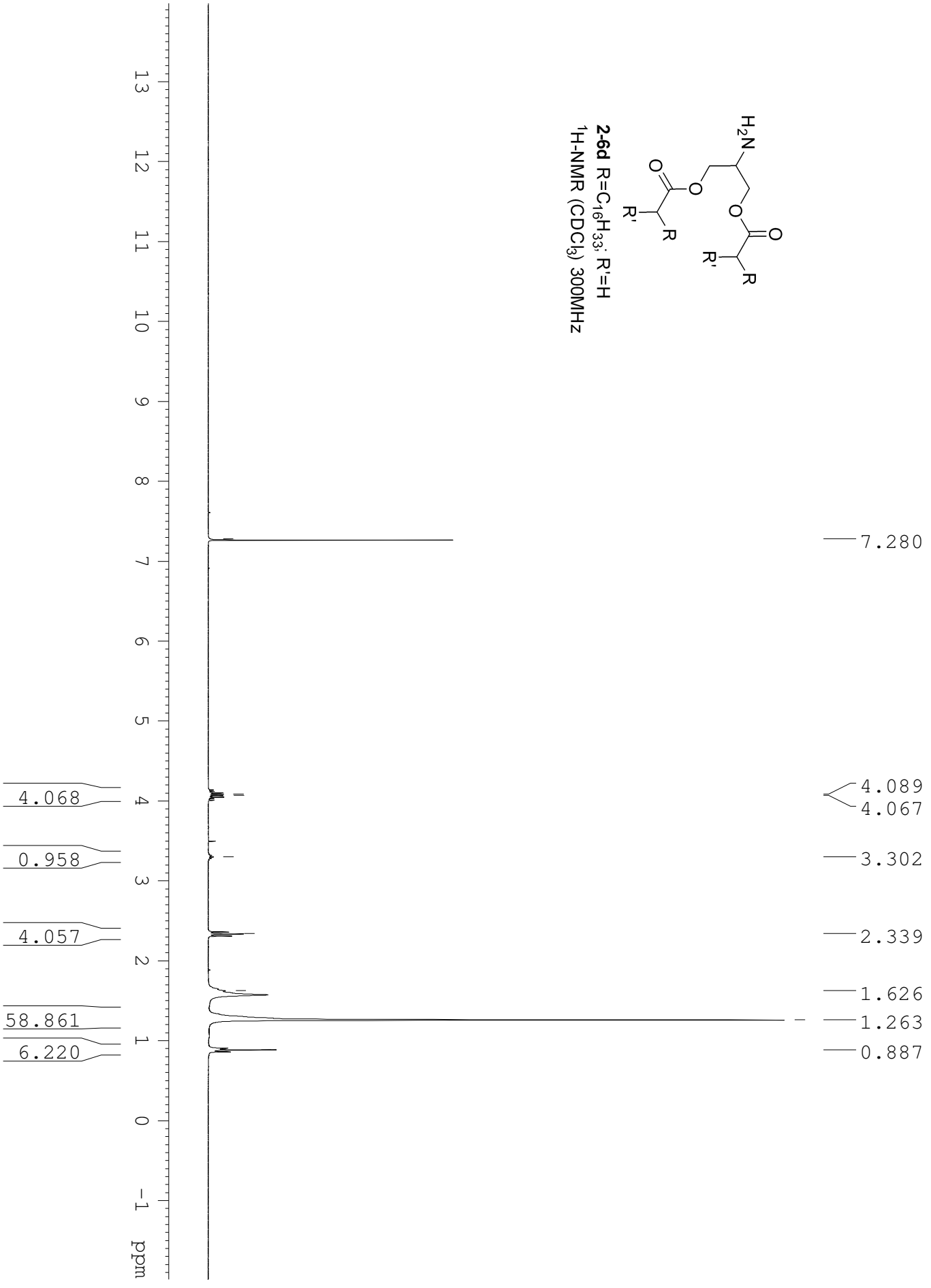
2-6d R=C16H33; R'=H
1H-NMR (CDCl3) 300MHz
H2N
O
R'
R
ppm
13
12
11
10
9
8
7
6
5
4
3
2
1
0
-1
7.280
4.089
4.067
3.302
2.339
1.626
1.263
0.887
4.068
0.958
4.057
58.861
6.220

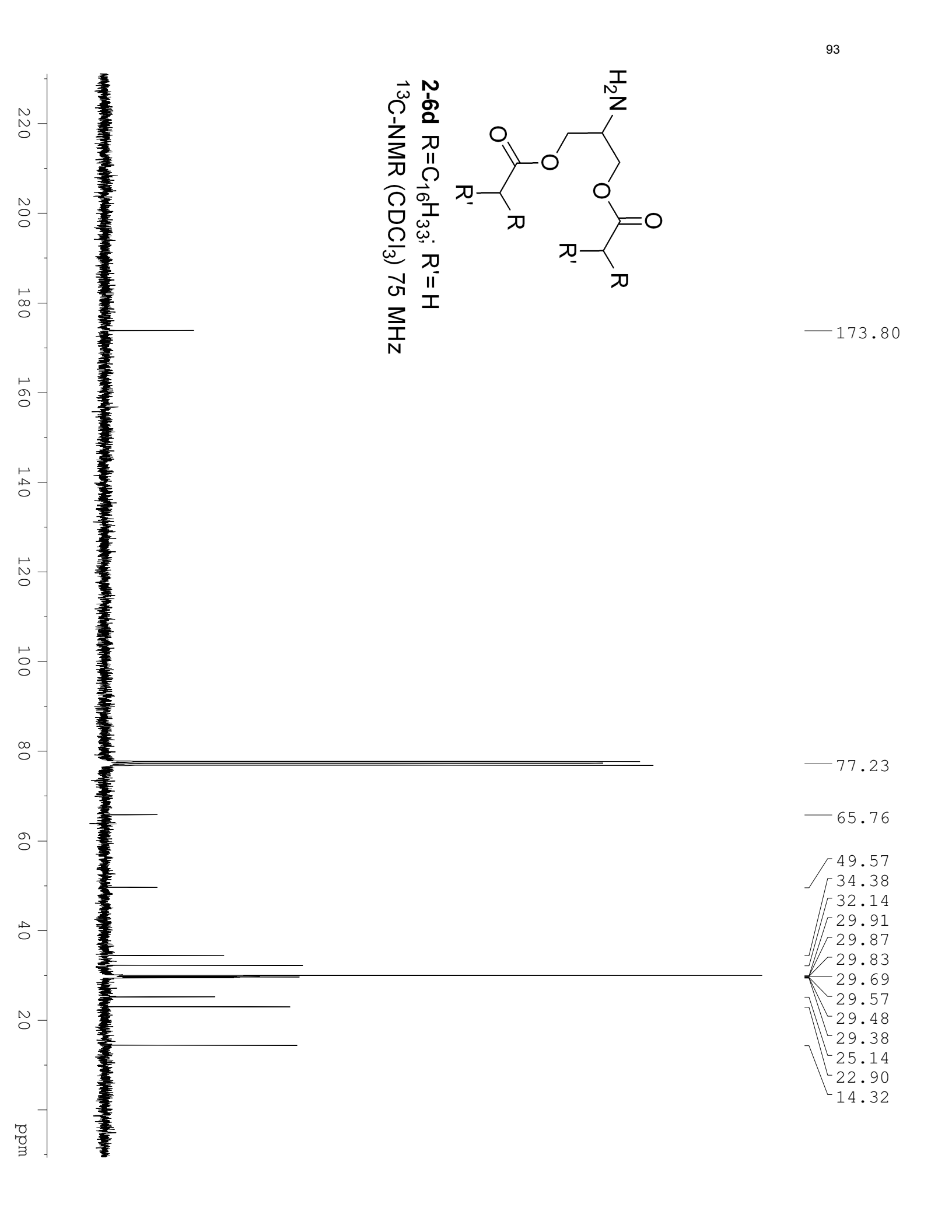
2-6d R=C16H33; R'= H
13C-NMR (CDCl3) 75 MHz
H2N
O
R'
R
173.80
77.23
65.76
49.57
34.38
32.14
29.91
29.87
29.83
29.69
29.57
29.48
29.38
25.14
22.90
14.32
220
200
180
160
140
120
100
80
60
40
20
ppm

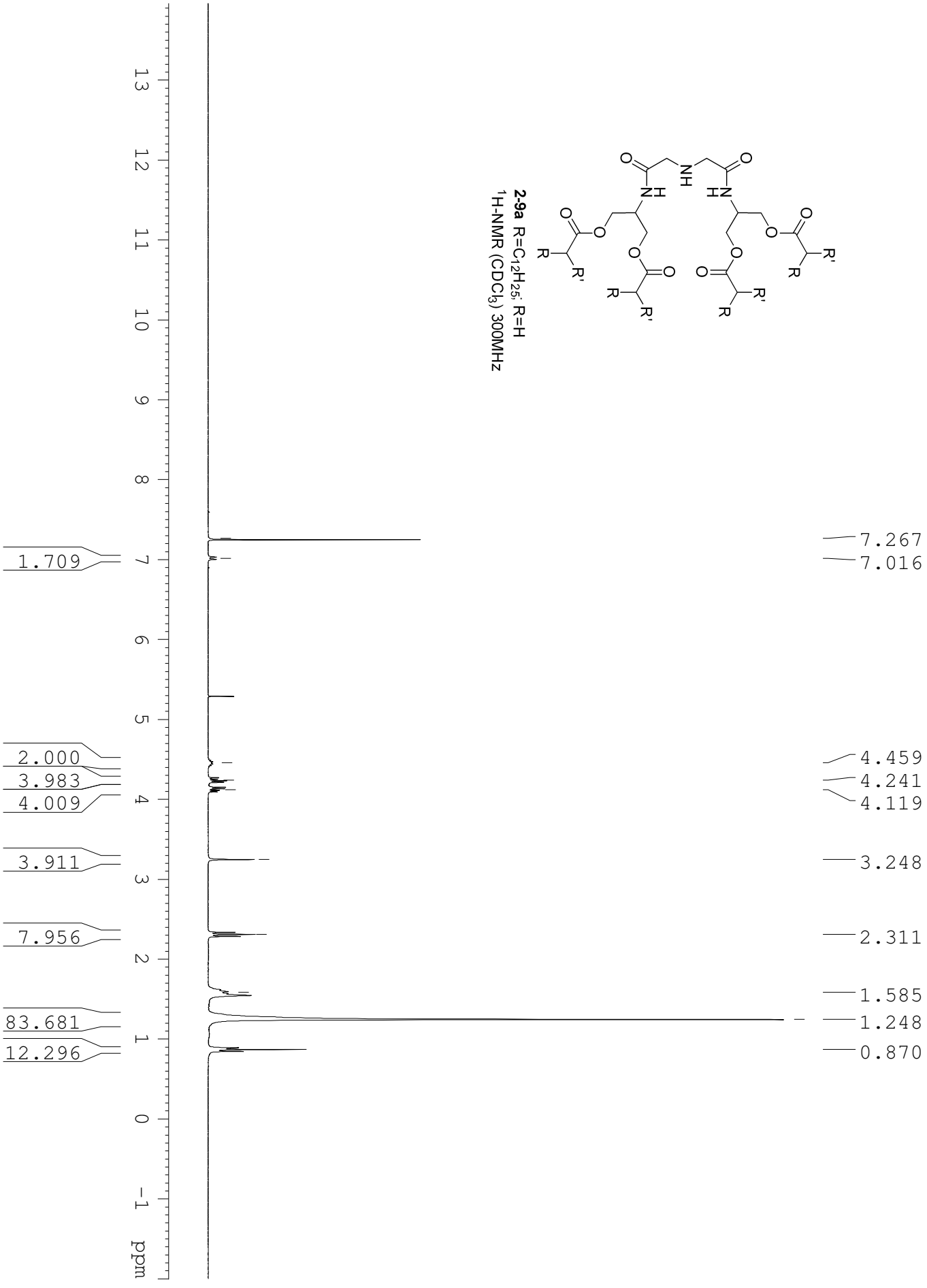
2-9a R=C12H25; R=H
1H-NMR (CDCl3) 300MHz
7.267
7.016
4.459
4.241
4.119
3.248
2.311
1.585
1.248
0.870
1.709
2.000
3.983
4.009
3.911
7.956
83.681
12.296
ppm

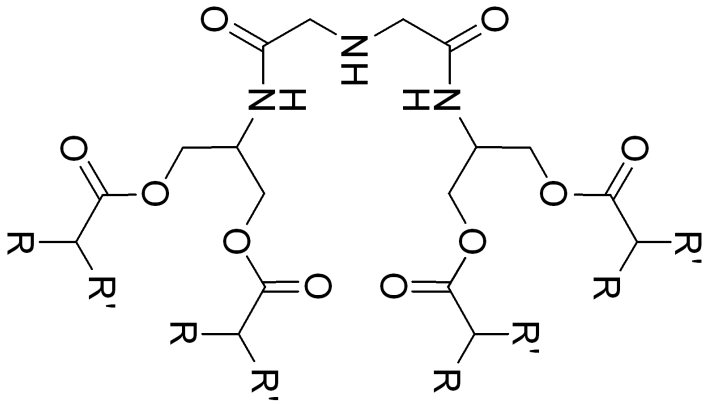

2-9a R= $C_{12}H_{25}$; R= H

^{13}C-NMR ($CDCl_3$) 75MHz

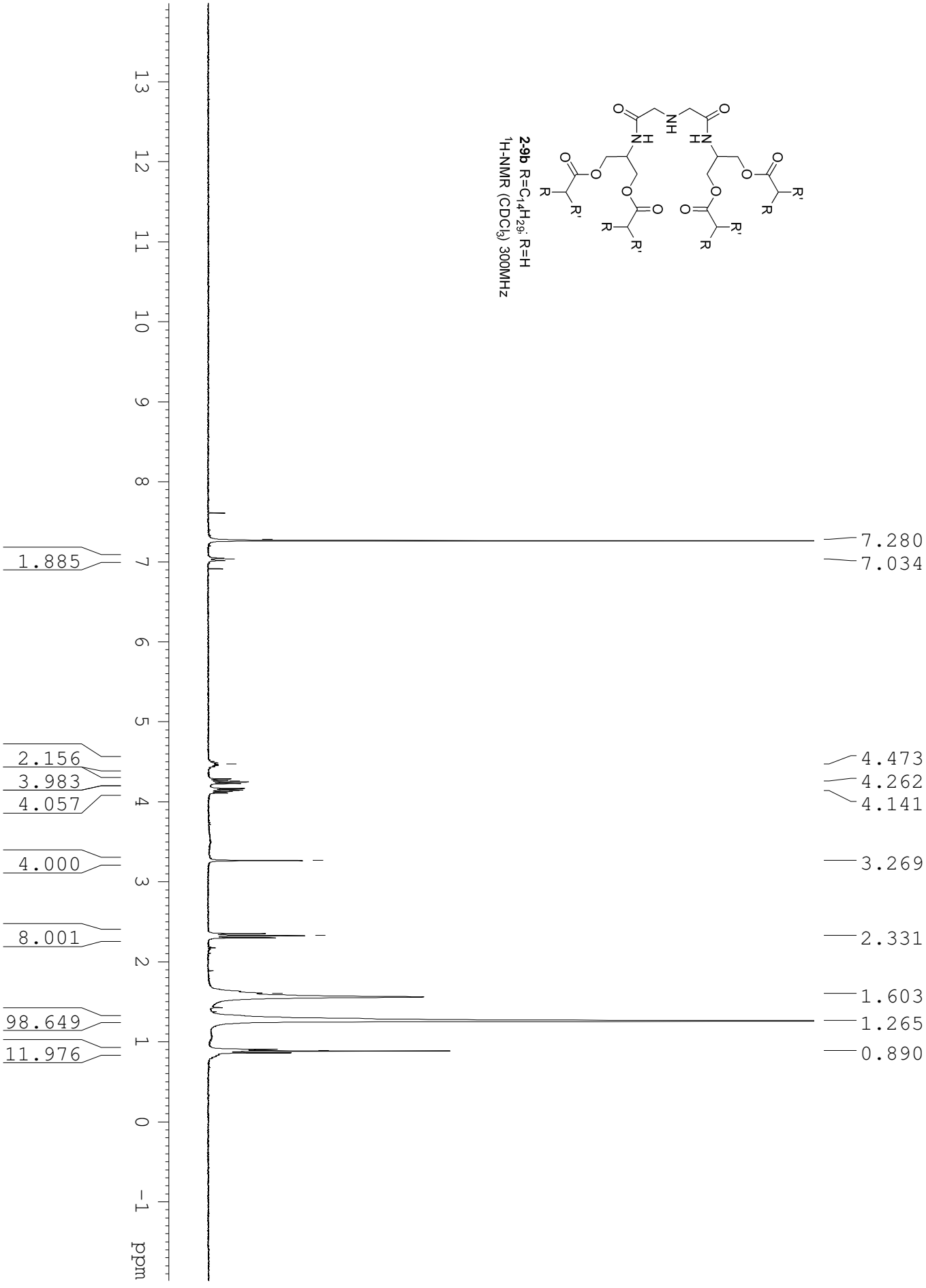
2-9b R=C14H29; R=H
1H-NMR (CDCl3) 300MHz
7.280
7.034
4.473
4.262
4.141
3.269
2.331
1.603
1.265
0.890
1.885
2.156
3.983
4.057
4.000
8.001
98.649
11.976
ppm

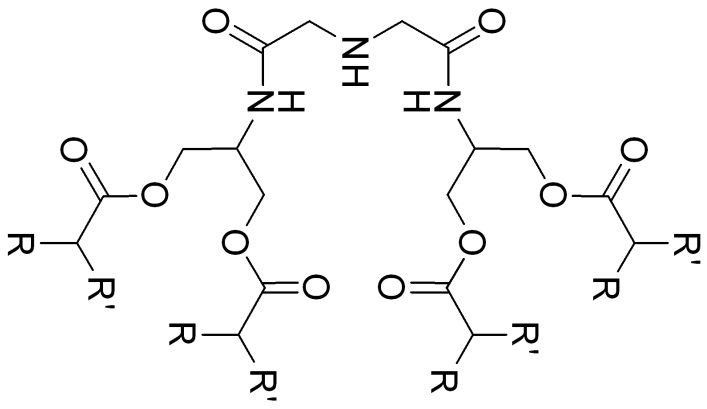

2-9b R= $C_{14}H_{29}$; R= H

^{13}C-NMR ($CDCl_3$) 75MHz

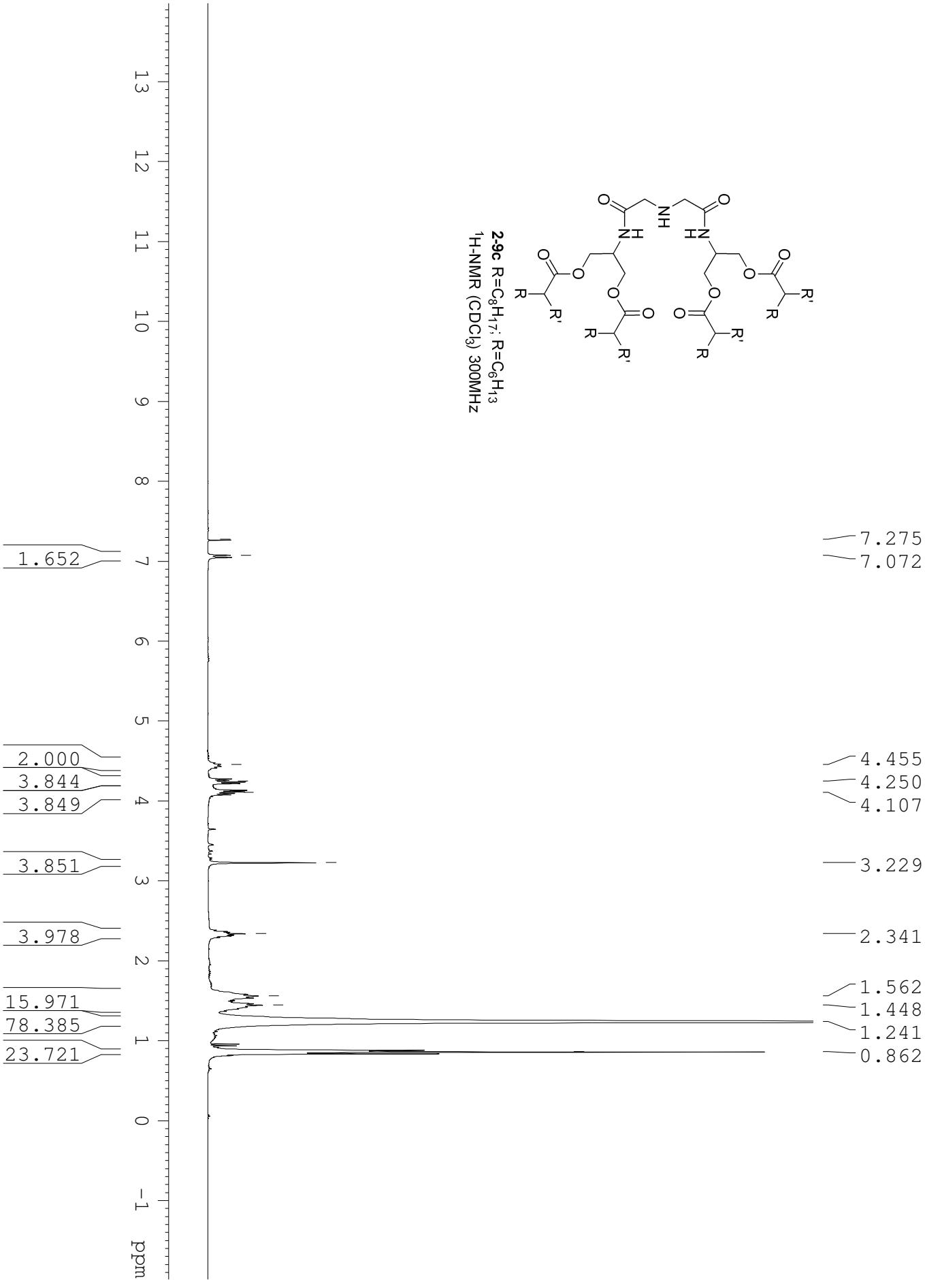
2-9c R=C8H17; R=C6H13
1H-NMR (CDCl3) 300MHz
13
12
11
10
9
8
7
6
5
4
3
2
1
0
-1
ppm
1.652
2.000
3.844
3.849
3.851
3.978
15.971
78.385
23.721
7.275
7.072
4.455
4.250
4.107
3.229
2.341
1.562
1.448
1.241
0.862

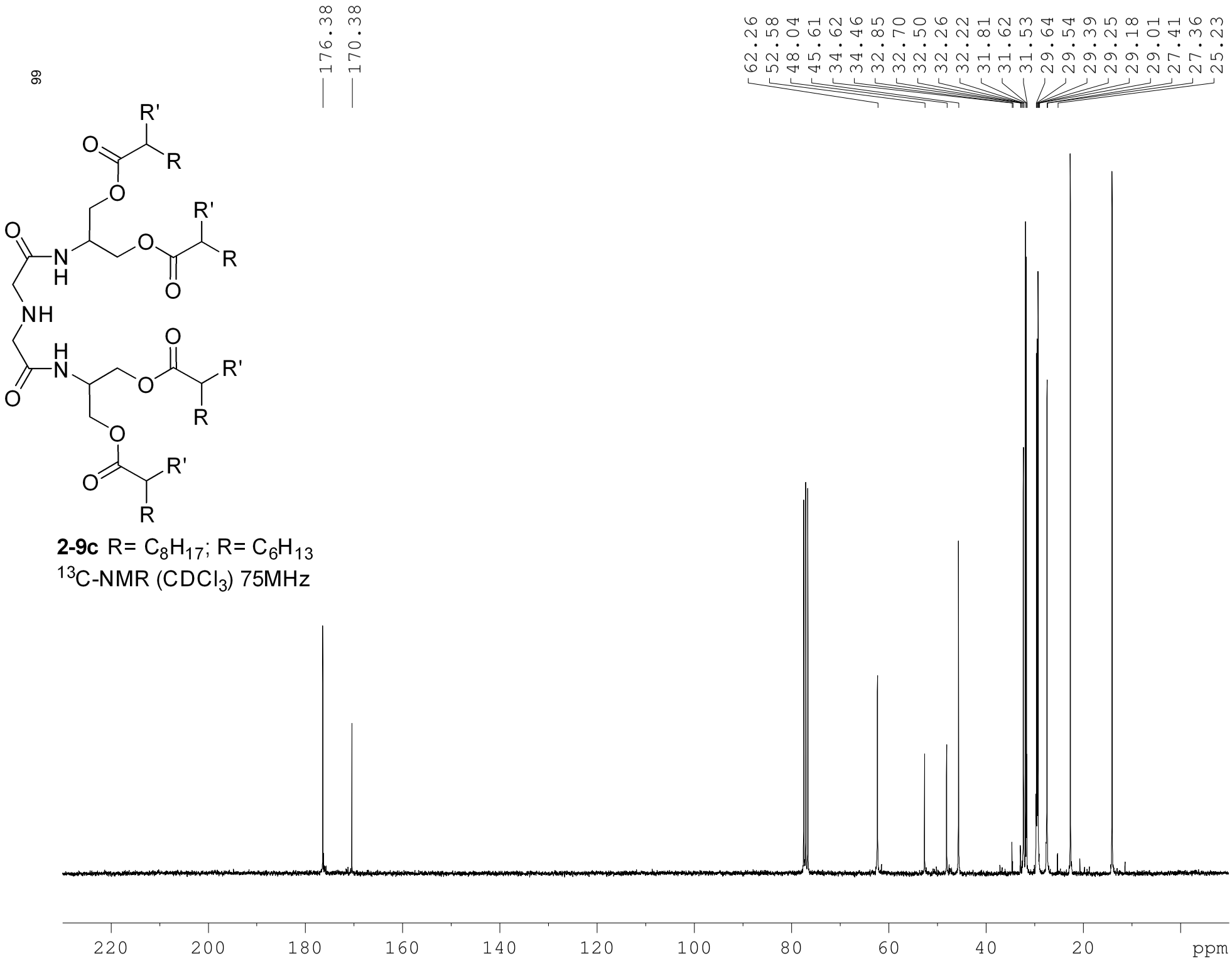

2-9c R= C_8H_{17}; R= C_6H_{13}

^{13}C-NMR ($CDCl_3$) 75MHz

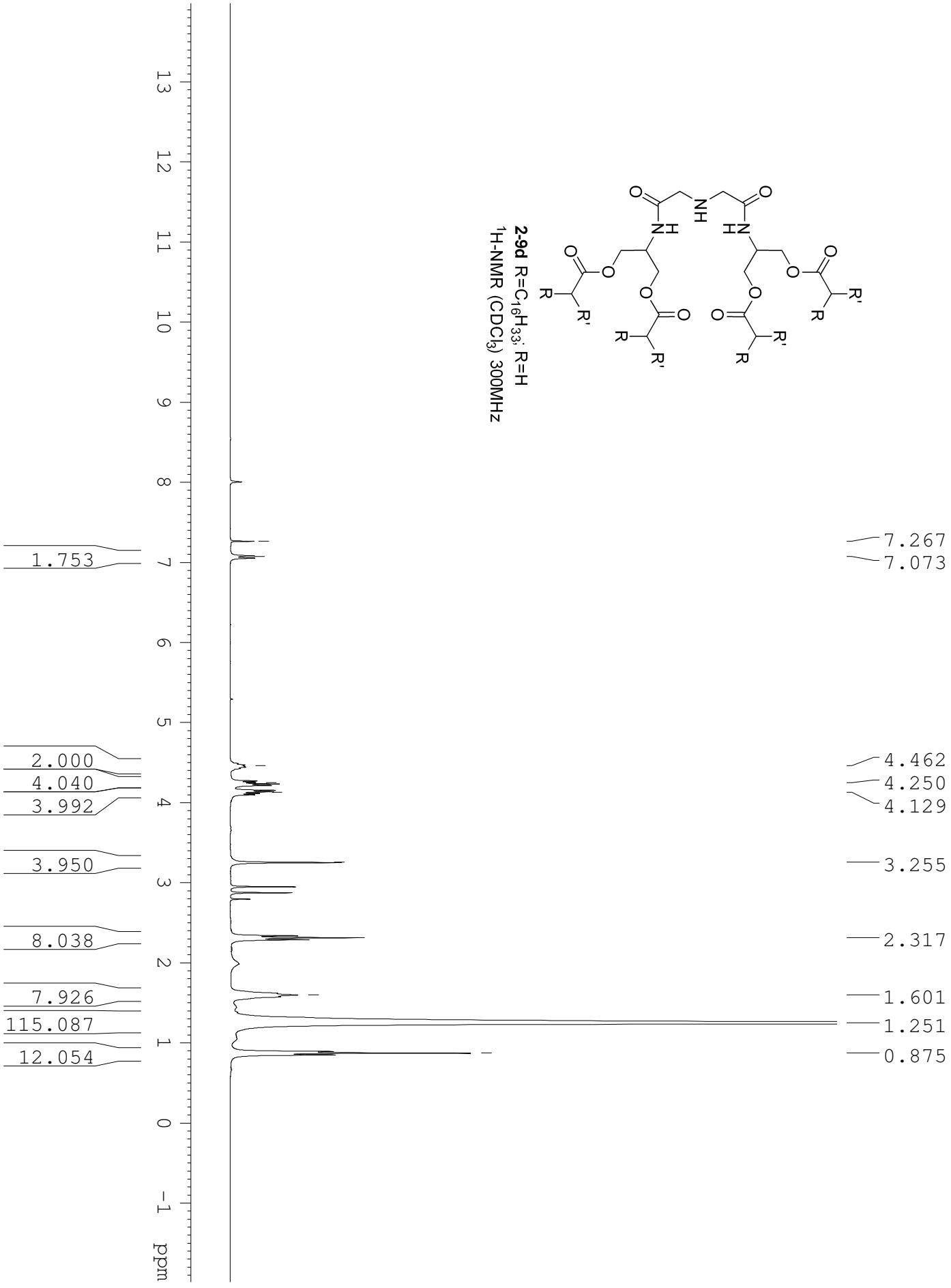
2-9d R=C16H33; R=H
1H-NMR (CDCl3) 300MHz
7.267
7.073
4.462
4.250
4.129
3.255
2.317
1.601
1.251
0.875
1.753
2.000
4.040
3.992
3.950
8.038
7.926
115.087
12.054
ppm

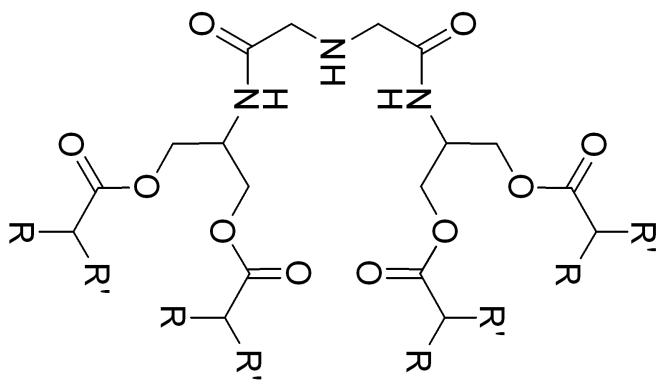

2-9d R= $C_{16}H_{33}$; R= H

^{13}C-NMR ($CDCl_3$) 75MHz

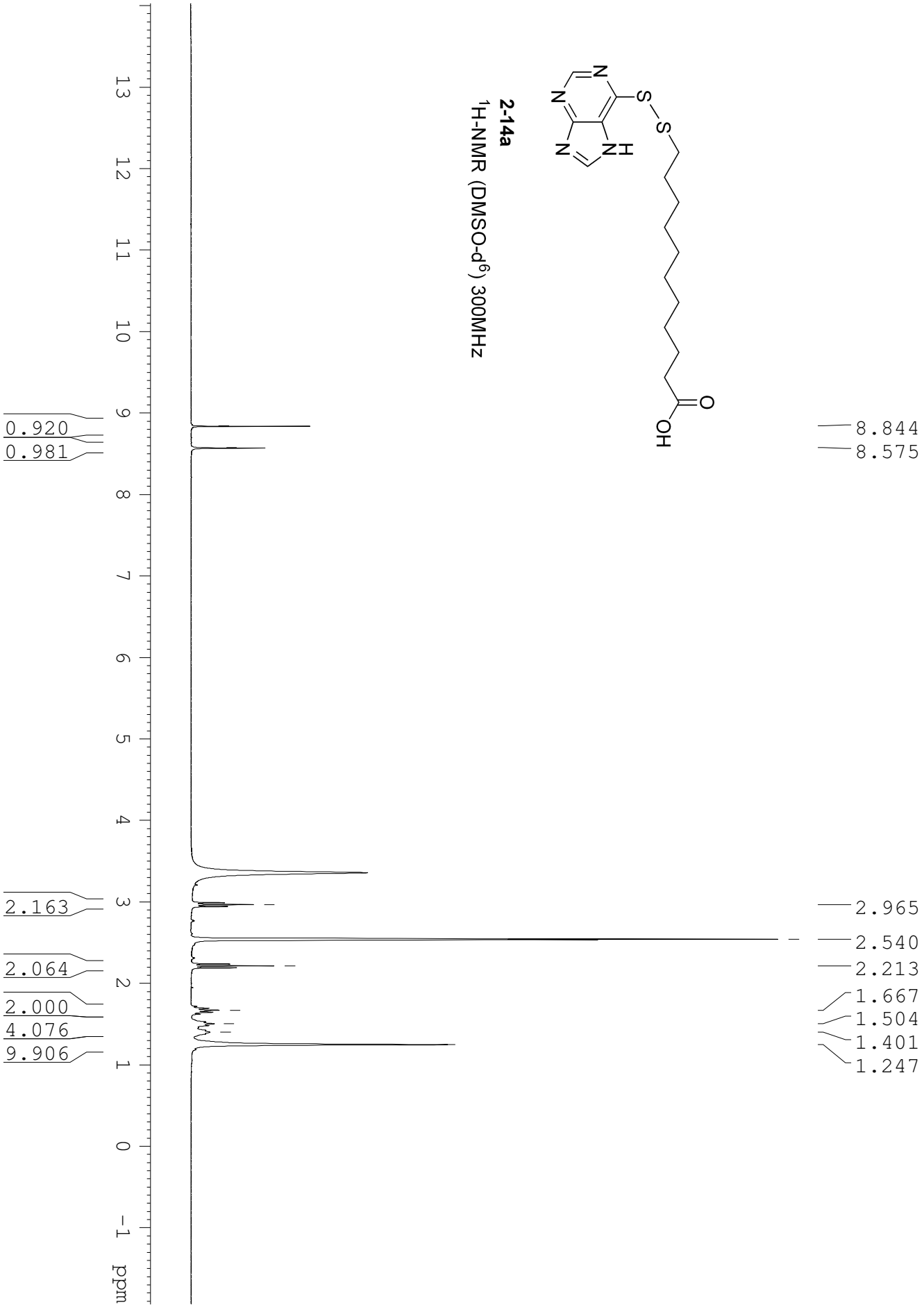
2-14a
^{1}H-NMR (DMSO-d^6) 300MHz
13
12
11
10
9
8
7
6
5
4
3
2
1
0
−1
ppm
0.920
0.981
2.163
2.064
2.000
4.076
9.906
8.844
8.575
2.965
2.540
2.213
1.667
1.504
1.401
1.247
N
N
N
H
S
S
O
OH

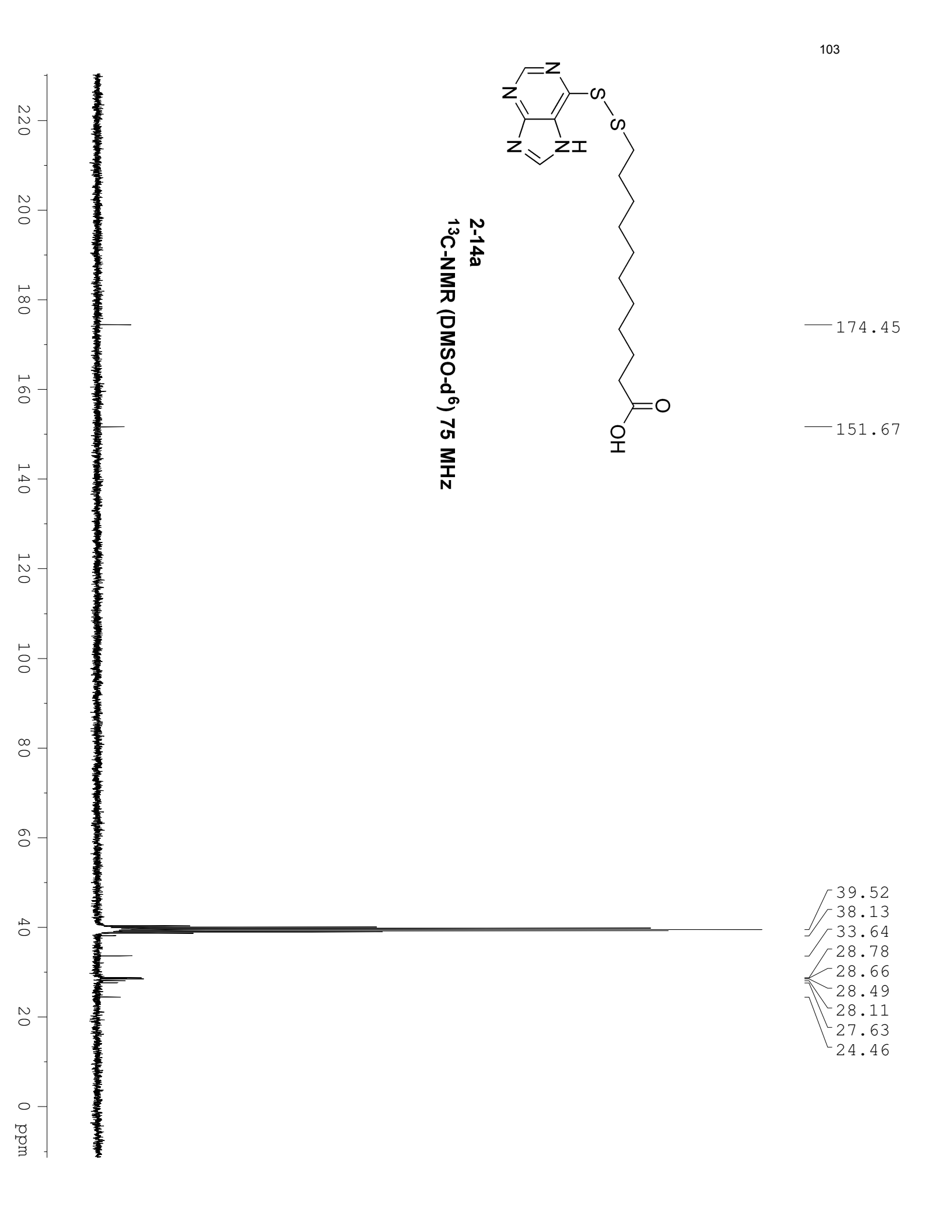
2-14a
13C-NMR (DMSO-d6) 75 MHz
174.45
151.67
39.52
38.13
33.64
28.78
28.66
28.49
28.11
27.63
24.46
220
200
180
160
140
120
100
80
60
40
20
0
ppm

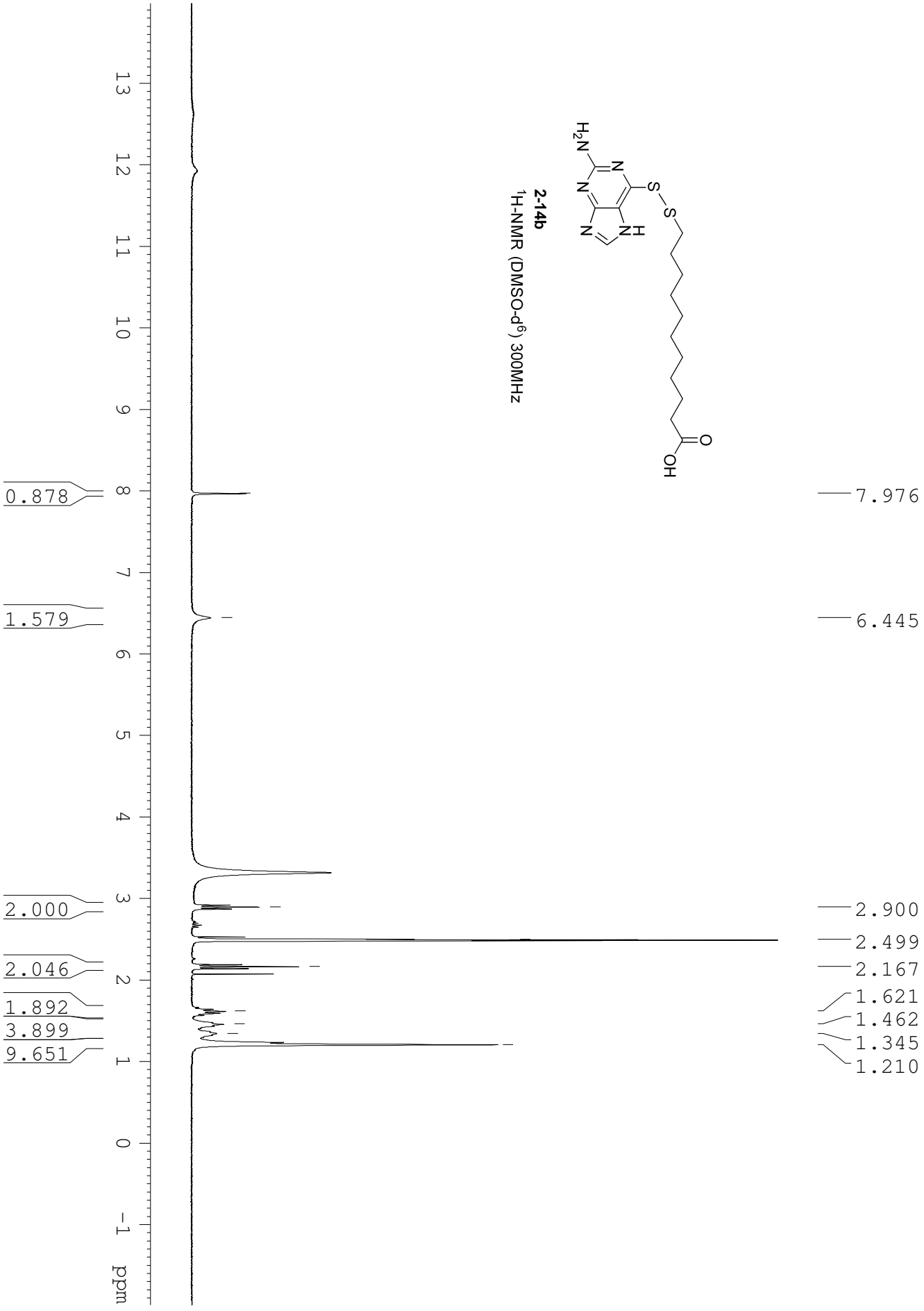
2-14b
1H-NMR (DMSO-d6) 300MHz
H2N
N
N
S
S
N
H
N
O
OH
13
12
11
10
9
8
7
6
5
4
3
2
1
0
-1
ppm
0.878
1.579
2.000
2.046
1.892
3.899
9.651
7.976
6.445
2.900
2.499
2.167
1.621
1.462
1.345
1.210

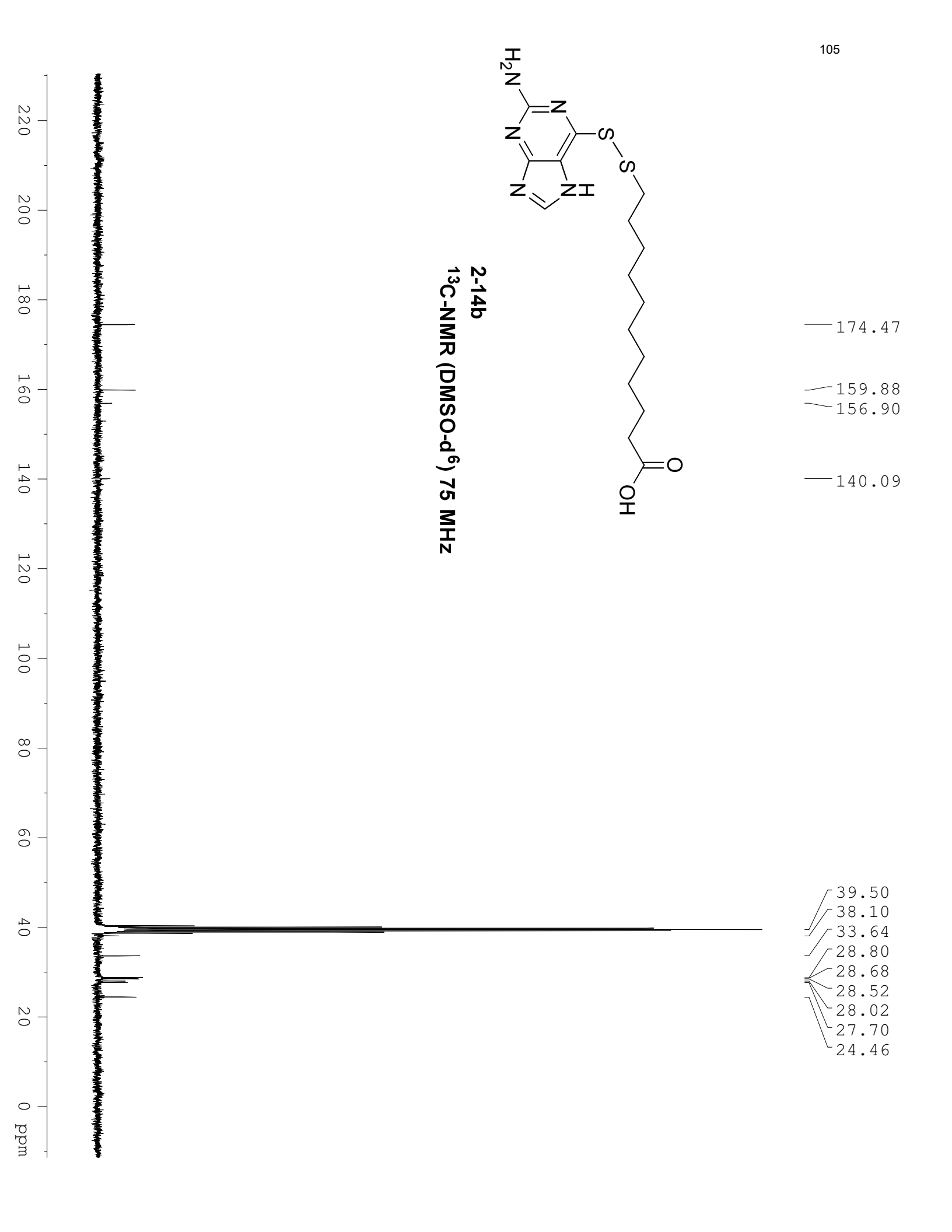
2-14b
13C-NMR (DMSO-d6) 75 MHz
174.47
159.88
156.90
140.09
39.50
38.10
33.64
28.80
28.68
28.52
28.02
27.70
24.46
220
200
180
160
140
120
100
80
60
40
20
0
ppm

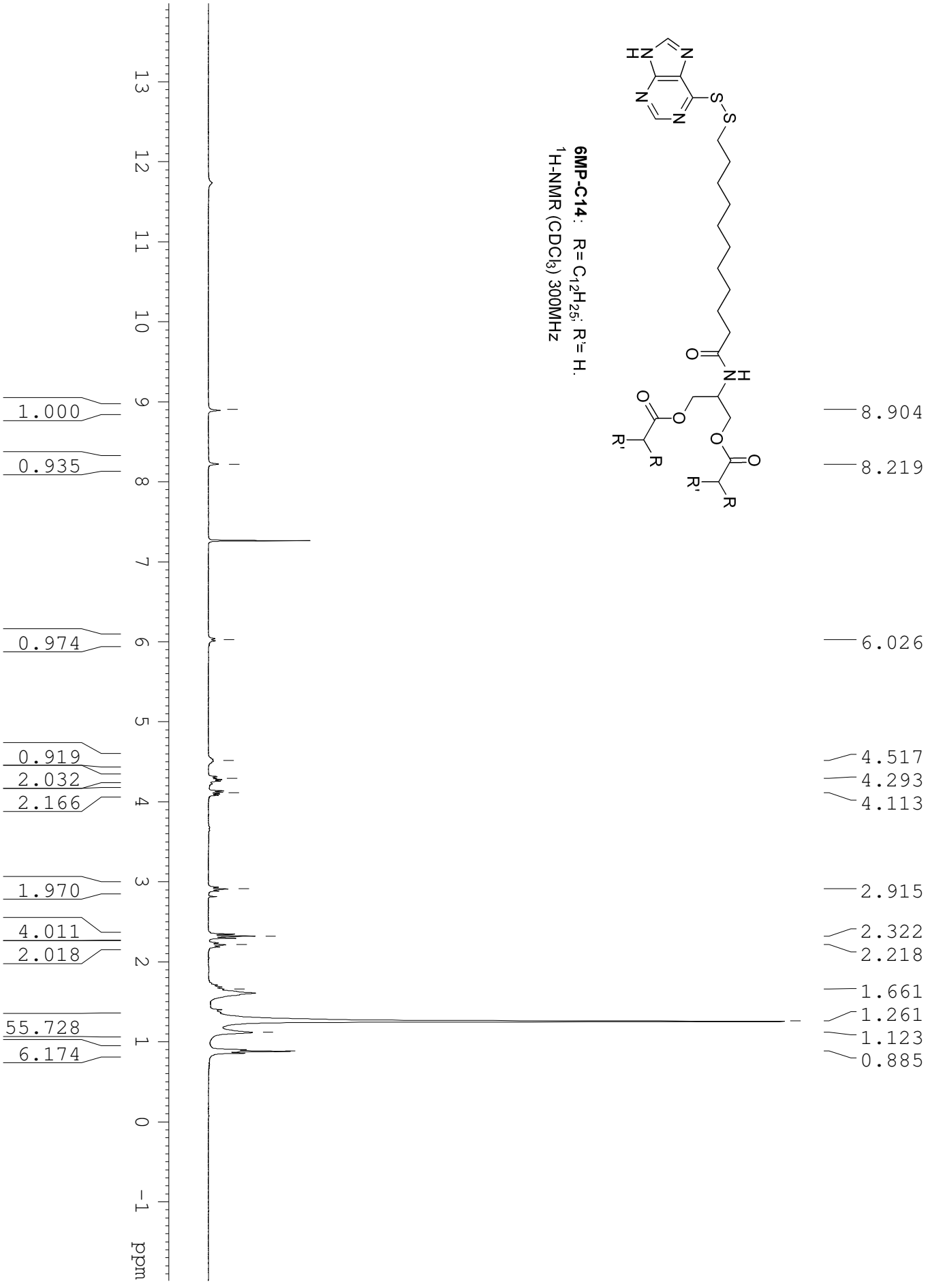
6MP-C14: R= C12H25; R'= H.
1H-NMR (CDCl3) 300MHz
1.000
0.935
0.974
0.919
2.032
2.166
1.970
4.011
2.018
55.728
6.174
8.904
8.219
6.026
4.517
4.293
4.113
2.915
2.322
2.218
1.661
1.261
1.123
0.885
ppm

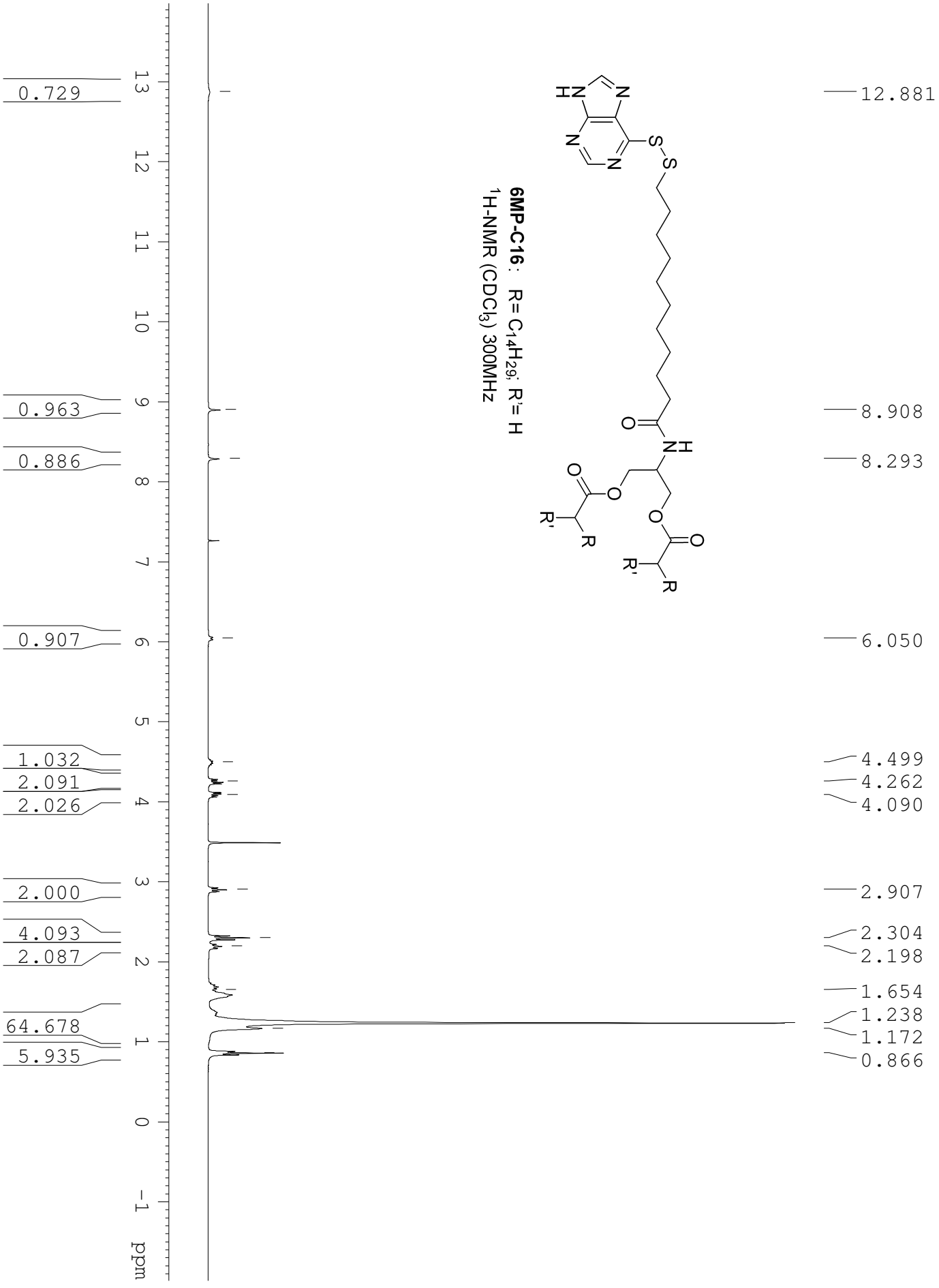
6MP-C16: R= C14H29; R'= H
1H-NMR (CDCl3) 300MHz
0.729
0.963
0.886
0.907
1.032
2.091
2.026
2.000
4.093
2.087
64.678
5.935
12.881
8.908
8.293
6.050
4.499
4.262
4.090
2.907
2.304
2.198
1.654
1.238
1.172
0.866
13
12
11
10
9
8
7
6
5
4
3
2
1
0
-1
ppm

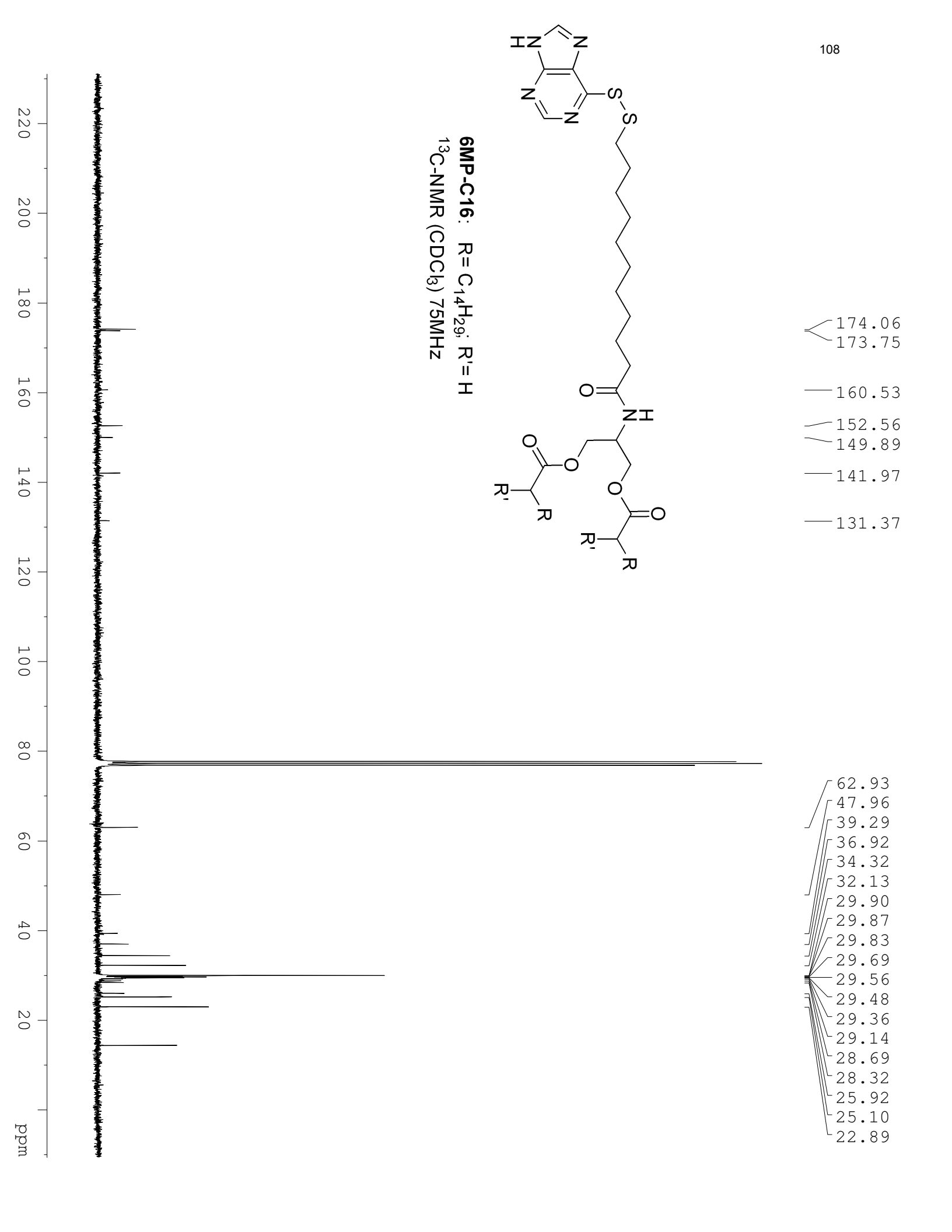
6MP-C16: R= C14H29; R'= H
13C-NMR (CDCl3) 75MHz
174.06
173.75
160.53
152.56
149.89
141.97
131.37
62.93
47.96
39.29
36.92
34.32
32.13
29.90
29.87
29.83
29.69
29.56
29.48
29.36
29.14
28.69
28.32
25.92
25.10
22.89
220
200
180
160
140
120
100
80
60
40
20
ppm

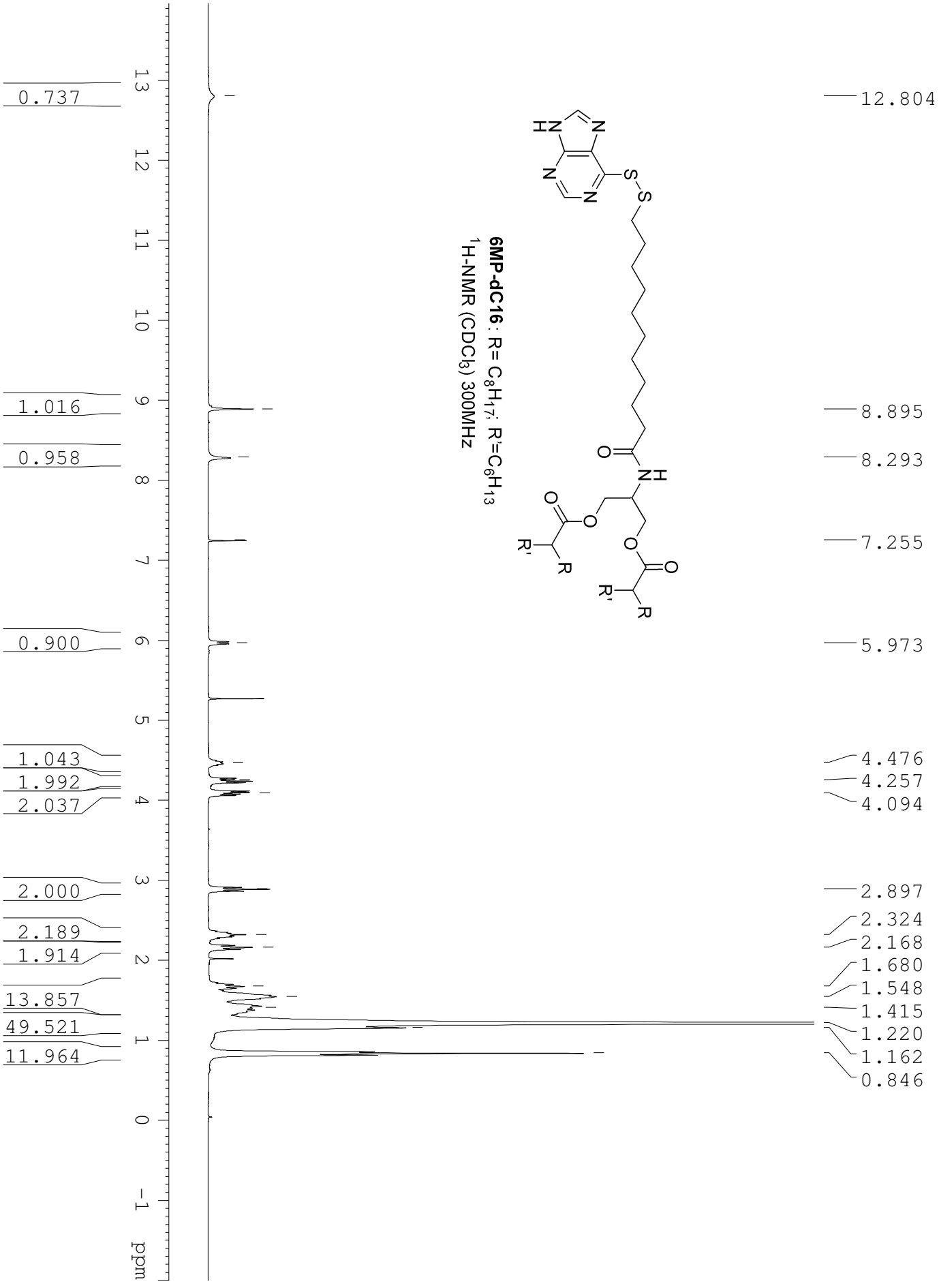
0.737
1.016
0.958
0.900
1.043
1.992
2.037
2.000
2.189
1.914
13.857
49.521
11.964
12.804
8.895
8.293
7.255
5.973
4.476
4.257
4.094
2.897
2.324
2.168
1.680
1.548
1.415
1.220
1.162
0.846
13
12
11
10
9
8
7
6
5
4
3
2
1
0
-1
ppm
6MP-dC16: R= C8H17; R'=C6H13
1H-NMR (CDCl3) 300MHz

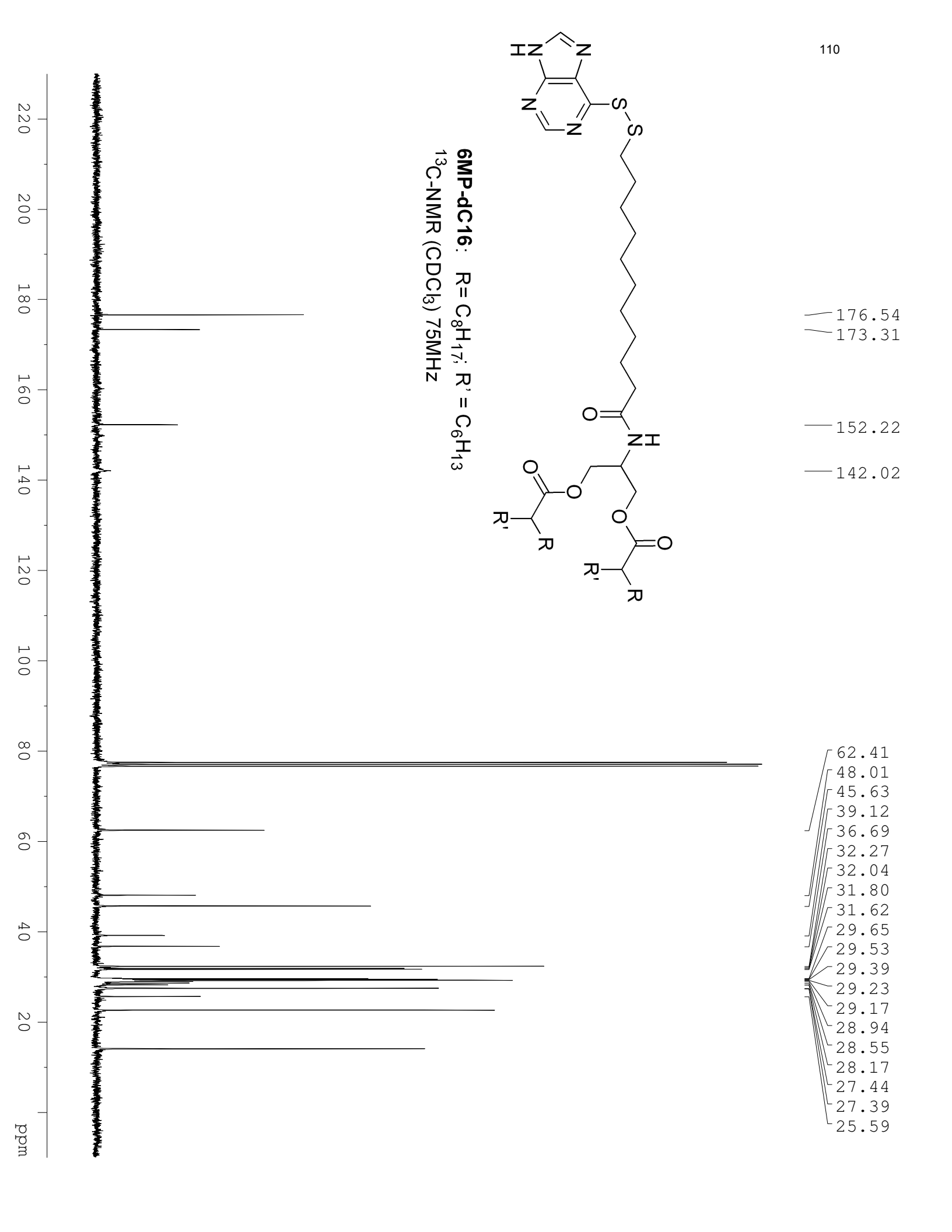
6MP-dC16: R= C8H17; R' = C6H13
13C-NMR (CDCl3) 75MHz
176.54
173.31
152.22
142.02
62.41
48.01
45.63
39.12
36.69
32.27
32.04
31.80
31.62
29.65
29.53
29.39
29.23
29.17
28.94
28.55
28.17
27.44
27.39
25.59
220
200
180
160
140
120
100
80
60
40
20
ppm

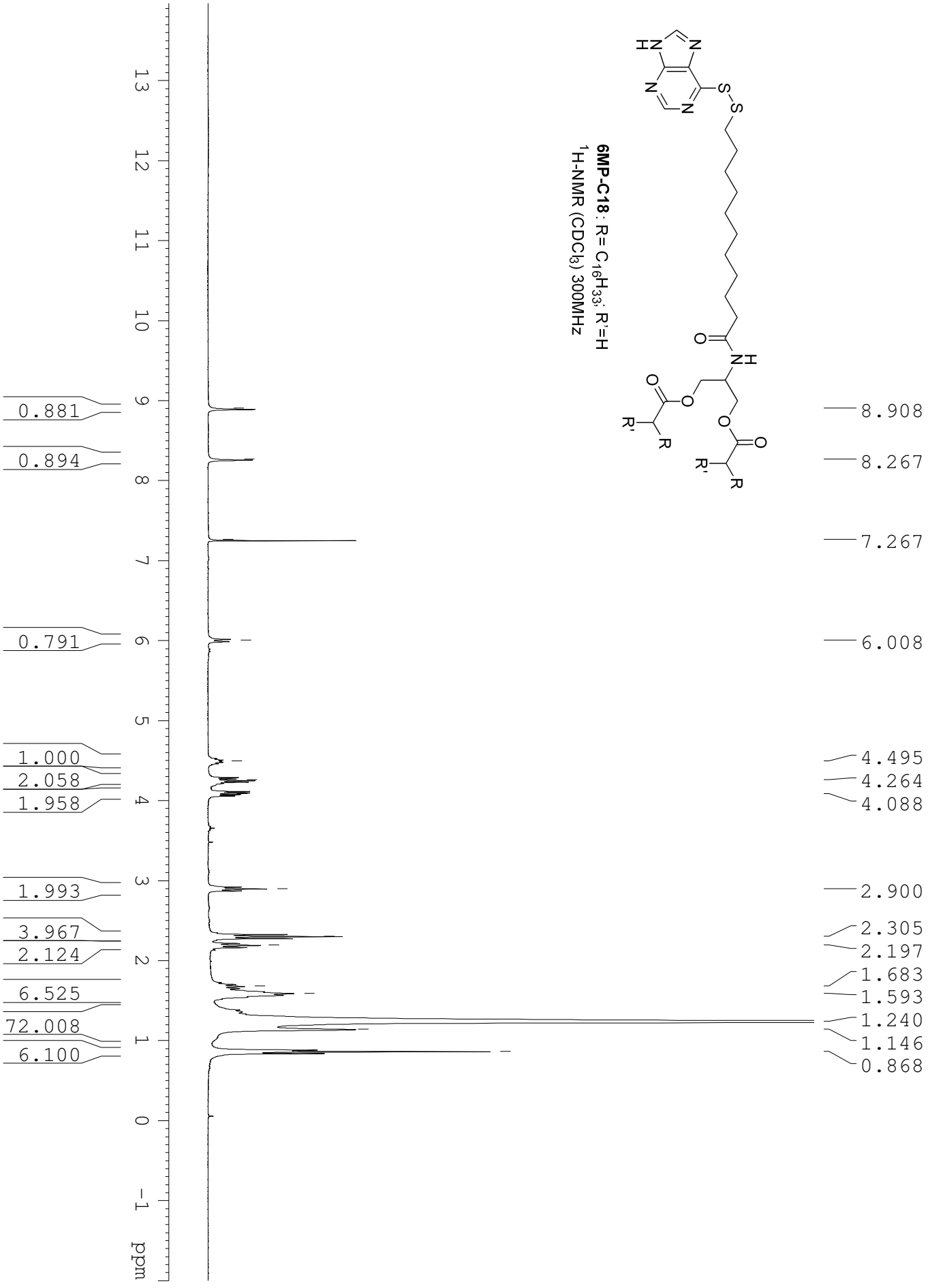
6MP-C18 : R= C16H33; R'=H
1H-NMR (CDCl3) 300MHz
0.881
0.894
0.791
1.000
2.058
1.958
1.993
3.967
2.124
6.525
72.008
6.100
8.908
8.267
7.267
6.008
4.495
4.264
4.088
2.900
2.305
2.197
1.683
1.593
1.240
1.146
0.868
ppm

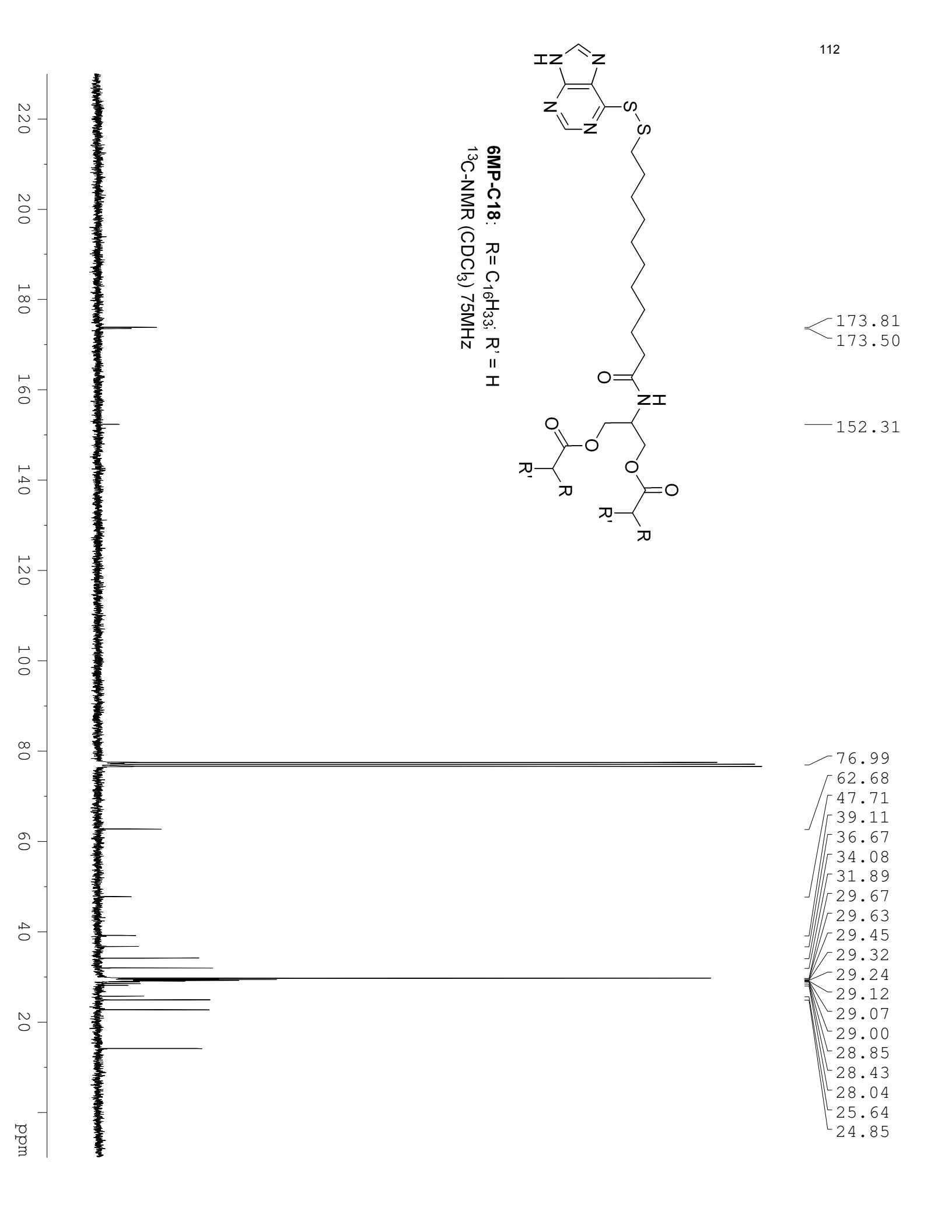
6MP-C18: R= C16H33; R' = H
13C-NMR (CDCl3) 75MHz
173.81
173.50
152.31
76.99
62.68
47.71
39.11
36.67
34.08
31.89
29.67
29.63
29.45
29.32
29.24
29.12
29.07
29.00
28.85
28.43
28.04
25.64
24.85
220
200
180
160
140
120
100
80
60
40
20
ppm

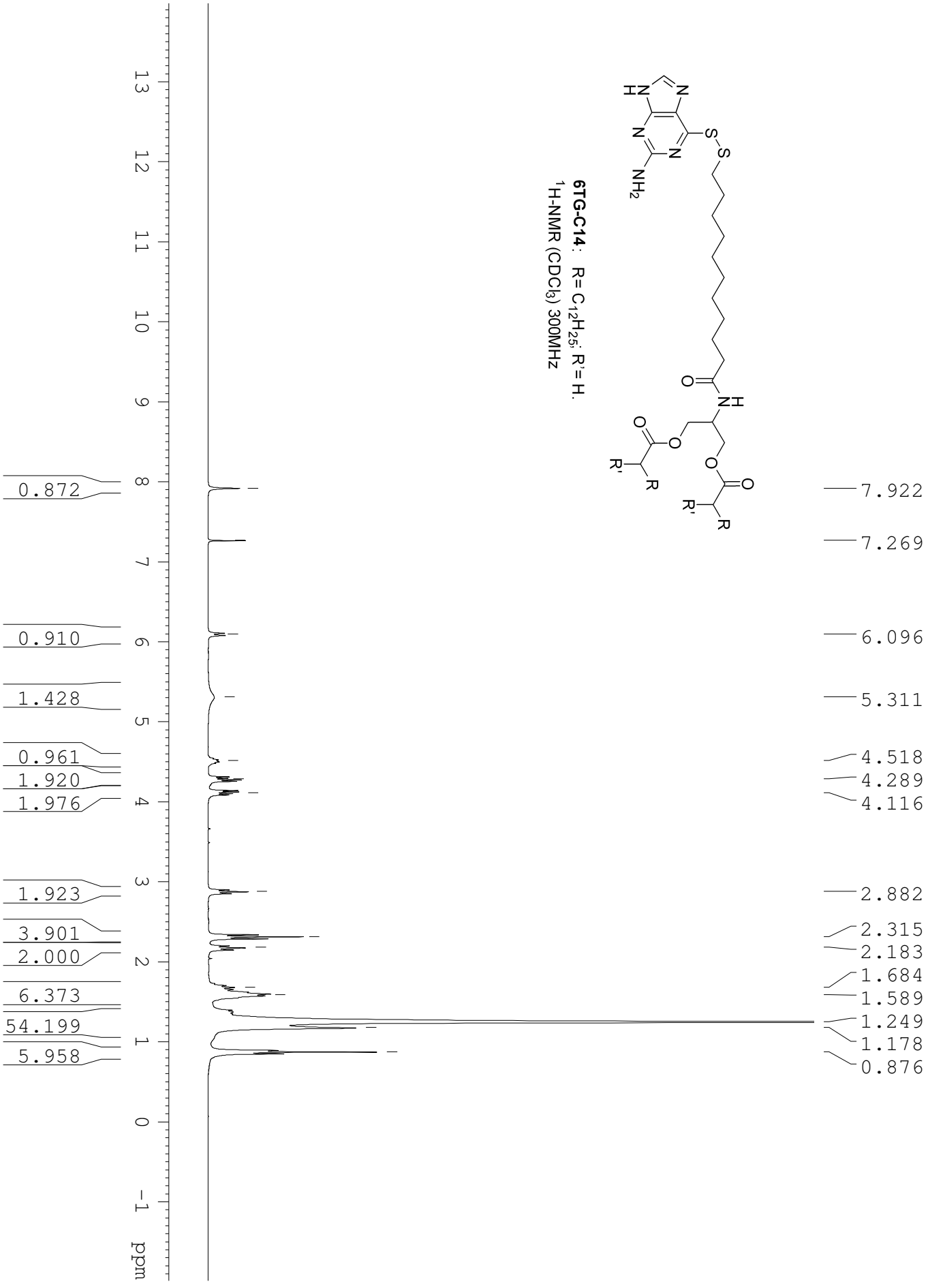
6TG-C14: R= C12H25; R'= H.
1H-NMR (CDCl3) 300MHz
0.872
0.910
1.428
0.961
1.920
1.976
1.923
3.901
2.000
6.373
54.199
5.958
7.922
7.269
6.096
5.311
4.518
4.289
4.116
2.882
2.315
2.183
1.684
1.589
1.249
1.178
0.876
ppm

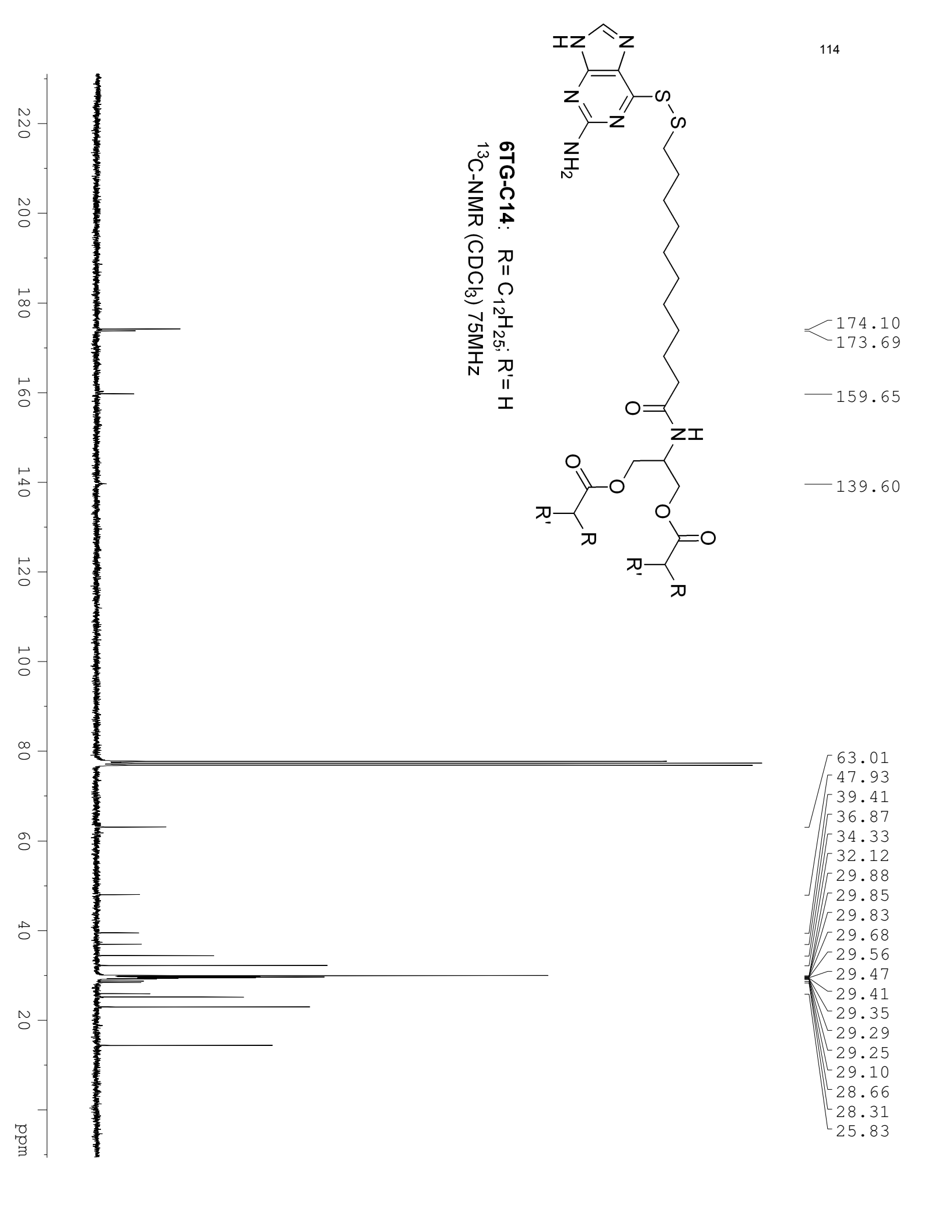
6TG-C14: R= C12H25; R'= H
13C-NMR (CDCl3) 75MHz
174.10
173.69
159.65
139.60
63.01
47.93
39.41
36.87
34.33
32.12
29.88
29.85
29.83
29.68
29.56
29.47
29.41
29.35
29.29
29.25
29.10
28.66
28.31
25.83
220
200
180
160
140
120
100
80
60
40
20
ppm

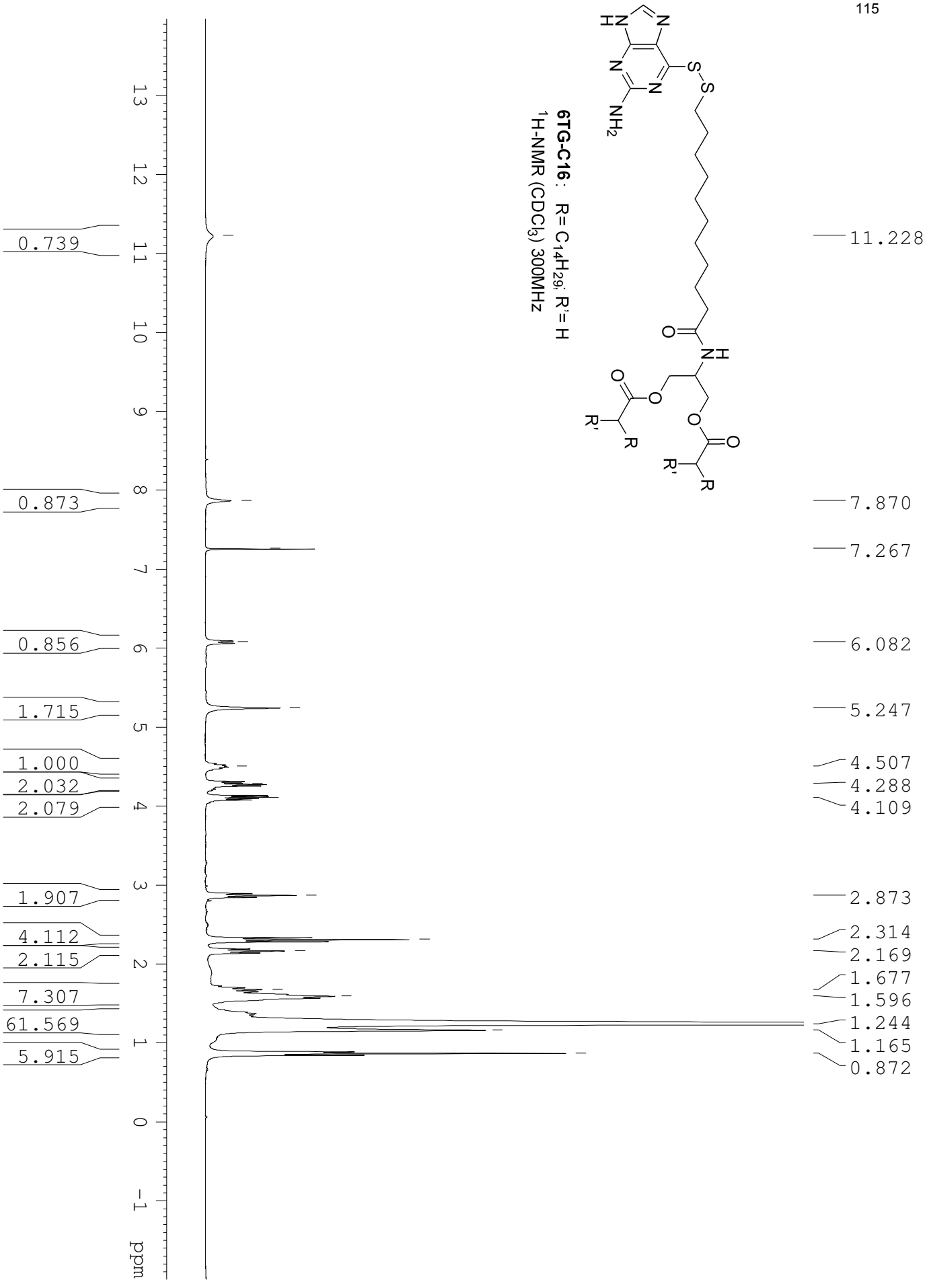
6TG-C16: R= C14H29; R'= H
1H-NMR (CDCl3) 300MHz
0.739
0.873
0.856
1.715
1.000
2.032
2.079
1.907
4.112
2.115
7.307
61.569
5.915
11.228
7.870
7.267
6.082
5.247
4.507
4.288
4.109
2.873
2.314
2.169
1.677
1.596
1.244
1.165
0.872
13
12
11
10
9
8
7
6
5
4
3
2
1
0
-1
ppm

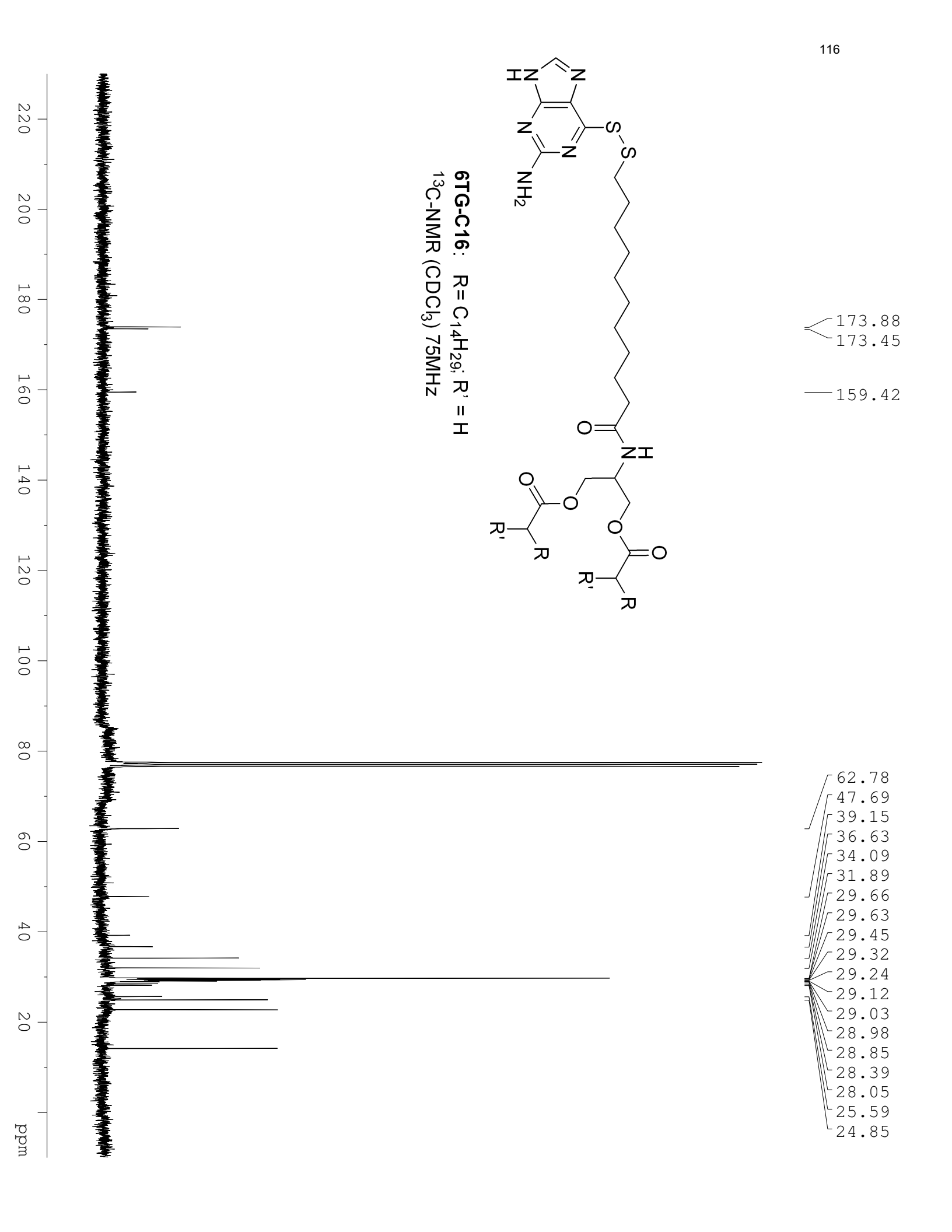
6TG-C16: R= C14H29; R' = H
13C-NMR (CDCl3) 75MHz
NH2
173.88
173.45
159.42
62.78
47.69
39.15
36.63
34.09
31.89
29.66
29.63
29.45
29.32
29.24
29.12
29.03
28.98
28.85
28.39
28.05
25.59
24.85
220
200
180
160
140
120
100
80
60
40
20
ppm

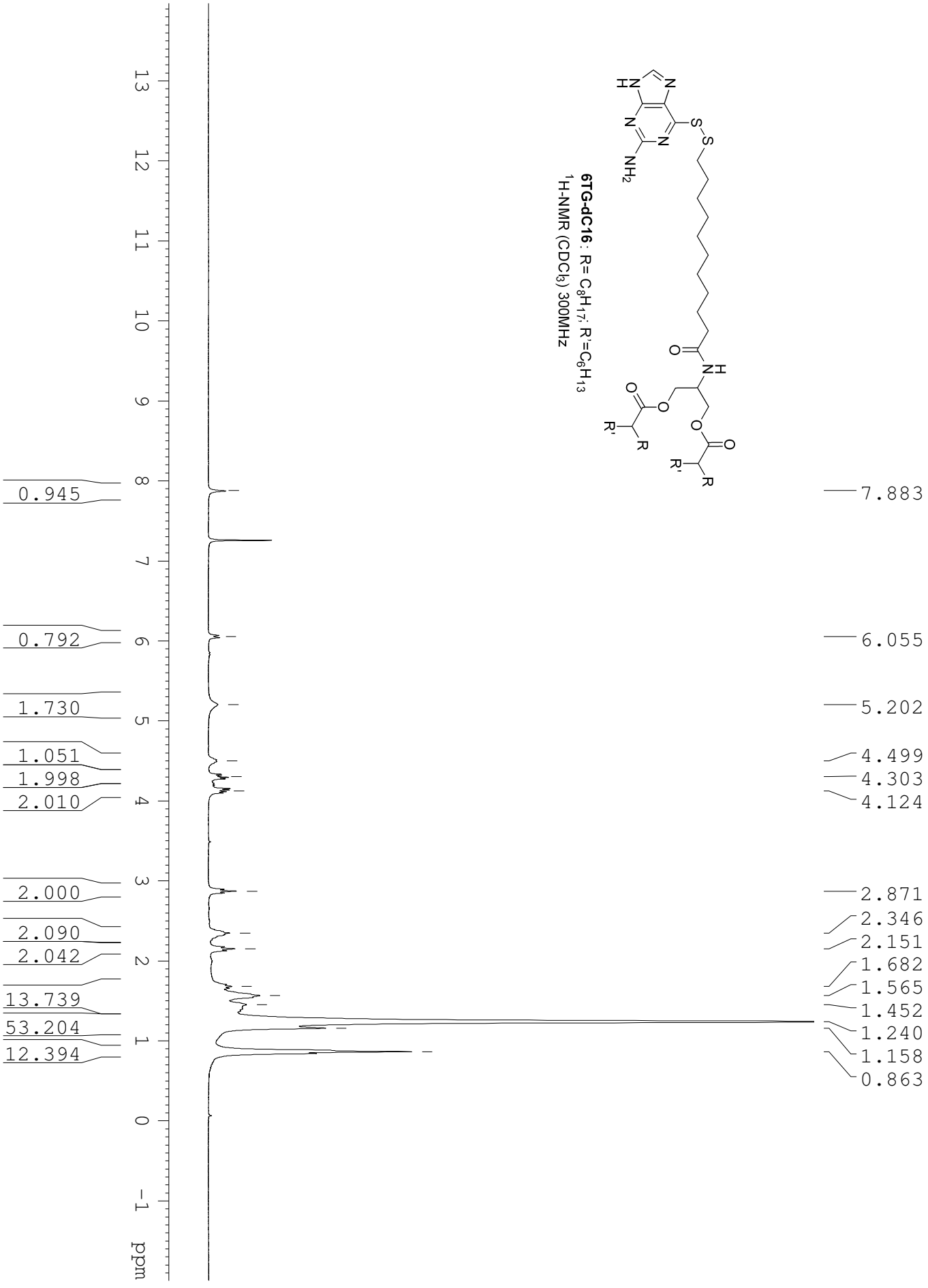
6TG-dC16: R= C8H17; R'=C6H13
1H-NMR (CDCl3) 300MHz
13
12
11
10
9
8
7
6
5
4
3
2
1
0
-1
ppm
0.945
0.792
1.730
1.051
1.998
2.010
2.000
2.090
2.042
13.739
53.204
12.394
7.883
6.055
5.202
4.499
4.303
4.124
2.871
2.346
2.151
1.682
1.565
1.452
1.240
1.158
0.863

118

176.65
173.29
159.40

62.55
47.99
45.66
39.12
36.63
32.29
31.82
31.63
29.67
29.55
29.41
29.25
29.19
29.05
29.01
28.97
28.84
28.37
28.04
27.45
27.40

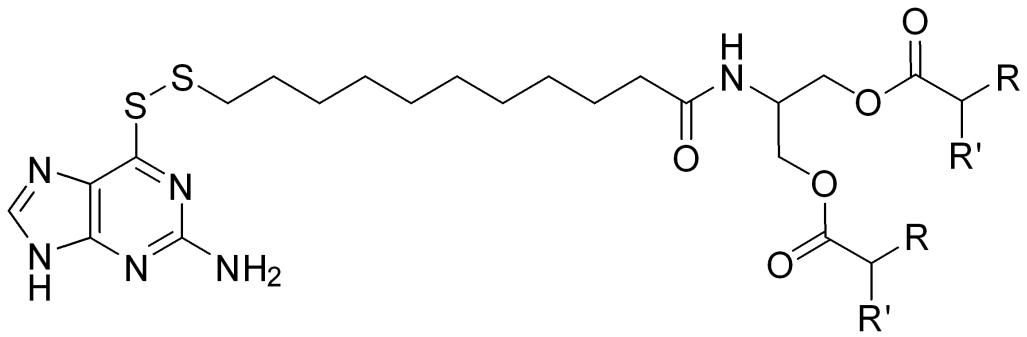

6TG-dC16: R= C_8H_{17}; R' = C_6H_{13}

^{13}C-NMR ($CDCl_3$) 75MHz

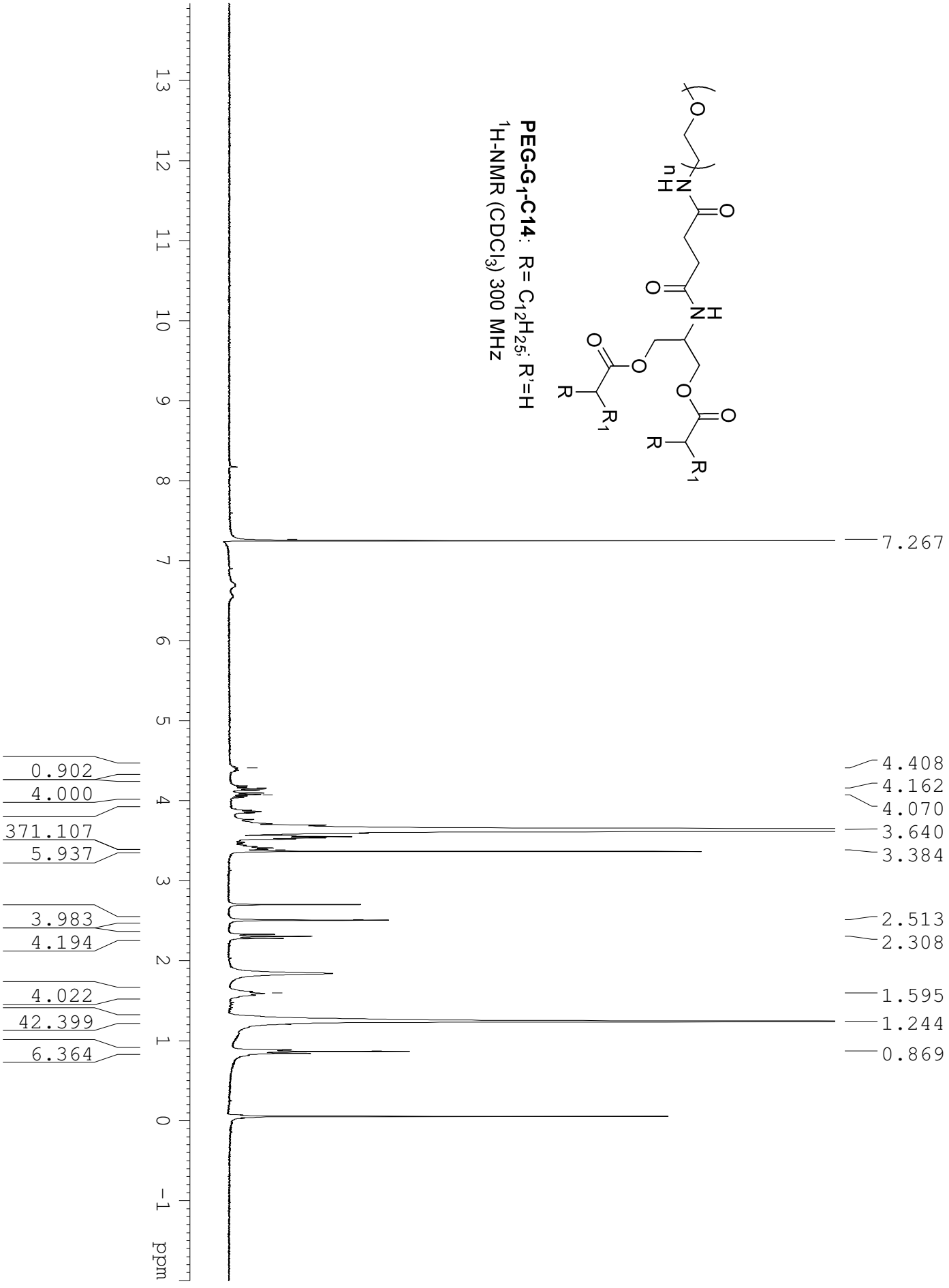
PEG-G1-C14: R= C12H25; R'=H
1H-NMR (CDCl3) 300 MHz
7.267
4.408
4.162
4.070
3.640
3.384
2.513
2.308
1.595
1.244
0.869
0.902
4.000
371.107
5.937
3.983
4.194
4.022
42.399
6.364
ppm

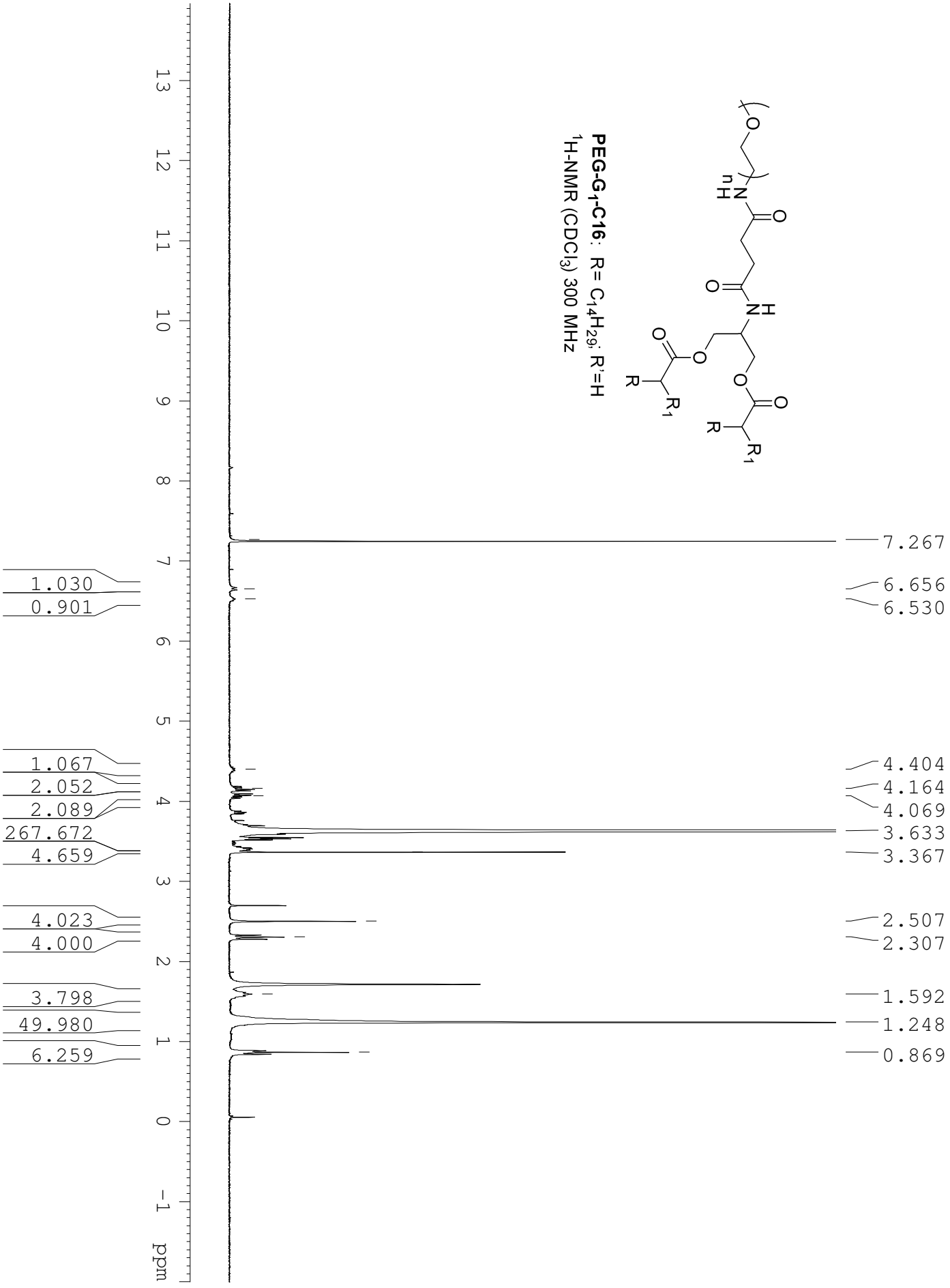
PEG-G1-C16: R= C14H29; R'=H
1H-NMR (CDCl3) 300 MHz
7.267
6.656
6.530
4.404
4.164
4.069
3.633
3.367
2.507
2.307
1.592
1.248
0.869
1.030
0.901
1.067
2.052
2.089
267.672
4.659
4.023
4.000
3.798
49.980
6.259
ppm

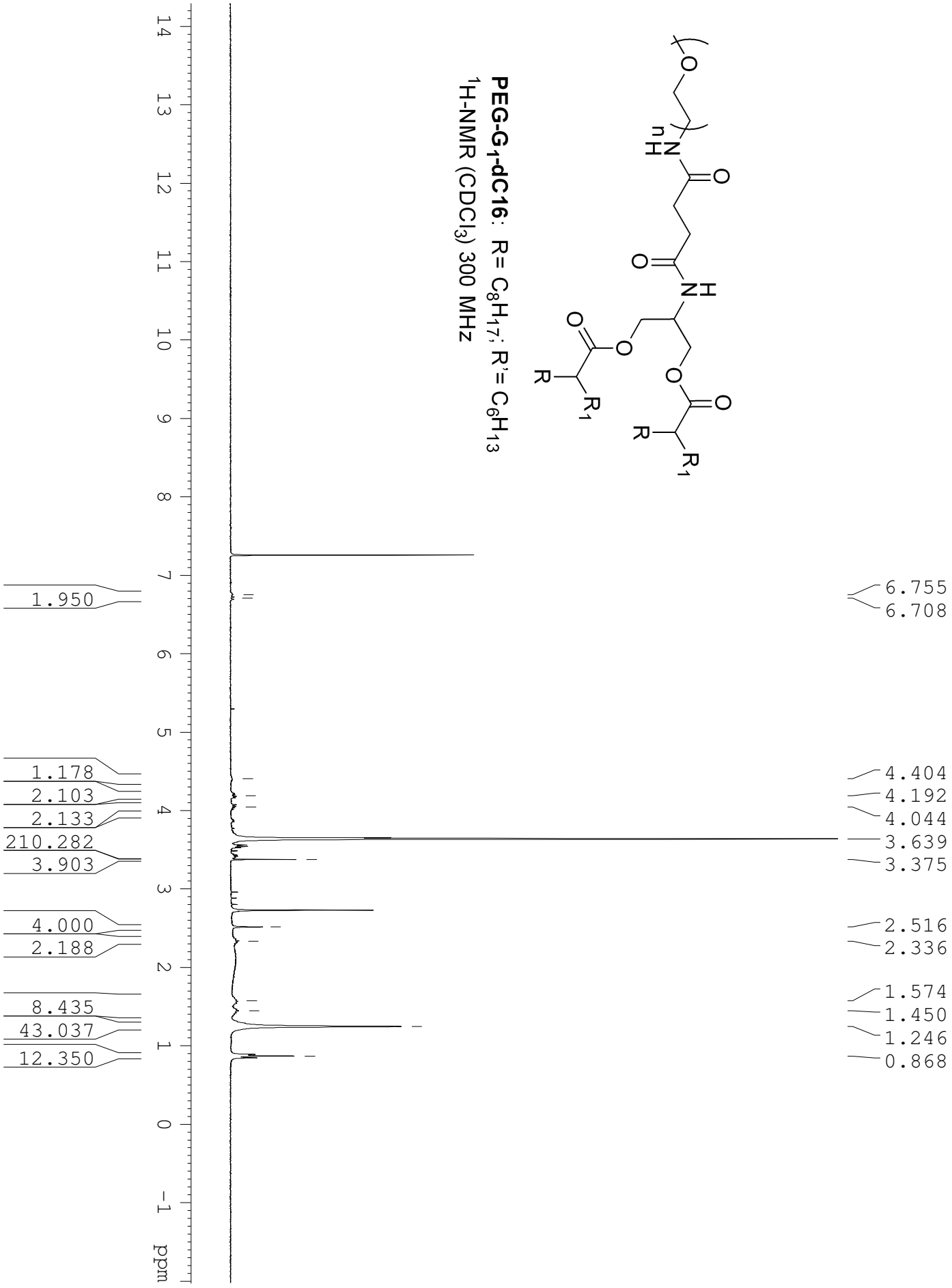
PEG-G1-dC16: R= C8H17; R'= C6H13
1H-NMR (CDCl3) 300 MHz
6.755
6.708
4.404
4.192
4.044
3.639
3.375
2.516
2.336
1.574
1.450
1.246
0.868
1.950
1.178
2.103
2.133
210.282
3.903
4.000
2.188
8.435
43.037
12.350
ppm

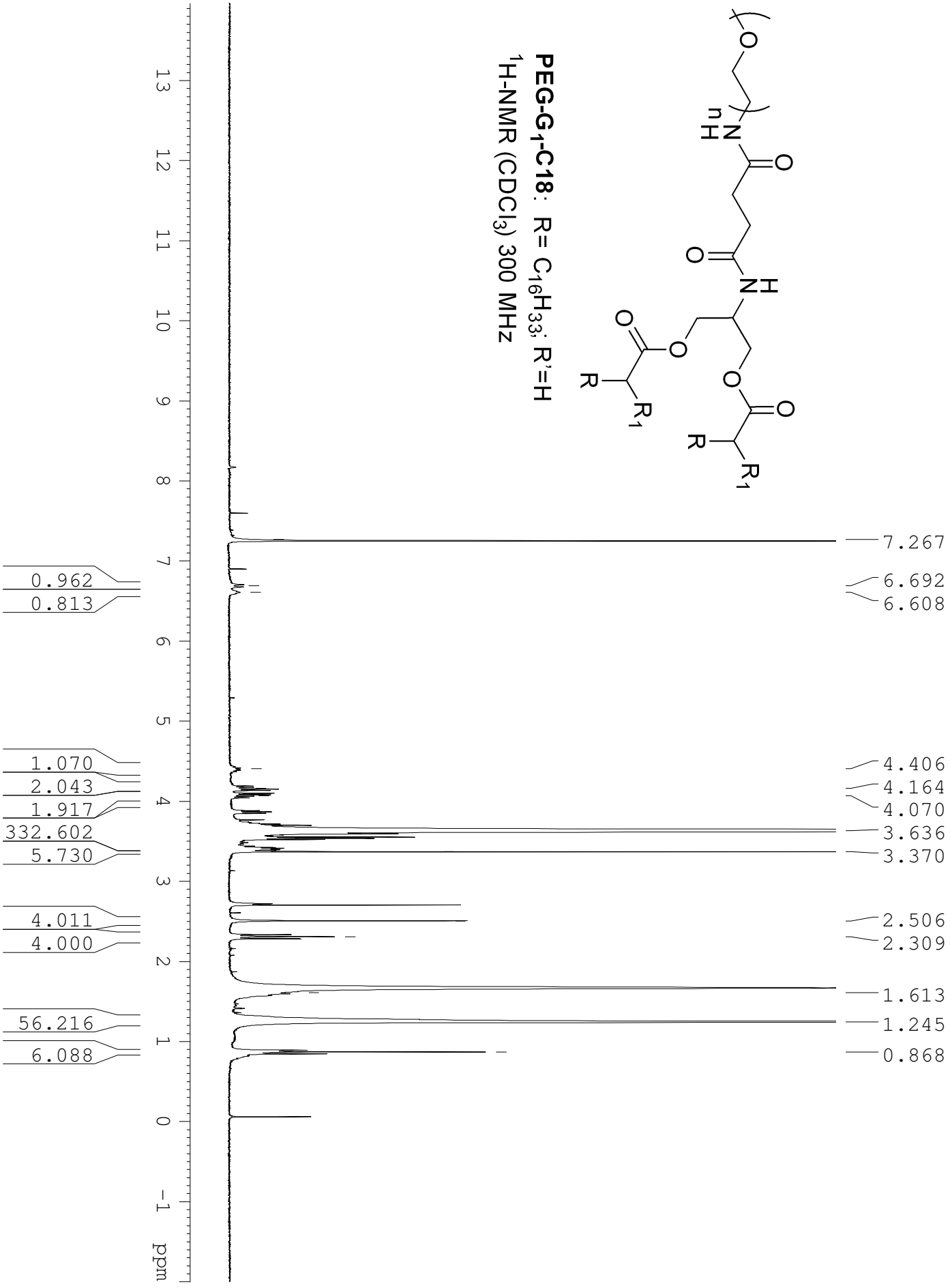
PEG-G1-C18: R= C16H33; R'=H
1H-NMR (CDCl3) 300 MHz
7.267
6.692
6.608
4.406
4.164
4.070
3.636
3.370
2.506
2.309
1.613
1.245
0.868
0.962
0.813
1.070
2.043
1.917
332.602
5.730
4.011
4.000
56.216
6.088
ppm

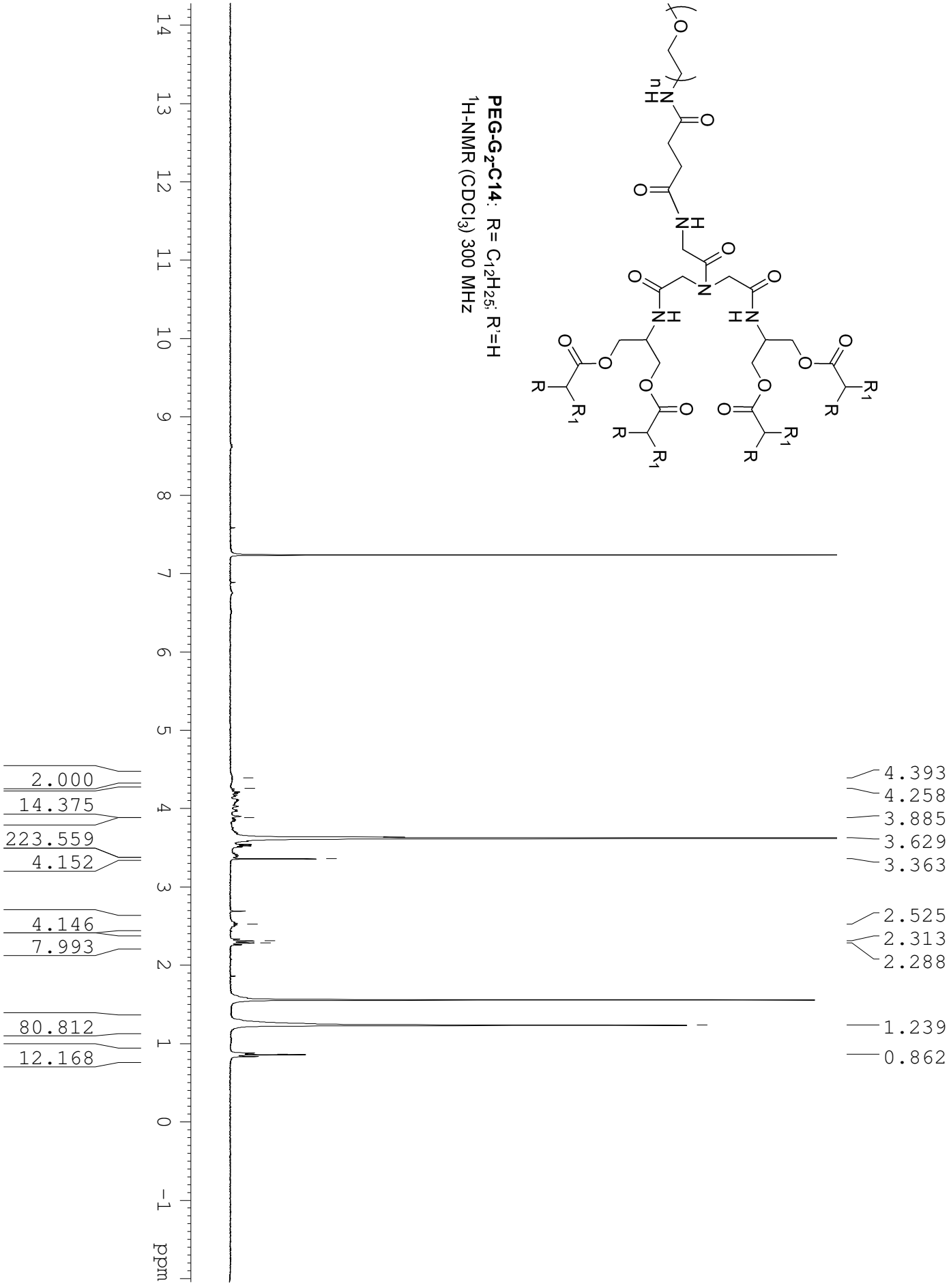
PEG-G2-C14: R= C12H25; R'=H
1H-NMR (CDCl3) 300 MHz
2.000
14.375
223.559
4.152
4.146
7.993
80.812
12.168
4.393
4.258
3.885
3.629
3.363
2.525
2.313
2.288
1.239
0.862
ppm

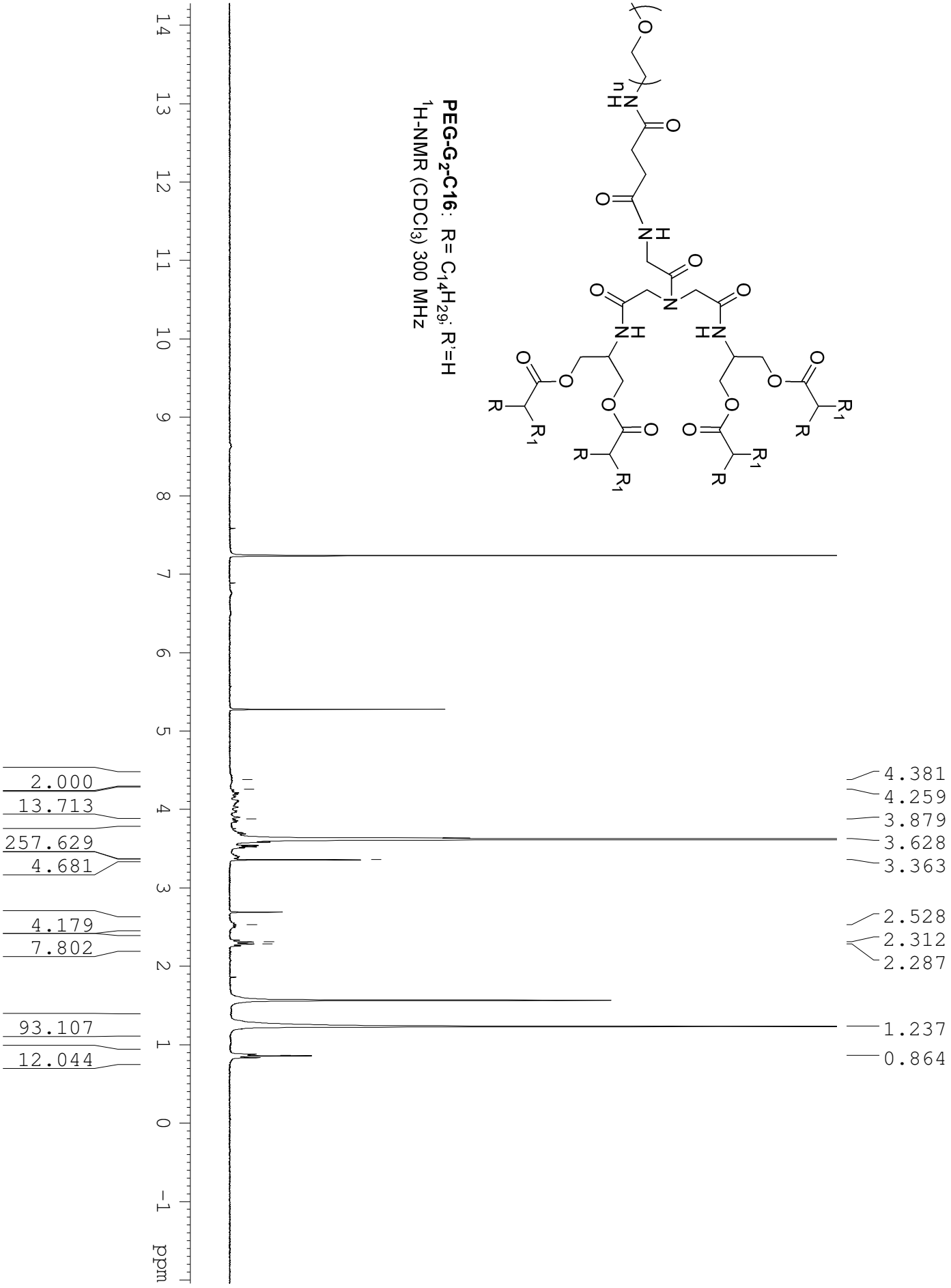
PEG-G2-C16: R= C14H29; R'=H
1H-NMR (CDCl3) 300 MHz
14
13
12
11
10
9
8
7
6
5
4
3
2
1
0
-1
ppm
2.000
13.713
257.629
4.681
4.179
7.802
93.107
12.044
4.381
4.259
3.879
3.628
3.363
2.528
2.312
2.287
1.237
0.864

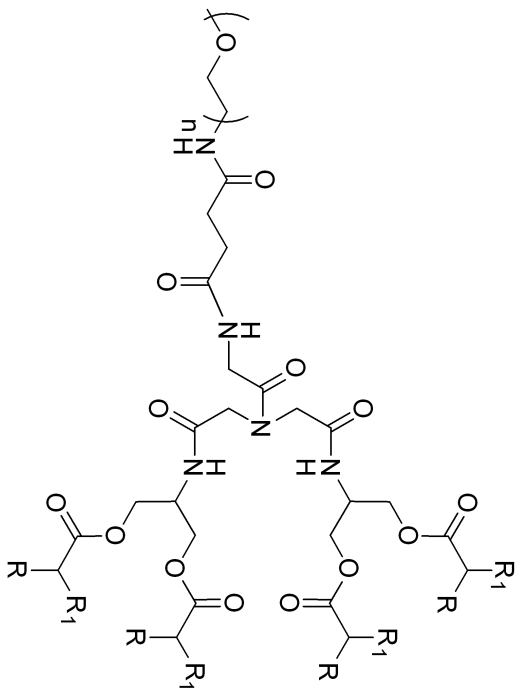

PEG-G_2-dC16: R= C_8H_{17}; R'=C_6H_{13}

^{1}H-NMR ($CDCl_3$) 300 MHz

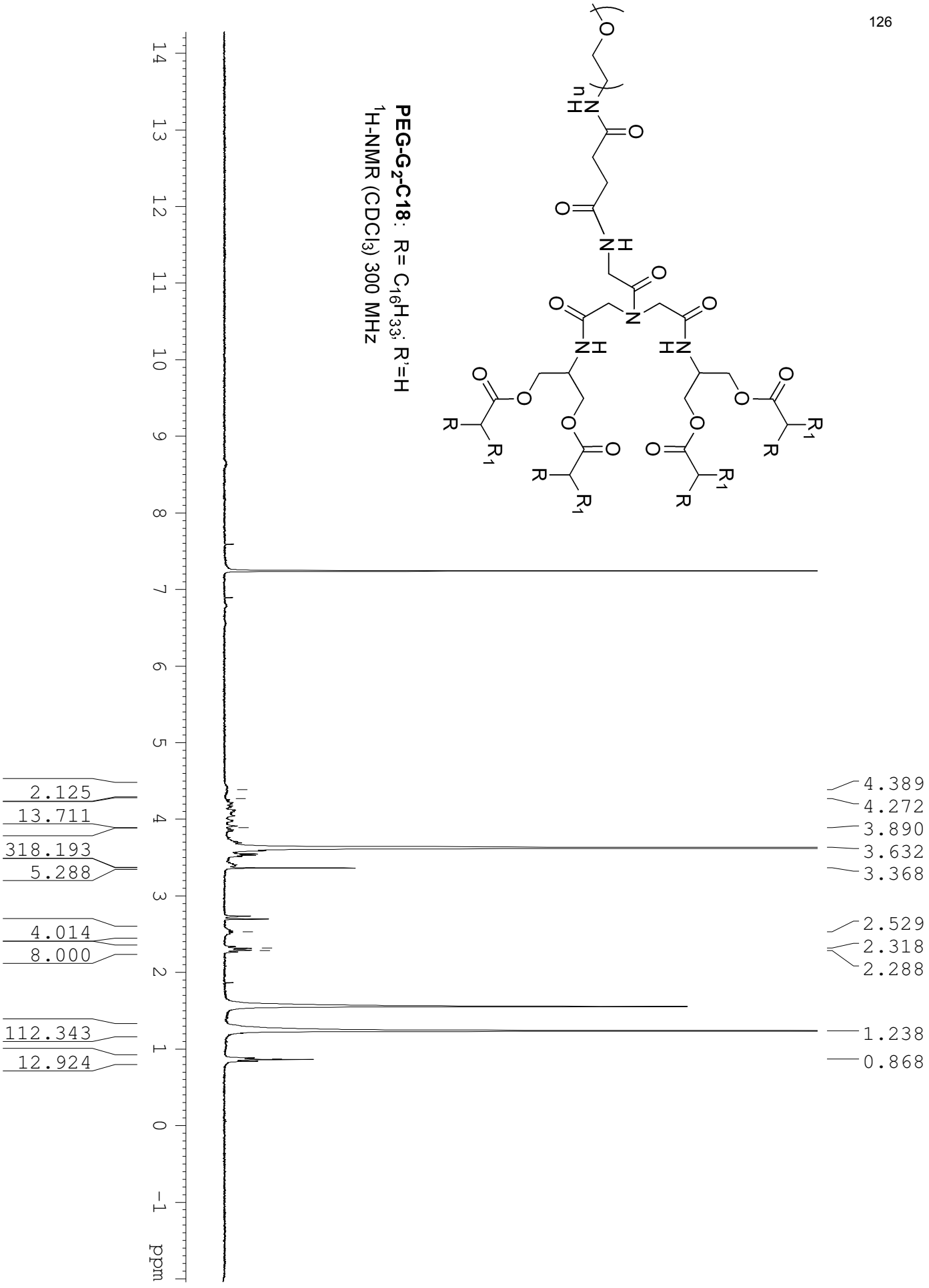
PEG-G2-C18: R= C16H33; R'=H
1H-NMR (CDCl3) 300 MHz
14
13
12
11
10
9
8
7
6
5
4
3
2
1
0
−1
ppm
2.125
13.711
318.193
5.288
4.014
8.000
112.343
12.924
4.389
4.272
3.890
3.632
3.368
2.529
2.318
2.288
1.238
0.868